Novel Lipid Nanoassemblies with Advanced Functionality: Design, Photosynthesis Mimicking and Self-Assembly

by

Mingming Wang

A dissertation submitted to the Graduate Faculty of
Auburn University
in partial fulfillment of the
requirements for the Degree of
Doctor of Philosophy of Science

Auburn, Alabama
August 5, 2017

Key words: Lipid bilayer, liposomes, self-assembly, photosynthetic mimicking, cholesterol-induced phase separation, Janus liposomes

Approved by

Wei Zhan, Chair, Associate Professor of Chemistry and Biochemistry
David Stanbury, Professor of Chemistry and Biochemistry
Christopher Easley, Associate Professor of Chemistry and Biochemistry
James Radich, Assistant Professor of Chemical Engineering

Abstract

Model lipid membranes have attracted considerable attention over the past several decades. They are ideal biomimetic models for studying cells and cellular processes. Due to their unique properties and functional versatility, they are widely used for drug delivery, biosensors and photosynthetic mimics. In this dissertation, we first demonstrated artificial photosynthetic mimics to mimic photosynthesis of green sulfur bacteria by using model lipid membranes including liposomes and solid supported lipid bilayers as scaffolds to host essential components for photoconversion. We specifically investigated the effect of different lipid phases such as lipid disorder phase, lipid ordered phase, gel phase on the photoconversion efficiency. We observed by incorporation of cholesterol, the photoconversion efficiency is greatly enhanced. The underlying photo-kinetics and morphology of such photosynthetic mimics are characterized by absorption spectroscopy, fluorescence spectroscopy, transient absorption spectroscopy, atomic force microscopy, scanning electron microscopy, and confocal microscopy. We next synthesized various kinds of Janus-like giant liposomes, exploiting cholesterol-induced phase separation. We specially investigated the self-assembly of biotinylated Janus-like liposomes and charged Janus-like liposomes, which is driven by biotin-avidin interaction and electrostatic interaction, respectively. By taking advantage of cholesterol-induced phase separation, we can regioselectively dope the biotinylated lipids and charged lipids into the desired domains. Using such Janus-like liposomes, we can obtain well controlled self-assembled lipid supercomplexes.

To my parents

Acknowledgments

Undertaking the Ph.D. has been a challenging yet rewarding experience in my life. By no means could I accomplish it without people who have offered their great and selfless help and support to me over the past five years. Here I would like to express my sincere gratitude to all of them.

First and foremost, I wish to thank my advisor, Dr. Wei Zhan, for his patience, valuable guidance, and consistent encouragement. Without him, I would not have had the great opportunity to pursue my Ph.D. at Auburn University. He is such an amicable and positive person. Whenever I come across tough times in the research work, he has always made himself available for me. I remember he used to say something like “you are one of the best students in the department”, “you need to look on the bright side”, and “you are getting there” to encourage me never to stop. It is Dr. Zhan who led me to one of my favorite research areas, lipid membranes. Not only did he teach me how to do experiments in person when I first joined his group, but also he shaped my attitude towards how to look at things that happened in research and life from different angles.

I am particularly thankful to all the previous and current group members. I feel lucky to have worked with them. With their help and support, I have been able to make progress in my projects. I sincerely thank Zening Liu. We attended the same Alma Mater (Huazhong Agricultural

University, China). We have collaborated on a Janus liposome project, which I did not include in this dissertation. I am also grateful to Qi Cui with whom I worked on a project on ultramicroelectrodes, which I did not cover in this dissertation; and Shamim Iqbal with whom I have had extensive discussion on our projects. I would also like to thank my other lab mates: Chao Li, Dr. Lixia Liu, and Matthew Ferguson.

I wish to thank all my committee members, Dr. David Stanbury, Dr. Christopher Easley, Dr. James Radich, and University reader, Dr. Juming Zhong, for their valuable suggestions in my research work. My thanks go as well to Dr. Tianquan Lian and his team member Dr. Jinquan Chen at Emory University for helping me perform transient absorption spectroscopy in his lab. I am very thankful to Dr. Anne Gordon, who gave me permission to use UV-Vis spectrometer and fluorometer in her lab. Dr. Byron Farnum and Dr. Jimmy Mills offered me great help with data interpretation and I really thank them. My thanks also go to Dr. Michael Miller for training me to master scanning electron microscopy and confocal microscopy.

I would like to give special thanks to Brandon C. Pope and his family. He has been my best friend at Auburn and has always supported and helped me whenever I go through hard times in life. His great family take me as their own child. This means a lot to me and makes me feel as if I have never left home and been away from my parents. I thank my great friend Dr. Xiangpeng Li, who helps me make PDMS sample holders for confocal microscopy. I would also like to thank my other friends back in China and USA: Zhiqiang Zhou, Xu Peng, Wenfeng Dun, Jinjun Tang, Lijin Su, Buhua Wang, Maya West. I sincerely value the friendship from my dear friends, which helps me get through the tough times in life. I am also grateful to my previous mentors, Dr. Yang

Qu, Dr. Hao Chen, and Professor Jing Shen from Huazhong Agricultural University and Hubei Academy of Agricultural Sciences in China, who led me to enter the academic world.

Last but not the least, my deepest and greatest thanks go to my parents and other family members for their endless support, encouragement and love.

Table of Contents

List of Tables

List of Figures

List of Abbreviations

SUV	Small Unilamellar vesicle
GUV	Giant Unilamellar Vesicle
MLV	Multilamellar Vesicle
BLM	Black Lipid Membrane
tBLM	Tethered Bilayer Lipid Membrane
SAM	Self-Assembled Monolayer
QCM	Quartz Crystal Microbalance
AFM	Atomic Force Microscopy
SLB	Solid Supported Lipid Bilayer
SPR	Surface Plasmon Resonance
FRET	Förster Resonance Energy Transfer
ITO	Indium Tin Oxide
T_m	Phase Transition Temperature
l_d	Liquid Disordered Phase
l_o	Liquid Ordered Phase
s_o	Gel Phase
GSB	Green Sulfur Bacteria

BChl	Bacteriochlorophyll
FMO	Fenna-Matthews-Olson
ET	Energy Transfer
PeT	Photo-Induced Electron Transfer
RC	Reaction Center
DOPC	1,2-dioleoyl-*sn*-glycero-3-phosphocholine
DOTAP	1,2-dioleoyl-3-trimethylammonium-propane
DPPC	1,2-dipalmitoyl-*sn*-glycero-3-phosphocholine
DPPG	1,2-dipalmitoyl-*sn*-glycero-3-phospho-*rac*-(1-glycerol) sodium salt
Rho-DPPE	1,2-dipalmitoyl-*sn*-glycero-3-phosphoethanolamine-N-(lissamine rhodamine B sulfonyl) (ammonium salt)
HEPES	4-(2-hydroxyethyl) piperazine-1-ethanesulfonic acid
CCD	Charge-coupled device
TA	Transient Absorption
CMOS	Complementary Metaloxide Semiconductor
IRF	Instrument Response Function
SEM	Scanning Electron Microscopy
AFM	Atomic Force Microscopy
QE	Photon-to-Electron Quantum Conversion Efficiency
POPC	1-palmitoyl-2-oleoyl-*sn*-glycero-3-phosphocholine
POPG	1-palmitoyl-2-oleoyl-*sn*-glycero-3-phospho-(1'-*rac*-glycerol) (sodium salt)
DPPE	1,2-dipalmitoyl-*sn*-glycero-3-phosphoethanolamine
Rho-DOPE	1,2-dioleoyl-*sn*-glycero-3-phosphoethanolamine-N-(lissamine rhodamine B

	sulfonyl) (ammonium salt)
DPTAP	1,2-dipalmitoyl-3-trimethylammonium-propane (chloride salt)
Biotin-DOPE	1,2-dioleoyl-*sn*-glycero-3-phosphoethanolamine-N-(biotinyl) (sodium salt)
BODIPY-Chol	23-(dipyrrometheneboron difluoride)-24-norcholesterol
BODIPY-PC	1-palmitoyl-2-(dipyrrometheneboron difluoride) undecanoyl-*sn*-glycero-3-phosphocholine
PBS	Phosphate Buffer Saline
PVA	Polyvinyl Alcohol

Chapter 1

Introduction

Recent years have witnessed notable advances in the development and application of model lipid membranes, due to their structural and functional resemblance to biomembranes, versatile functionalization, and simplicity. This chapter starts with outlining commonly used model lipid membranes, and proceeds with focusing on addressing the advancements in artificial photosynthesis based on model lipid membranes, despite their wide applications. Following that, a rather interesting and significant phenomenon in lipid membranes, phase separation, is briefly discussed. A special emphasis is placed on cholesterol induced phase separation. Janus particles and their application in self-assembly is then touched on in brief. This chapter is concluded with the scope of this dissertation.

1.1 Model Lipid Membranes

As the major structural component of biological membranes, lipids, once dispersed into water or deposited onto solid supports (e.g. glass[1-2] and metal surfaces[3-5]), spontaneously self-assemble into hierarchical lipid assemblies such as liposomes (vesicles)[6] and lipid bilayers[7]. Lipids possess amphiphilic characteristics, containing a hydrophilic headgroup and hydrophobic tails

(See Fig. 1.1 for example). The primary driving force for lipid self-assembly is the hydrophobic effect, contributed by hydrophobic tails. When exposed in aqueous environment, bilayer structure will form to minimize the exposure of hydrophobic moieties to water (Fig. 1.1). Within the bilayers, hydrophobic tails are placed together, forming the core of the bilayer, while the hydrophilic headgroups face toward water. On the other hand, entropic interactions between hydrophobic tails, and electrostatic and steric interactions between headgroups, counteract the formation of bilayers.[8] To date, various model lipid membranes have been developed as versatile systems not only for fundamental studies of membrane functions such as membrane fusion,[9,10] endocytosis/exocytosis,[10] lipid-protein interactions,[11] but also for practical applications such as drug delivery[7,12,13] and biosensors[7,12].

1.1.1 Liposomes

Liposomes comprising mostly phospholipids are artificial vesicles in which an aqueous solution core is surrounded by a lipid bilayer membrane (Fig. 1.1),[6] unlike micelles, which are enclosed monolayers with a hydrophobic core (tails) and hydrophilic surface (headgroups), or a hydrophobic core and hydrophilic surface (so-called inverted micelles). Dispersed in aqueous media, lipids spontaneously self-assemble into unilamellar/multilamellar liposomes with size ranging from nanometers to micrometers in diameters.[6] Liposomes are ideal biomimetic models for studying key cellular processes, including cell fusion and docking,[9,10] endocytosis/exocytosis,[10] membrane trafficking,[14] etc. Moreover, due to their structural versatility and facile surface functionalization, liposomes are promising carriers for drug delivery[12,13] and gene delivery[13-15]. Additionally, liposomes have been employed as scaffolds for solar energy conversion,[16-18] inspired by nature. Depending on their size and numbers of lamellae, liposomes can be categorized into

several types including small unilamellar vesicles (SUVs), giant unilamellar vesicles (GUVs), multilamellar vesicles (MLVs), etc.[6] (Fig. 1.1).

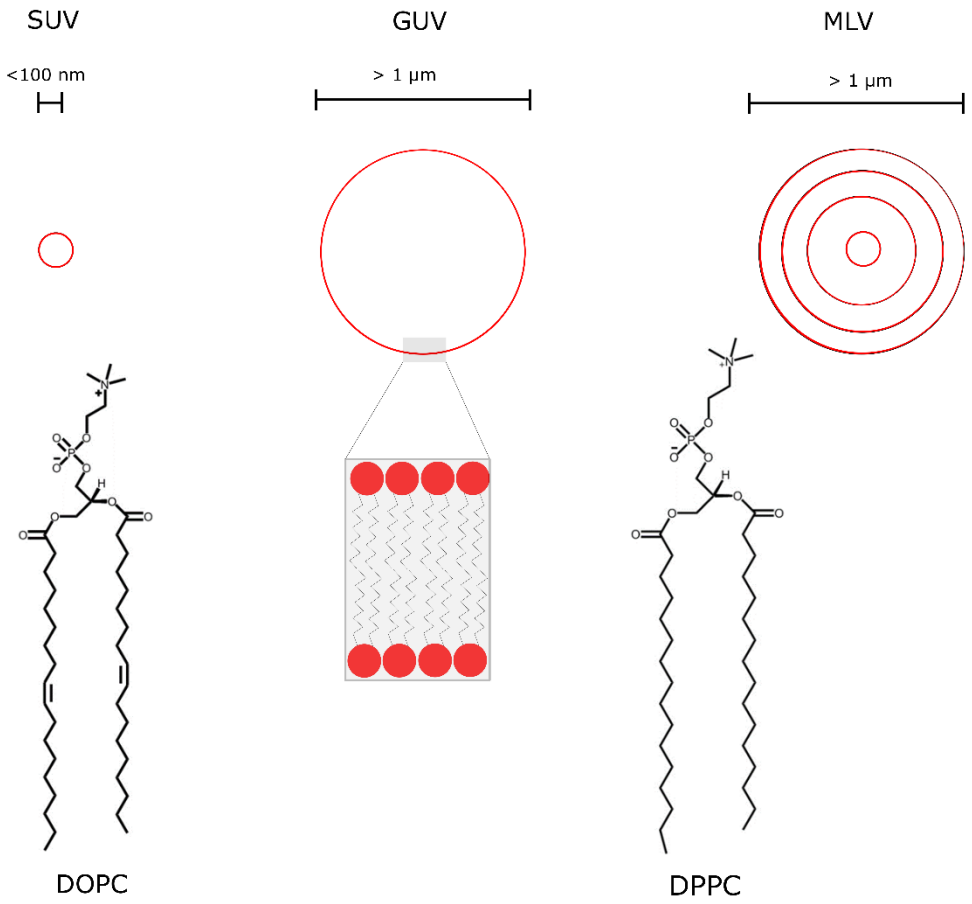

Figure 1.1 Schematic of liposomes including SUVs, GUVs and MLVs, and chemical structures of representative lipids: DOPC, 1,2-dioleoyl-sn-glycero-3-phosphocholine; DPPC, 1,2-dipalmitoyl-sn-glycero-3-phosphocholine.

SUVs contain a single lamella and have a typical size of 20-100 nm. They have been extensively used for targeted drug delivery[10,12,13] and gene delivery (typically cationic SUVs),[13,14]

and biosensors[19]. The general procedure to prepare SUVs involves hydration followed by sizing such as sonication and extrusion. GUVs represent an excellent model for cell mimicking due to their comparable size and readily being characterized by optical microscopes.[20-22] Several methods for GUV preparation have been developed including gentle hydration,[23-26] electroformation,[26-29] phase transfer,[30,31] and gel-assisted formation,[32,33] etc. MLVs have onion-like structures, generally consisting of five or more concentric lamellae composed of lipid bilayers interspersed with aqueous layers.[6] MLVs are therefore considered to be of great promise for incorporation or transportation of lipophilic materials.[34]

1.1.2 Black Lipid Membranes (BLMs)

BLMs are the earliest model lipid membrane developed by Mueller and coworkers.[35,36] To form BLMs, a lipid solution typically prepared in a viscous hydrophobic solvent (e.g. octane) is brushed onto an aperture in a thin layer of a hydrophobic material such as Teflon. Once in water, a lipid monolayer spontaneously forms at the interface between the organic and aqueous phases on either side of Teflon sheet; overtime, a continuous bilayer is formed in the center of the aperture (Fig. 1.2).[36,37] BLMs remain widely applied today mainly due to their being well suited to electrical characterization because two compartments separated by the bilayer are both accessible, which allows straightforward electrode placement and reagent exchange.[37] However, BLMs suffer from short lifetime and residual organic solvent,[37,38] which greatly limit the applications of BLMs on transmembrane protein studies.

1.1.3 Lipid Membranes on Solid Supports

Preparation of lipid membranes on solid supports have become popular practice in laboratory over the past several decades[7,39-41]. Not only can it afford the capability to study basic cell membrane functions such as lipid-protein interaction and ion channels[7,41], but it can serve as a robust platform for potential biotechnological applications, for instance, biosensors.[7,42] To date, a wealth of such lipid bilayer systems on solid supports have been invented, such as solid supported lipid bilayers,[43-47] hybrid lipid bilayers,[48-50] and tethered lipid bilayers[51,52] (Fig. 1.3).

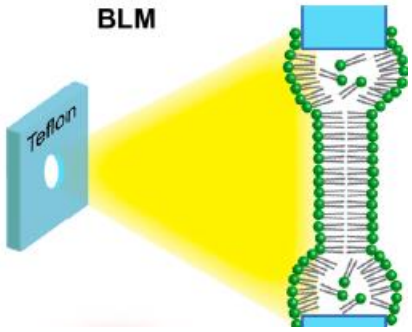

Figure 1.2 Schematic of black lipid membrane (BLM). Reprinted with permission from *Acc. Chem. Res*. **2016**, *49*, 2551-2559. Copyright (2016) American Chemical Society.

1.1.3.1 Solid Supported Lipid Bilayers (SLBs)

Formation of SLBs (Fig. 1.3A) necessitates a hydrophilic surface of solid supports such as glass, mica, and some metals.[7] One of the most widely used method to form SLBs is vesicle fusion on these solid surfaces.[7] In detail, hydrophilic substrates are immersed in a SUV solution typically for several hours. During hours incubation, these liposomes first adsorb, rupture, and ultimately spread into planar lipid bilayer during incubation.[39] Vesicle fusion represents a simple and robust route to produce SLBs. More exciting is that such SLBs allows lipids and lipid-associated proteins

to diffuse translationally and rotationally.[39] As such, SLBs are well applicable to studying lipid domains,[53,54] intermembrane interactions,[55,56] or membrane-protein interactions.[57] However, formation of SLBs has been found to be an intricate process. When lipid vesicles contact the surface of the solid substrate, they either do not adsorb, adsorb and remain intact, or adsorb and rupture instantaneously to form lipid bilayer, depending on the composition of vesicles.[58] The exact mechanism of formation of SLBs via vesicle fusion is not fully understood, and considerable work is underway by using a wide variety of analytical tools including quartz crystal microbalance (QCM),[39] atomic force microscopy (AFM),[39] neutron reflectometry,[59] and surface plasmon resonance (SPR)[60] as well as mathematical modeling[61].

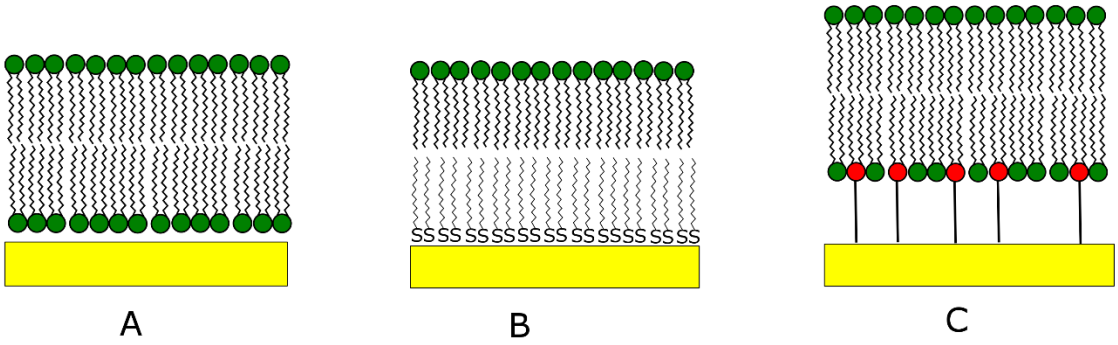

Figure 1.3 Solid supported lipid bilayers. A. SLBs; B, hybrid lipid bilayers; C, tethered lipid bilayers.

1.1.3.2 Hybrid Lipid Bilayers

Hybrid lipid bilayers (Fig. 1.3B) are made by placing a monolayer of phospholipids on an alkanethiol self-assembled monolayer (SAM) anchored typically on a gold surface[62]. Compared to lipid bilayers, hybrid bilayers exhibit higher stability and robustness[7,63]. On the other hand,

direct interface with metal surfaces renders the feasibility of applications of surface-sensitive techniques, e.g. SPR,[64] surface-enhanced Raman/IR,[65] and electrochemical techniques including cyclic voltammetry,[62] impedance spectroscopy,[62] and QCM.[66] For instance, investigation on electron transfer between a redox species and a hybrid lipid bilayer covered gold electrode can shed light on the formation of the bilayer qualitatively and quantitatively by using cyclic voltammetry and impedance spectroscopy.[62] Ever since their first introduction by Plant in 1993,[62] hybrid lipid bilayers have been often employed for biomembrane mimicking as well as biosensing.[8,67] Ferri and coworkers,[67] for example, incorporated a glutamate receptor in a hybrid lipid bilayer to detect glutamate at nM levels due to transmembrane current amplification. There lacks adequate space for incorporating membrane proteins, however, making biomembrane mimicking problematic.

1.1.3.3 Tethered Bilayer Lipid Membranes (tBLMs)

Tethered lipid bilayers (Fig. 1.3C) are based on thiolipids, which comprise a lipid tail and a hydrophilic spacer linked to a solid substrate, preferably gold.[68,69] As to the tethered molecules, alkyl chains, phospholipids, or cholesterols have been used as thiolipid tails, whereas peptides, oligomers, or polymers have been chosen as spacers.[68] This submembraneous space affords an ionic reservoir as well as provides adequate space for incorporated membrane proteins,[70] which makes tBLMs well suited to mimic biomembranes. However, their high capacitance and impedance limit the ability of tBLMs to match the electric properties of biological membranes.[68]

1.1.4 Tethered Vesicles

Lipid vesicles have been tethered to SLBs via DNA hybridization or biotin-avidin interaction.[71-73] In doing so, proteins incorporated into tethered vesicles can be shielded from the solid surface by SLBs thus minimizing the molecule-surface interaction.[71] Haran et al.[73] tethered protein-trapped vesicles to a SLB via biotin-avidin chemistry for single biomolecule detection. These vesicles remain intact and often motionless after being attached to the surface. Quite differently, DNA-tethered vesicles have been shown to diffuse and collide with each other, although their diffusion is constrained into two dimensions.[71] This raises the potential to use DNA tethered vesicles to study membrane reactions including protein-mediated docking and fusion.[74]

1.2 Model Lipid Membranes for Artificial Photosynthesis

As the ultimate energy source, solar power is clean, abundant and sustainable, and has thus been considered the ideal replacement to carbon-based energy sources, such as oil, gas and coal. Ever-growing use of fossil fuels will eventually exhaust them and unfortunately has brought severe environmental issues, such as air pollution and the greenhouse effect.[75] Considerable attention has been therefore directed towards finding efficient and sustainable ways to capture and convert solar energy on a large scale. Photosynthesis in nature is a system that has the capability to harness energy provided by the sun, which has inspired generations of researchers in biomimetic light energy utilization due to its grand scale, ultimate efficiency, and sustainability.[37]

Following nature's lead, considerable artificial photosynthetic systems have hitherto been constructed with promising efficiency, where light-harvesting antenna initially captures light, and transfers excitation energy ultimately to adjacent reaction center. Inspired by nature, several light-driven methodologies have been developed such as photo-electrochemical cells,[76-78] photocatalytic

water splitting,[78-80] light-driven carbon dioxide reduction,[81] and photobiological fuel production[82]. A wide variety of materials developed for achieving these goals have been reported and reviewed elsewhere.[83-86] Here, we specifically focus on artificial systems built in a lipid membrane setting.

As an essential and ubiquitous component in all photosynthetic machinery, lipids and their assemblies have long been recognized as powerful molecular scaffolds in building artificial photosynthetic systems.[37] Photovoltaic effect and photoconductivity in BLMs was demonstrated by Tien in 1968 for the first time.[87] The membrane, constituted from natural photosynthetic pigments such as chlorophyll and xanthophyll, is considered as a photocell capable of effecting water photolysis. On the other hand, artificial photoconversion based on liposomes containing chlorophyll and carotene was first described in 1976 by Mangel.[88] Upon illumination, charge transport is observed provided that a redox potential gradient exists across the liposome membrane. One significant finding in this report is that chlorophyll aggregates are present in the liposomes and are responsible for energy conversion. This is in accordance with spectroscopic characterization for some photosynthetic bacteria, e.g. green sulfur bacteria,[89] whose light harvesting antenna comprise such aggregated bacteriochlorophylls. It has been proposed such aggregation results in molecular exciton formation upon irradiation.[90] Model membrane system based artificial photosynthesis has become an active research area ever since.[37]

Using model lipid membranes, two approaches have been generally employed to establish artificial photosynthetic systems. One is directly copying natural systems by reconstitution of photosynthetic antenna protein and/or reaction center in lipid bilayers. Reconstituting photosynthetic proteins into membrane is not only a promising way to fabricate photoconverting devices, but also sheds light on mechanisms how nature performs photosynthesis. Earlier work on reconstituted photosynthetic in SLBs was done by Gruszecki et al.[91] In this work, monomolecular

layers of LHCII complex were formed on a glass support, where efficient excitation energy transfer was observed to chlorophyll b respectively from chlorophyll a, neoxanthin, lutein, and violaxanthin. This work demonstrated the viability to fabricate artificial light-to-current converters using reconstituted photosynthetic proteins. One notable drawback of such monolayer system is that direct contact in solid supports presumably denatures and therefore malfunction proteins. Later, reconstituting transmembrane proteins in lipid bilayers has become a frequent practice.[92-94] For instance, Nango et al.[92] assembled two types of photosynthetic membrane proteins from purple bacteria, i.e. the peripheral antenna complex (LHII) and the core antenna/reaction center complex (LHI-RC), into domain-structured planar lipid bilayer, where intermolecular energy transfer from LHII to LHI-RC was clearly observed (Fig. 1.4). More recently, Sinner and coworkers[93] developed a stable, highly controllable, and sustainable light harvesting system by reconstitution of light-harvesting complex II (LHCII) into a polymeric membrane, in both spherical and planar configurations. It has been found that LHCII is capable of binding pigments in a certain way akin to that found in the chloroplasts of living cells. Kumar and coworkers[94] designed a photo-electrochemical cell by using a biomimetic interface, where photosystem I complex is reconstituted into a tethered lipid bilayer intercalated by conjugated oligoelectrolyte molecules at a high concentration to form ordered two-dimensional crystals. This approach may provide a potential platform for photosystem I based H_2 production. The studies reviewed above show the capability of reconstitution of photosynthetic proteins in model lipid membranes to establish artificial photosynthetic systems. However, this approach suffers from vulnerability of photosynthetic bacteria especially when the lipid bilayer interfaces with a solid support.

The other approach, more robust, is to incorporate synthetic molecules/nanoparticles into model membranes. Given that unique nano-environment of lipid bilayer, one needs to exquisitely

design molecules in order for successful embedment. In 1979, Calvin and coworkers[16] demonstrated efficient photosensitized electron transport across lipid vesicle membranes. In these lipid vesicles, an amphiphilic tris(2,2'-bipyridine) ruthenium(II) derivative is incorporated into the lipid bilayer, which isolates two aqueous compartments including an exterior viologen solution and an interior ethylenediaminetetraacetate (EDTA) solution. This ruthenium species,

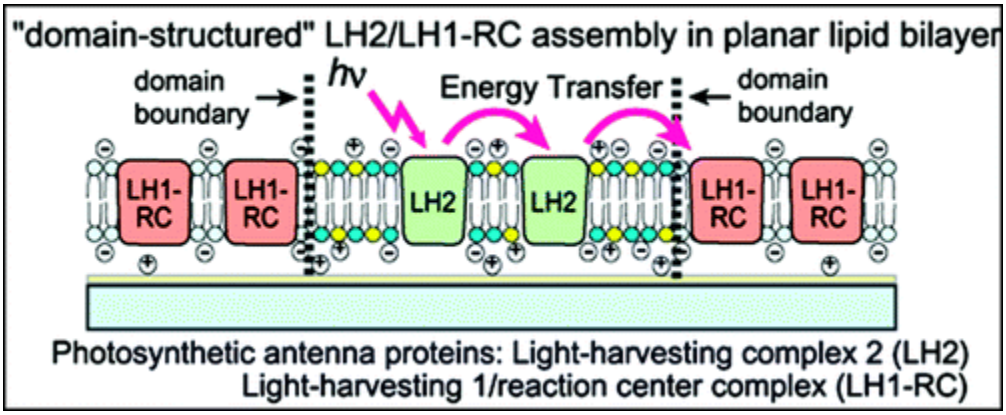

Figure 1.4 Reconstitution of light-harvesting complex 2/light-harvesting complex 1-reaction center into planar lipid bilayers supported on a solid substrate. Reprinted with permission from *Langmuir* **2011**, *27*, 1092-1099. Copyright (2011) American Chemical Society.

upon irradiation, photosensitizes the irreversible oxidation of EDTA and reduction of viologen. Within the membrane, electron transport is plausibly due to electron exchange (electron tunneling) rather than a diffusional mechanism. Later, Moore et al.[17] reported a quinone-porphyrin-carotene triad that is incorporated into the lipid bilayer of liposomes to generate a proton gradient across liposomal bilayers to drive adenosine triphosphate (ATP) synthesis (Fig. 1.5). By rational design, Matile and coworkers[95] created a photosystem where helical tetrameric π-stacks of naphthalene diimides are successfully incorporated in liposomes by using rigid p-octiphenyl rods as

preorganizing scaffolds. Such π-stacks are demonstrated to support sufficient charge-separation lifetimes for conversion into proton gradients. Without extensive molecular engineering, Lindsey and coworkers[96] developed an approach to build a light-harvesting system that may afford broad solar collection and efficient energy transfer using lipid vesicles. Using lipid vesicles and DNA as scaffolds, Albinsson and coworkers[97] reported self-assembled light-harvesting complexes comprising DNA-intercalating YO-PRO-1 (energy donor) and membrane-bound porphyrin (energy acceptor). Thanks to DNA, chromophores can be arranged on a nanometer scale to significantly enhance the effective absorption coefficient of light harvesting antenna. In addition to these synthetic molecules, nanoparticles that can fit within either the bilayer or aqueous core have been used as photosensitizers and/or electron mediators. Hwang and Mauzerall[98] embedded fullerenes (C_{60} and C_{70}) in a lipid bilayer, serving as efficacious electron acceptors from membrane surface-bound photoexcited zinc porphyrin. Apart from being an electron transport mediator, C_{70} was further shown to be an efficient photosensitizer. This C_{70}-lipid bilayer system outclassed previously the most efficient artificial photosynthetic system, i.e. carotene-porphyrin-quinone system, in terms of photocurrent density, stability, and turnover number.[98] Baral and Fendler[99] demonstrated successful photovoltage generation by using CdS quantum dots, which are generated *in situ* on one side of a BLM to mediate photoelectric effects.

Additionally, integration of these two approaches have been done to establish hybrid artificial photosynthetic systems. For instance, CdTe quantum dots were immobilized on the surface of a purple membrane containing a photochromic protein bacteriorhodopsin. Exogeneous quantum dots capture light and transfer excitation energy via highly efficient Förster energy transfer (FRET) to the surrounding purple membrane system. Significant enhancement in efficiency of light-driven transmembrane proton pumping was further demonstrated in this

integrated system, which is the main biological function of bacteriorhodopsin.[100] Another example[101] is to embed photosynthetic reaction centers combined with CdSe/ZnS quantum dots into liposomes. The stability of reaction centers in this hybrid complex is even increased yet their function is completely maintained. Remarkably, even for dried films of such hybrid complexes, the efficiency of energy transfer from quantum dots to reaction centers and electron transport activity of reaction centers remain for several months. This demonstrates the possibility to develop an efficient and robust light-harvesting antenna for photosynthetic reaction centers in films and potential for developing novel bio-hybrid light-harvesting modules.

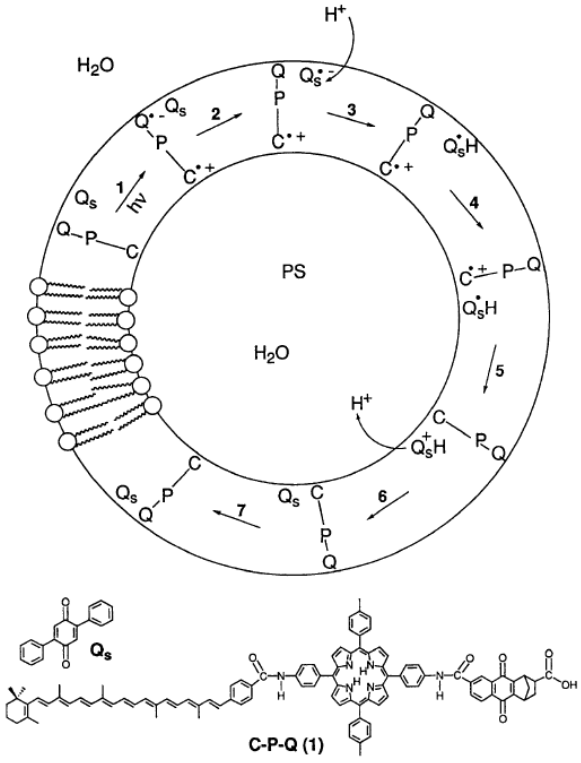

Figure 1.5 Schematic artificial photosynthetic reaction centers composed of carotene-porphyrin-quinone (C-P-Q) triads incorporated in liposomes. Reprinted with permission from *Nature* **1997**, *385*, 239-241. Copyright (1997) Nature Publishing Group.

Besides photovoltaics reviewed above, photocatalytic water splitting as another promising way of storing and converting solar energy has blossomed into active fields of research.[85,86] Hydrogen, where the converted energy is stored, is an ideal energy carrier in that water is the only product when the energy is released. To accomplish this process, typically a photosensitizer creates an electron and a hole upon irradiation, which are respectively transferred to adjacent hydrogen evolving catalyst and oxygen evolving catalyst. In doing so, water is photo-catalytically reduced and oxidized to generate hydrogen and oxygen.[102] Herein, we reviewed the literatures on photocatalytic water splitting carried out at the lipid membranes. Taking advantage of lipid vesicles, amphiphilic photosensitizers and a cobaloxime catalyst are co-assembled in a lipid bilayer for water reduction by Troppmann and König.[103] Within lipid membrane, these complexes are within close spatial proximity and membrane fluidity furthermore allows their dynamic reorganization, resulting in efficient electron transfer and improved photocatalytic activity for water reduction. Later, by employing the same approach, they anchored a ruthenium complex photosensitizer and a ruthenium complex catalyst to a lipid membrane for water oxidation.[104] This system shows superior photocatalytic activity even at low concentration of the water oxidation catalysts plausibly due to appearance of phase separation and patch formation, which might facilitate the intermolecular electron transfer and thus enhance photocatalytic efficiency. Bonnet et al.[105] studied the kinetics of photocatalytic water oxidation at liposomes, using a ruthenium complex as the photosensitizer and Ru-, Co-, or Ir-based water-oxidation catalysts incorporated into the liposomes. It appears that oxidative quenching of photosensitizer is the rate-determining step of the photocatalytic water oxidation reaction. Membrane anchoring is found to be able to stabilize the photosensitizer.

Research on artificial photosynthesis in our lab is focused on solid supported lipid bilayers, which are employed as scaffolds to host light-harvesting antenna and electron-transfer mediators for fabricating photo-electrochemical cells. By precise molecular design, we synthesized a photoactive fullerene molecule ([6,6]-closed-ring bridged malonic fullerene) with desired amphiphilicity, size and relatively undisturbed electronic structure, which can be quantitatively assembled in liposomes. Subsequent liposome rupturing on indium tin oxide (ITO), a transparent conducting substrate, forms a lipid bilayer. Stable photocurrents are generated from these ITO-supported lipid nanoassemblies.[47] Later, we introduced a photoactive species $[Ru(bpy)_3]^{2+}$ into a hybrid lipid bilayer for photocurrent generation. We investigated the dependence of photocurrent generation on the underlying *n*-alkanethiol based SAM. Among the three *n*-alkanethiols (C6, C12, and C18) studied, the C12 SAM based bilayers produced higher photocurrent, presumably due to well formation of top lipid bilayer and suitable electron-tunneling distance.[50] Continuing in this direction, we then incorporated multi-components including porphyrin as the photosensitizer and fullerene as the electron mediator into tethered lipid bilayers supported by ITO electrodes.[52] We found out the photosensitizer and electron acceptor should be present in both lipid monolayers in order to facilitate photoexcited electrons to tunnel through low-dielectric hydrocarbon region of lipid bilayer. Taking advantage of sequential formation of bilayers, we are able to facilely decorate each lipid monolayer with desired components, either photosensitizer and/or electron mediator. In doing so, very efficient vectorial electron transfer was observed with concomitant photocurrents enhanced by more than 50-fold. Tailoring the underlying SAMs in hybrid lipid bilayers by affording new functionality, we can introduce new electronic states and modify oriented surface dipole. Specifically, we prepared a new hybrid lipid bilayer comprising a ferrocene-terminated undecanethiol SAM and top lipid monolayer.[106] New electronic states brought by ferrocene

moieties for photo-generated charges hopping on and off, act either as an electron sink or a relay for photoinduced electron transfer, depending on the redox potentials of incorporated photoactive species. On the other hand, oriented surface dipole can be well tuned by forming desired SAMs. Two hybrid lipid bilayers were formed by first grafting two thiols (*n*-dodecanethiol and heptadecafluoro-1-decanethiol) with opposite molecular dipoles onto gold and then laying the same lipid monolayer containing either fullerene or porphyrin on top. Thus-formed hybrid lipid bilayers allow us to investigate the effect of surface dipole on photogenerated charge injection. As envisaged, we observed strikingly different photocurrent/photovoltage from these two bilayer systems, which can be well explained by the different dipole potentials associated with the two SAMs, modifying the Fermi level of gold and thus its alignment with the HOMO/LUMO level of photoactive species. These systems are simple to build, stable yet inexpensive, however, they are less efficient compared to other thin-layer photoconverting devices.

1.3 Cholesterol-Induced Phase Separation

Phospholipids in lipid bilayers exhibit a unique feature of gel-to-liquid-crystalline phase transition upon temperature change. The temperature at which such structural phase transition occurs is called phase transition temperature (T_m). Each lipid has its characteristic T_m.[6] Generally, lipids with longer and saturated acyl chains tend to have higher T_m, whereas those with shorter and unsaturated diacyl chains have lower T_m. Phospholipids tend to adopt *trans* conformation (Fig. 1.6) at $T < T_m$, due to low-lying energy in this state.[107] In the lipid bilayers, they are fully extended and tightly packed to maximize Van der Waals interaction. This lipid phase is called gel phase (s_o), in which individual lipids have rather limited lateral diffusivity and freedom of motion. As the temperature increases up to T_m, the phospholipids instead adopt *gauche* conformation (Fig. 1.6).

Such a transition is called *trans* to *gauche* isomerization.[107] Under this circumstance, the tight packing of acyl chains will loosen, leading to the liquid disordered phase (l_d) emerging,[107] characterized by that lipids have high rotational and lateral mobility.

As a ubiquitous component in biological membranes, cholesterol plays an essential role in maintaining membrane integrity and fluidity. In detail, the presence of cholesterol in membranes condenses the acyl chains of unsaturated lipids in l_d phase and fluidizes those of saturated lipids in s_o phase.[6,108] Incorporation of cholesterol into l_d/s_o binary systems induces a separate phase, i.e. liquid ordered (l_o) phase,[109] which is a hybrid of l_d phase and s_o phase. Lipids in l_o phase have comparable lateral diffusivity to l_d phase and similarly tight packing as in s_o phase (Fig. 1.7).

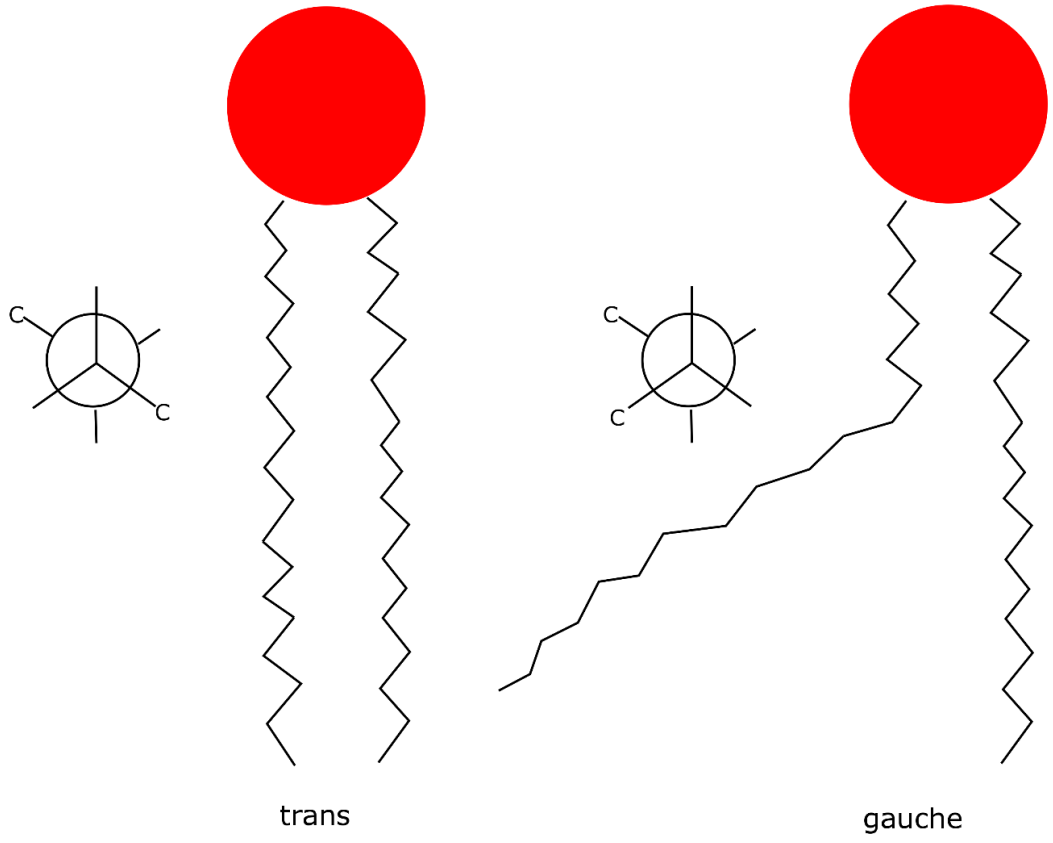

Figure 1.6 Disposition of phospholipid diacyl chains.

Such l_o phase shares similar feature with lipid rafts, which is thought to function in membrane trafficking and signaling.[110] Lipid rafts have thus received much attention over the past two decades ever since this concept was proposed. Their existence, however, is still enormously controversial, which is in part due to that the methods for their detection remain far from perfect.[110,111]

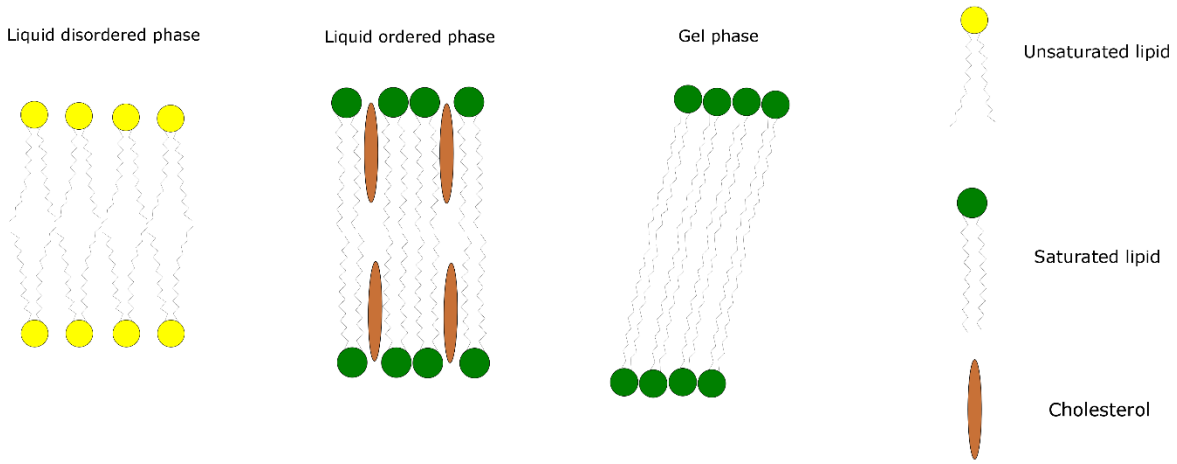

Figure 1.7 Schematic of liquid-disordered (l_d), liquid-ordered (l_o), and gel (s_o) phase membranes.

Intrigued by lipid rafts, model membranes such as GUVs are often employed to study l_o phase and associated biological processes.[112-114] Typical GUVs comprise ternary mixtures of saturated lipids, unsaturated lipids, and cholesterol, which allow for direct observation of micron-sized domains by optical microscopy and precise control of formation of lipid domains.[115] A plethora of ternary lipid systems containing a variety of phospholipids, sphingolipids, and sterols have been developed, and corresponding phase diagrams have been depicted and reviewed elsewhere[116] (see Fig. 1.8 for example). Fluorescence microscopy is the most commonly used method to visualize the phase separation and lipid domains in GUVs that are labelled with fluorescent probes. A number of fluorescent probes that prefer to partition into a single lipid phase

either l_d or l_o phase, have been synthesized and reviewed elsewhere.[117] Knowing the whereabouts of the fluorescent probe by fluorescence microscopy, the lipid phase can be easily discerned.

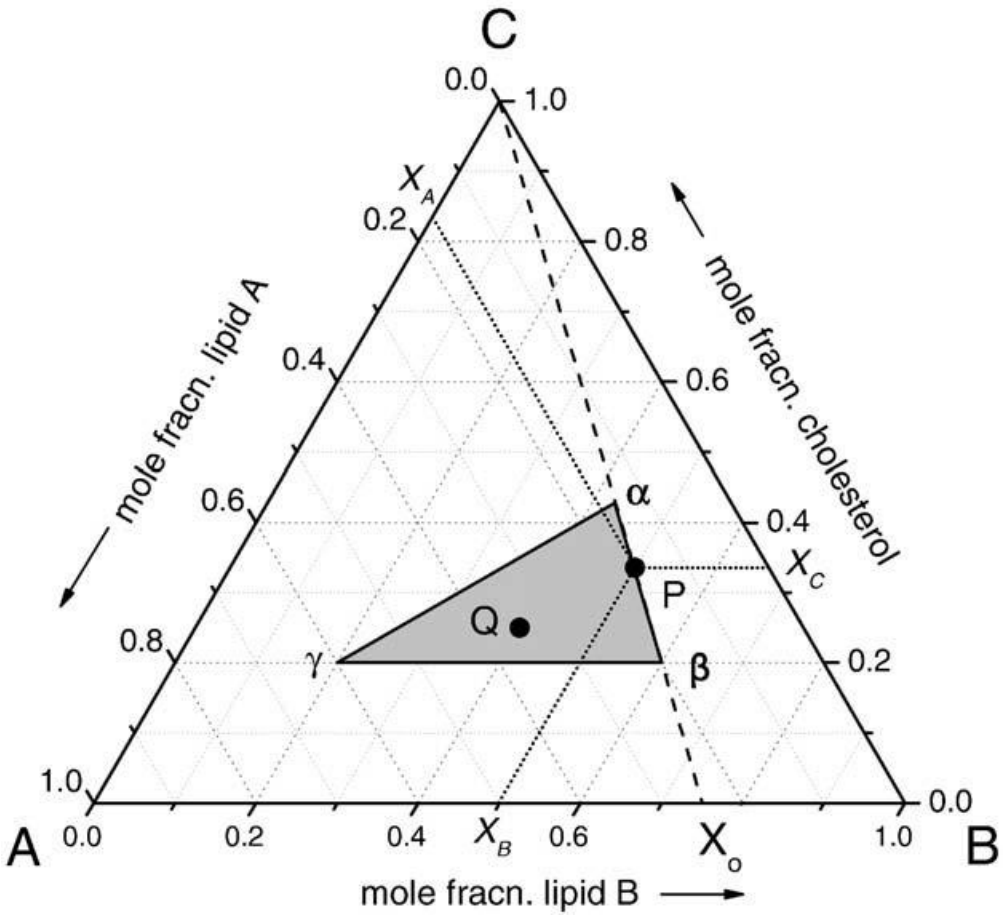

Figure 1.8 Phase diagram of ternary mixtures of lipid A and lipid B together with cholesterol C. The axes to which mole fraction coordinates (XA, XB, XC) are referred are tilted at 60° to one another. α-β, β-γ and α-γ are tie lines and αβγ is a three-phase triangle. Reprinted with permission from *Biochim. Biophys. Acta*. **2009**, *1788*, 2114-2123. Copyright (2009) Elsevier.

1.4 Janus Particles

Janus particles (Fig. 1.9), named after the Roman double-faced god, possess two distinct sides with contrasting functionality. They have attracted enormous attention in recent years,

because they are building blocks of great promise for hierarchical functional materials and potential models for biological structures.[118-120] For example, incorporating stimuli-responsive moieties selectively into certain region, Janus particles are promising "smart" drug carriers,[121] where the morphology/fluidity of the particles can be changed to trigger release of encapsulated materials. Moreover, Janus particles have exhibited self-propelled motion in the presence of catalysts.[122] So far, various shaped Janus particles have been invented and synthesized including spherical, cylindrical, disc-shaped, and dumbbell-shaped ones.[118]

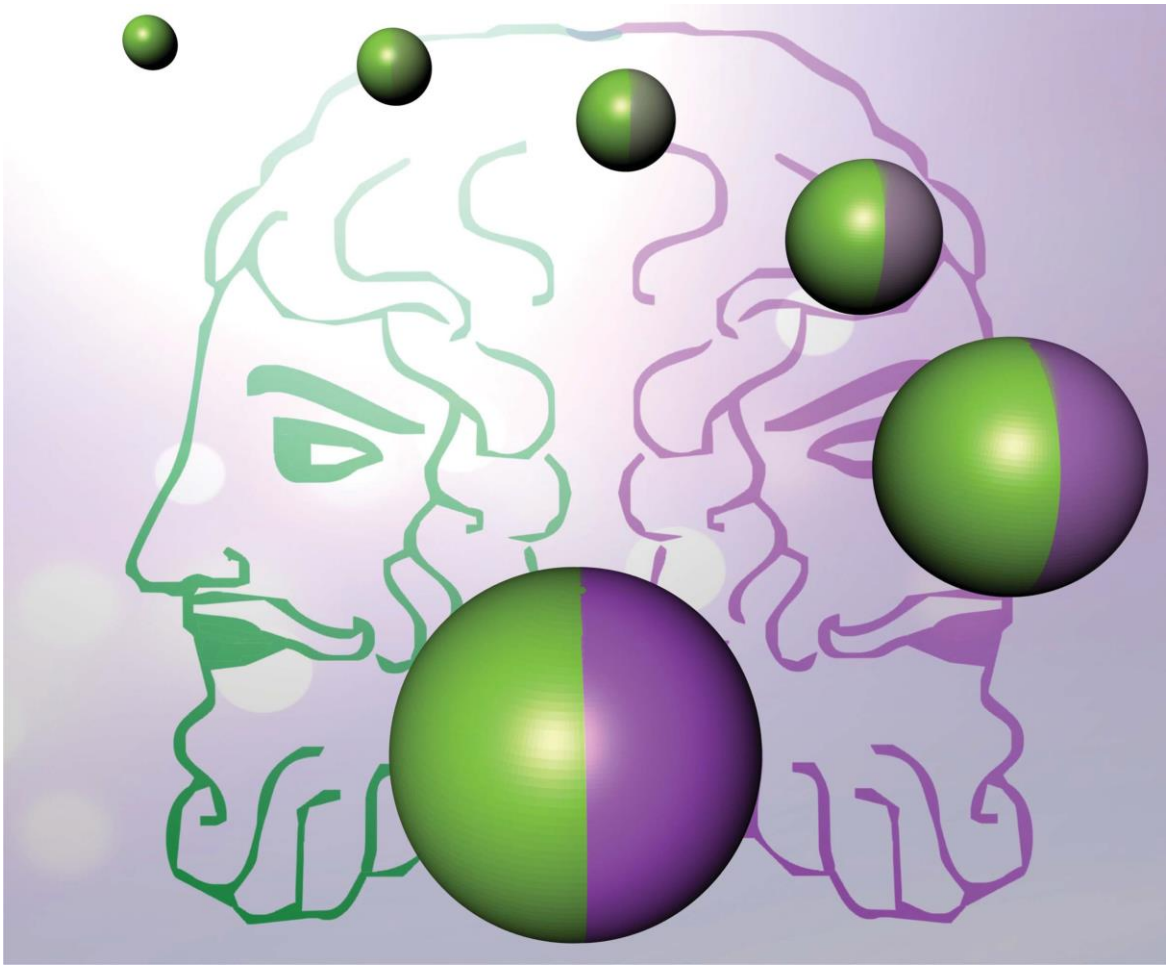

Figure 1.9 Janus and Janus particles. Reprinted with permission from *J. Mater. Chem*. **2012**, *22*, 15457-15474. Copyright (2012) Royal Society of Chemistry.

1.4.1 Synthesis of Janus Particles

To date, there are several general methods to synthesize Janus particles, among which toposelective surface modification is one of the most commonly used method. Toposelective surface modification breaks the symmetry at a single interface.[120]

Interface immobilization is a straightforward and probably most used way to break the symmetry.[120] In detail, homogeneous precursor particles are first immobilized at an interface, say, a solid substrate, to form a monolayer (Fig. 1.10). In doing so, only a portion of each particle surface is exposed for further functionalization while the rest portion thereof is masked and protected. Particles can be immobilized via Langmuir-Blodgett, thiol chemistry (e.g. forming Au-S bond), spin coating, and drop casting.[120] For instance, Tang et al.[123] demonstrated the synthesis of bifunctional Janus microparticles with spatially segregated proteins using interface immobilization based modification, in which polystyrene microparticles were firstly deposited onto glass substrates by drop casting to form a monolayer, and then the exposed side of particles was coated with a layer of gold by metal evaporation. Such gold-coated hemisphere was then activated via thiol-PEG-biotin, by which desired proteins can be conjugated to the surface of particles.

Another often used method to break the symmetry is Pickering emulsion[124]. Particles tend to adsorb at the emulsion interface. As a consequence, one side of each particle is immersed in oil phase, while the other side thereof is exposed in water phase, allowing for toposelective modification.[120] As a case in point, Suzuki et al.[125] reported synthesis of Janus microgel by using Pickering emulsion-based modification (Fig. 1.11) , where poly(*N*-Isopropylacrylamide-*co*-acrylic acid) microgels were dispersed into hexadecane-in-water emulsions, and subsequent

functionalization by tethering amino groups to the side of each microgel exposed to water phase was accomplished through a carbodiimide coupling reaction using ethylenediamine and 1-ethyl-3-(3-dimethylaminopropyl)-carbodiimide hydrochloride. In so doing, the microgels have untreated carboxyl groups on one hemisphere and functionalized amino groups on the other. Thus-prepared Janus microgels were collected by destabilizing the emulsion via freezing/melting process.

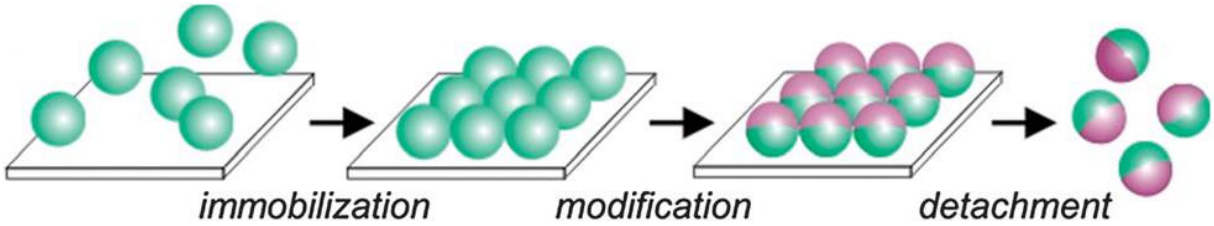

Figure 1.10 Interface immobilization based modification for synthesis of Janus particles. Reprinted with permission from *J. Mater. Chem.* **2012**, *22*, 15457-15474. Copyright (2012) Royal Society of Chemistry.

1.4.2 Self-Assembly of Janus Particles

Self-assembly is a process by which individual components spontaneously form ordered and well-defined hierarchical superstructures, whose collective properties differ from their starting materials.[126] In fact, an astounding range of complex/supercomplex structures in cell are formed by self-assembly, such as lipid membranes, intermembrane proteins, protein aggregates, and molecular machines. The understanding of self-assembly processes is of paramount fundamental interest, not only for developing advanced materials, but for gaining insight into sophisticated biological functions of cells and organelles. The connection of specific organelles such as Golgi, peroxisomes, and lipid droplets etc. by membrane contact sites, for instance, is particularly important in cellular signaling, promotion of ion passage, and non-vesicular lipid trafficking.[127]

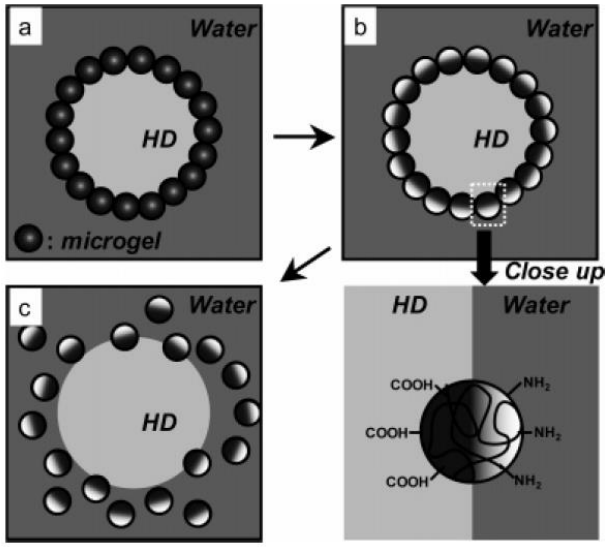

Figure 1.11 Pickering emulsion based modification for synthesis of Janus microgels. (a) Stabilization of a hexadecane (HD) droplet by microgels, (b) modification of one hemisphere of each microgel with amino groups, (c) collection of Janus microgels by destabilizing emulsion. Reprinted with permission from *J. Am. Chem. Soc*. **2007**, *129,* 8088-8089. Copyright (2012) American Chemical Society.

A variety of interaction patterns have been introduced into Janus particles, including hydrophobic interaction, electrostatic interaction, supramolecular binding, etc. driving their self-assembly.[118]

Granick and coworkers[128] have endeavored experimentally and by simulation to investigate the self-assembly of micron-sized colloids. For example, they synthesized dipolar Janus particles, which carry opposite electric charge on the two hemispheres of each particle. Using carboxylate-modified polystyrene colloids, one hemisphere was coated with a thin layer of gold, which was then treated with amine terminated thiols. In this way, colloids carry opposite charge on two hemispheres, rendered by untreated carboxylate and amine group, respectively. Triggered by

electrostatic attraction (Debye screening length was set below 10 nm), a series of clusters with different structures were obtained, which quantitatively agree with computed structures. Rather than clusters, Suzuki et al.[125] observed string structures by using dipolar microgels with carboxyl groups on one hemisphere and amino groups on the other (vide supra). At pH 4.0, such microgels carried opposite charge on each hemisphere forming a large dipole, therefore triggering the formation of aggregates with string structure.

Granick and coworkers[129] also studied self-assembly behavior of amphiphilic particles, of which one side is hydrophobic and the other side is charged, thus generating anisotropy. Interestingly, the self-assembled clusters show a strong dependence on ionic strength. In DI water, due to strong electrostatic repulsion, Janus particles remain separate, but when Debye screening length falls to 10 nm in the solution, appreciable aggregation was observed, forming clusters. When the ionic strength of the solution is further increased, lower ordered clusters aggregated into extended, branched, wormlike superstructures.

Supramolecular chemistry has in addition been employed to achieve self-assembly of Janus particles. Maye et al.[130] demonstrated self-assembly of Janus nanoclusters driven by DNA hybridization. In this report, ssDNA modified gold nanoparticles were immobilized onto paramagnetic beads that were coated with complementary ssDNA. Introducing a second nanoparticle modified with suitable ssDNA, Janus nanoclusters can be fabricated and finally released from the paramagnetic bead support by adding another ssDNA that has energetically more favorable hybridization.

1.5 The Scope of this Dissertation

The motivation of this dissertation is to explore the applications of model lipid membranes in artificial photosynthesis and self-assembly. We focus mainly on solid supported lipid bilayers, small unilamellar vesicles, and giant liposomes.

In Chapter 2, we demonstrate two-tier lipid nanoassemblies to mimic photosynthesis of green sulfur bacteria. Two-tier lipid nanoassemblies consist of a liposome layer electrostatically held on a solid supported lipid bilayer. Specifically, we prepared liposomes mainly composed of DPPC. Wired to an ITO electrode, photoaction spectrum is recorded. We further demonstrated that photoconversion efficiency is greatly enhanced by incorporation of cholesterol into DPPC liposomes. UV-Vis absorption spectroscopy, fluorescence spectroscopy, transient absorption spectroscopy, atomic force microscopy, scanning electron microscopy, and confocal microscopy were performed to characterize such lipid supercomplexes and elucidate the role of cholesterol in the system.

In Chapter 3, we expand the work to study the effect of lipid phases on photo-to-electrochemical conversion. To this end, we built photosynthetic mimics using the same approach as in chapter 2. Instead of using DPPC as the main component, herein we employed POPC and DPPE, as the main lipids in the two new mimics, respectively. To comprehend the photokinetics of such mimics, UV-Vis absorption spectroscopy, fluorescence spectroscopy, transient absorption spectroscopy, atomic force microscopy, and confocal microscopy were carried out.

Chapter 4 reports the synthesis and characterization of various Janus-like liposomes including zwitterionic, anionic, cationic and biotinylated liposomes. Symmetry of liposomes is broken by cholesterol-induced phase separation.

We report the self-assembly of biotinylated Janus-like liposomes via biotin-avidin interaction in Chapter 5. Taking advantage of cholesterol-induced phase separation, biotinylated lipid can be regio-selectively doped into liposomes. Thanks to the resulting anisotropic property of liposomes, well-controlled chain-like aggregates were formed.

We demonstrate in Chapter 6 the self-assembly of charged liposomes. Two mechanisms are used to drive self-assembly, including electrostatic interaction between oppositely charged giant liposomes, and between oppositely charged giant liposomes and SUVs.

References

1. Tamm, L. K.; McConnell, H. M. Supported Phospholipid Bilayers. *Biophys. J*. **1985**, *47*, 105-113.
2. Beyer, D.; Elender, G.; Knoll, W.; Kuhner, M.; Maus, S; Ringsdorf, H.; Sackmann, E. Influence of Anchor Lipids on the Homogeneity and Mobility of Lipid Bilayers on Thin Polymer Films. *Angew. Chem. Int. Ed.* **1996**, *35*, 1682-1685.
3. Bunjes, N.; Schmidt, E.K.; Jonczyk, A.; Rippmann, F.; Beyer, D.; Ringsdorf, H.; Graber, P.; Knoll, W.; Naumann, R. Thiopeptide-Supported Lipid Layers on Solid Substrates. *Langmuir* **1997**, *13*, 6188-6194.
4. Salamon, Z.; Wang, Y.; Tollin, G.; Macleod, H. A. Assembly and Molecular Organization of Self-Assembled Lipid Bilayers on Solid Substrates Monitored by Surface Plasmon Resonance Spectroscopy. *Biochim. Biophys. Acta Biomembranes* **1994**, *1195*, 267-275.
5. Puu, G.; Gustafson, I. Planar Lipid Bilayers on Solid Supports from Liposomes – Factors of Importance for Kinetics and Stability. *Biochim. Biophys. Acta Biomembranes* **1997**, *1327*, 149-161.

6. New, R. R. C. Liposomes: A Practical Approach; IRL Press: Oxford, U.K., **1990**.
7. Castellana, E. T.; Cremer, P. S. Solid Supported Lipid Bilayers: From Biophysical Studies to Sensor Design. *Surf. Sci. Rep*. **2006**, *61*, 429-444.
8. Iglič, A.; Kulkarni, C. V.; Tien, H. T.; Liu, A. L. Advances in Planar Lipid Bilayers and Liposomes, Volume 18, 1st Edition. Academic Press, 2013.
9. Weber, T; Zemelman, B. V.; McNew, J. A.; Westermann, B.; Gmachl, M.; Parlati, F.; Söllner, T. H.; Rothman, J. E. SNAREpins: Minimal Machinery for Membrane Fusion. *Cell* **1998**, *92*, 759-772.
10. Rizo. J.; Chen, X.; Arac, D. Unraveling the Mechanisms of Synaptotagmin and SNARE Function in Neurotransmitter Release. *Trends Cell Biol*. **2006**, *16*, 339-350.
11. Smith, A. W. Lipid-Protein Interactions in Biological Membranes: A Dynamic Perspective. *Biochim. Biophys. Acta-Biomembranes* **2012**, *1818*, 172-177.
12. Plant, A. L. Supported Hybrid Bilayer Membranes as Rugged Cell Membrane Mimics. *Langmuir* **1999**, *15*, 5128-5135
13. Torchilin, V. P. Recent Advances with Liposomes as Pharmaceutical Carriers. *Nat. Rev. Drug Discov*. **2005**, *4*, 145-160.
14. Sakurai, F.; Inoue, R.; Nishino, Y.; Okuda, A.; Matsumoto, O.; Taga, T.; Yamashita, F.; Takakura, Y. Effect of DNA/Liposome Mixing Ratio on the Physicochemical Characteristics, Cellular Uptake and Intracellular Trafficking of Plasmid DNA/Cationic Liposome Complexes and Subsequent Gene Expression. *J. Control. Release* **2000**, *66*, 255-269.
15. Jesorka, A.; Orwar, O. Liposomes: Technologies and Analytical Applications. *Annu. Rev. Anal. Chem*. **2008**, *1*, 801-832.

16. Ford, W. E.; Otvos, J. W.; Calvin, M. Photosensitized Electron Transport across Lipid Vesicle Walls - Quantum Yield Dependence on Sensitizer Concentration. *Proc. Natl. Acad. Sci. U. S. A.* **1979**, *76*, 3590-3593.
17. Steinberg-Yfrach, G.; Liddell, P. A.; Hung, S-C.; Moore, A.; Gust, D.; Moore, T. A. Conversion of Light Energy to Proton Potential in Liposomes by Artificial Photosynthetic Reaction Centres. *Nature* **1997**, *385*, 239-241.
18. Steinberg-Yfrach, G.; Rigaud, J. L.; Durantini, E. N.; Moore, A. L.; Gust, D.; Moore, T. A. Light-Driven Production of ATP Catalysed by F0F1-ATP Synthase in an Artificial Photosynthetic Membrane. *Nature* **1998**, *392*, 479−482.
19. Liu, Q.; Boyd, B. J. Liposomes in Biosensors. *Analyst* **2013**, *138*, 391-409.
20. Menger, F. M.; Angelova, M. I. Giant Vesicles: Imitating the Cytological Processes of Cell Membranes. *Acc. Chem. Res*. **1998**, *31*, 789-797.
21. Dimova, R.; Aranda, S.; Bezlyepkina, N.; Nikolov, V.; Riske, K. A.; Lipowsky, R. A Practical Guide to Giant Vesicles. Probing the Membrane Nanoregime via Optical Microscopy. *J. Phys. Condens. Matter* **2006**, *18*, S1151-S1176.
22. Hotani, H.; Nomura, F.; Suzuki, Y. Giant Liposomes: from Membrane Dynamics to Cell Morphogenesis. *Curr. Opin. Colloid Interface Sci*. **1999**, *4*, 358-368.
23. Reeves, J. P.; Dowben, R. M. Formation and Properties of Thin-Walled Phospholipid Vesicles. *J. Cell. Physio*. **1969**, *73*, 49-60.
24. Akashi, K.; Miyata, H.; Itoh, H.; Kinosita, K. Preparation of Giant Liposomes in Physiological Conditions and Their Characterization under an Optical Microscope. *Biophys. J*. **1996**, *71*, 3242-3250.

25. Yamashita, Y.; Oka, M.; Tanaka, T.; Yamazaki, M. A New Method for the Preparation of Giant Liposomes in High Salt Concentrations and Growth of Protein Microcrystals in Them. *Biochim. Biophys. Acta* **2002**, *1561*, 129-134.
26. D'Onofrio, T. G.; Hatzor, A.; Counterman, A. E.; Heetderks, J. J.; Sandel, M. J.; Weiss, P. S. Controlling and Measuring the Interdependence of Local Properties in Biomembranes. *Langmuir* **2003**, *19*, 1618-1623.
27. Angelova, M. I.; Dimitrov, D. S. Liposome Electroformation. *Faraday Discussions of the Chemical Society* **1986**, *81*, 303-311.
28. Estes, D. J.; Mayer, M. Electroformation of Giant Liposomes from Spin-Coated Films of Lipids. *Colloids Surf. B* **2005**, *42*, 115-123.
29. Menger, F. M.; Seredyuk, V. A. Internally Catalyzed Separation of Adhered Lipid Membranes. *J. Am. Chem. Soc*. **2003**, *125*, 11800-11801.
30. Pautot, S.; Frisken, B. J.; Weitz, D. A. Production of Unilamellar Vesicles Using an Inverted Emulsion. *Langmuir* **2003**, *19*, 2870-2879.
31. Pautot, S.; Frisken, B. J.; Weitz, D. A. Engineering asymmetric vesicles. *Proc. Natl. Acad. Sci. U. S. A.* **2003**, *100*, 10718-10721.
32. Horger, K. S.; Estes, D. J.; Capone, R.; Mayer, M. Films of Agarose Enable Rapid Formation of Giant Liposomes in Solutions of Physiologic Ionic Strength. *J. Am. Chem. Soc*. **2009**, *131*, 1810-1819.
33. Weinberger, A.; Tsai, F.-C.; Koenderink, G. H.; Schmidt, T. H.; Itri, R.; Meier, W.; Schmatko, T.; Schröder, A.; Marques, C. Gel-Assisted Formation of Giant Unilamellar Vesicles. *Biophys. J*. **2013**, *105*, 154-164.

34. Wallach, D. F. H. Lipid Vesicles Formed of Surfactants and Steroids. US patent. US4917951 A

35. Mueller, P.; Rudin, D. O.; Tien, H. T.; Wescott, W. C. Methods for the Formation of Single Bimolecular Lipid Membranes in Aqueous Solution. *J. Phys. Chem*. **1963**, *67*, 534-535.

36. Mueller, P.; Rudin, D. O.; Tien, H. I.; Wescott, W. C. Reconstitution of Cell Membrane Structure in Vitro and Its Transformation into an Excitable System. *Nature* **1962**, *194*, 979-980.

37. Wang, M.; Zhan, W. Mimicking Photosynthesis with Electrode-Supported Lipid Nanoassemblies. *Acc. Chem. Res*. **2016**, *49*, 2551-2559.

38. Sugihara, K.; Vörös, J.; Zambelli, T. A Gigaseal Obtained with a Self-Assembled Long-Lifetime Lipid Bilayer on a Single Polyelectrolyte Multilayer Filled Nanopore. *ACS Nano* **2010**, *4*, 5047-5054.

39. Richter, R. P.; Bérat, R.; Brisson, A. R. Formation of Solid-Supported Lipid Bilayers: An Integrated View. *Langmuir* **2006**, *22*, 3497-3505.

40. Wang, L.; Roth, J. S.; Han, X.; Evans, S. D. Photosynthetic Proteins in Supported Lipid Bilayers: Towards a Biokleptic Approach for Energy Capture. *Small* **2015**, *11*, 3306-3318.

41. Tanaka, M.; Sackmann, E. Polymer-Supported Membranes as Models of the Cell Surface. *Nature* **2005**, *437*, 656-663.

42. Nikoleli, G. P. ; Nikolelis, D. P. ; Evtugyn, G ; Hianik, T. Advances in Lipid Film Based Biosensors. TrAC. **2016**, *79*, 210-221.

43. Reviakine, I.; Brisson, A. Streptavidin 2D Crystals on Supported Phospholipid Bilayers: Toward Constructing Anchored Phospholipid Bilayers. *Langmuir* **2001**, *17*, 8293-8299.

44. Larsson, C.; Rodahl, M.; Höök, F. Characterization of DNA Immobilization and Subsequent Hybridization on a 2D Arrangement of Streptavidin on a Biotin-Modified Lipid Bilayer Supported on SiO_2. *Anal. Chem.* **2003**, *75*, 5080-5087.

45. Brian, A. A.; McConnell, H. M. *Proc. Natl. Acad. Sci. U. S. A.* **1984**, *81*, 6159-6163.

46. Lenz, P.; Ajo-Franklin, C. M.; Boxer, S. G. Patterned Supported Lipid Bilayers and Monolayers on Poly(dimethylsiloxane). *Langmuir* **2004**, *20*, 11092-11099.

47. Zhan, W.; Jiang, K. A Modular Photocurrent Generation System Based on Phospholipid-Assembled Fullerenes. *Langmuir* **2008**, *24*, 13258-13261.

48. Silin, V. I.; Wieder, H.; Woodward, J. T.; Valincius, G.; Offenhausser, A.; Plant, A. L. The Role of Surface Free Energy on the Formation of Hybrid Bilayer Membranes. *J. Am. Chem. Soc*. **2002**, *124*, 14676-14683.

49. Terrettaz, S.; Mayer, M.; Vogel, H. Highly Electrically Insulating Tethered Lipid Bilayers for Probing the Function of Ion Channel Proteins. *Langmuir* **2003**, *19*, 5567-5569.

50. Jiang, K.; Xie, H.; Zhan, W. Photocurrent Generation from $Ru(bpy)_3^{2+}$ Immobilized on Phospholipid/Alkanethiol Hybrid Bilayers. *Langmuir* **2009,** *25*, 11129-11136.

51. Purrucker, O.; Förtig, A.; Jordan, R.; Tanaka, M. Supported Membranes with Well-Defined Polymer Tethers-Incorporation of Cell Receptors. *ChemPhysChem*. **2004**, *5*, 327-335.

52. Zhan, W.; Jiang, K.; Smith, M. D.; Bostic, H. E.; Best, M.; Auad, M. L.; Ruppel, J. V.; Kim, C.; Zhang, X. P. Photocurrent Generation from Porphyrin/Fullerene Complexes Assembled in a Tethered Lipid Bilayer. *Langmuir* **2010**, *26*, 15671-15679.

53. Reviakine, I.; Simon, A.; Brisson, A. Effect of Ca^{2+} on the Morphology of Mixed DPPC-DOPS Supported Phospholipid Bilayers. *Langmuir* **2000**, *16*, 1473-1477.

54. Schneider, J.; Dufrêne, Y. F.; Barger, W. R., Jr.; Lee, G. U. Atomic Force Microscope Image Contrast Mechanisms on Supported Lipid Bilayers. *Biophys. J.* **2000**, *79*, 1107-1118.

55. Parthasarathy, R.; Groves, J. T. Protein Patterns at Lipid Bilayer Junctions. *Proc. Natl. Acad. Sci. U. S. A.* **2004**, *101*, 12798-12803.

56. Fix, M.; Melia, T. J.; Jaiswal, J. K.; Rappoport, J. Z.; You, D.; Söllner, T. H.; Rothman, J. E.; Simon, S. M. Imaging Single Membrane Fusion Events Mediated by SNARE Proteins. *Proc. Natl. Acad. Sci. U. S. A.* **2004**, *101*,7311-7316.

57. Andree, H. A. M.; Stuart, M. C. A.; Hermens, W. T.; Reutelingsperger, C. P. M.; Hemker, H. C.; Frederik, P. M.; Willems, G. M. Clustering of Lipid-bound Annexin V May Explain Its Anticoagulant Effect. *J. Biol. Chem*. **1992**, *267*, 17907-17912.

58. Richter, R. P.; Mukhopadhyay, A.; Brisson, A. Pathways of Lipid Vesicle Deposition on Solid Surfaces: A Combined QCM-D and AFM Study. *Biophys. J.* **2003**, *85*, 3035-3047.

59. Lind, T. K.; Cárdenas, M.; Wacklin, H. P. Formation of Supported Lipid Bilayers by Vesicle Fusion: Effect of Deposition Temperature. *Langmuir* **2014**, *30*, 7259-7263.

60. Morigaki, K.; Tawa, K. Vesicle Fusion Studied by Surface Plasmon Resonance and Surface Plasmon Fluorescence Spectroscopy. *Biophys. J*. **2006**, *91*, 1380-1387.

61. Zheng, Z.,; Stroumpoulis, D.; Parra, A.; Petzold, L.; Tirrell, M. A Monte Carlo Simulation Study of Lipid Bilayer Formation on Hydrophilic Substrates from Vesicle Solutions. *J. Chem. Phys*. **2006**, *126*, 064904.

62. Plant, A. L. Self-Assembled Phospholipid/Alkanethiol Biomimetic Bilayers on Gold. *Langmuir* **1993**, *9*, 2764-2767.

63. Meuse, C. W.; Krueger, S.; Majkrzak, C. F.; Dura, J. A.; Fu, J.; Connor, J. T.; Plant, A. L. Hybrid Bilayer Membranes in Air and Water: Infrared Spectroscopy and Neutron Reflectivity Studies. *Biophys. J*. **1998**, *74*, 1388-1398.

64. Plant, A. L.; Brighamburke, M.; Petrella, E. C.; Oshannessy, D. J. Phospholipid/Alkanethiol Bilayers for Cell-Surface Receptor Studies by Surface Plasmon Resonance. *Anal. Biochem*. **1995**, 226, 342-348.

65. Meuse, C. W.; Niaura, G.; Lewis, M. L.; Plant, A. L. Assessing the Molecular Structure of Alkanethiol Monolayers in Hybrid Bilayer Membranes with Vibrational Spectroscopies. *Langmuir* **1998**, *14*, 1604-1611.

66. Kastl, K.; Ross, M.; Gerke, V.; Steinem, C. Kinetics and Thermodynamics of Annexin A1 Binding to Solid-Supported Membranes: A QCM Study. *Biochemistry* **2002**, *41*, 10087-10094.

67. Favero, G.; Campanella, L.; Cavallo, S.; D'Annibale, A.; Perrella, M.; Mattei, E.; Ferri, T. Glutamate Receptor Incorporated in a Mixed Hybrid Bilayer Lipid Membrane Array, as a Sensing Element of a Biosensor Working under Flowing Conditions. *J. Am. Chem. Soc*. **2005**, *127*, 8103-8111.

68. Schiller, S. M.; Naumann, R.; Lovejoy, K.; Kunz, H.; Knoll, W. Archaea Analogue Thiolipids for Tethered Bilayer Lipid Membranes on Ultrasmooth Gold Surfaces. *Angew. Chem. Int. Ed*. **2003**, *42*, 208-211.

69. Naumann, R.; Schiller, S. M.; Giess, F.; Grohe, B.; Hartman, K. B.; Kärcher, I.; Köper, I.; Lübben, J.; Vasilev, K.; Knoll, W. Tethered Lipid Bilayers on Ultraflat Gold Surfaces. *Langmuir* **2003**, *19*, 5435-5443.

70. Giess, F.; Friedrich, M. G.; Heberle, J.; Naumann, R. L. Knoll, W. The Protein-Tethered Lipid Bilayer: A Novel Mimic of the Biological Membrane. *Biophys. J.* **2004**, *87*, 3213-3220.

71. Chan, Y. M.; Boxer, S. G. Model Membrane Systems and Their Applications. *Curr. Opin. Chem. Biol*. **2007**, *11*, 1-7.

72. Yoshina-Ishii, C.; Boxer, S. G. Arrays of Mobile Tethered Vesicles on Supported Lipid Bilayers. *J. Am. Chem. Soc*. **2003**, *125*, 3696-3697.

73. Boukobza, E.; Sonnenfeld, A.; Haran, G. Immobilization in Surface-Tethered Lipid Vesicles as a New Tool for Single Biomolecule Spectroscopy. *J. Phys. Chem. B* **2001**, *105*, 12165-12170.

74. Chan, Y. M.; Lenz, P.; Boxer, S. G. Kinetics of DNA-Mediated Docking Reactions Between Vesicles Tethered to Supported Lipid Bilayers. *Proc. Natl. Acad. Sci. U. S. A.* **2007**, *104*, 18913-18918.

75. Collings, A. F.; Critchley, C. Artificial Photosynthesis: From Basic Biology to Industrial Application. Wiley-VCH Verlag GmbH, **2005**.

76. O'Regan, B.; Grätzel, M. A Low-Cost, High-Efficiency Solar Cell Based on Dye-Sensitized Colloidal TiO_2 Films. *Nature* **1991**, *353*, 737-740.

77. Kalyanasundaram, K.; Grätzel, M. Artificial Photosynthesis: Biomimetic Approaches to Solar Energy Conversion and Storage. *Curr. Opin. Biotechnol*. **2010**, *21*, 298-310.

78. Andreiadis, E. S.; Chavarot-Kerlidou, M.; Fontecave, M.; Artero, V. Artificial Photosynthesis: From Molecular Catalysts for Light-driven Water Splitting to Photoelectrochemical Cells. *Photochem. Photobio*. **2011**, *87*, 946-964.

79. Yerga, R. M. N.; Álvarez-Galván, M. C.; del Valle, F.; de la Mano, J. A. V.; Fierro, J. L. G. Water Splitting on Semiconductor Catalysts under Visible-Light Irradiation. *ChemSusChem*. **2009**, *2*, 471-485.

80. Carraro, M.; Sartorel, A.; Toma, F.; Puntoriero, F.; Scandola, F.; Campagna, S.; Prato, M.; Bonchio, M. Artificial Photosynthesis Challenges: Water Oxidation at Nanostructured Interfaces. *Top. Curr. Chem*. **2011**, *303*, 121-50.

81. Dubois, M. R.; Dubois, D. L. Development of Molecular Electrocatalysts for CO_2 Reduction and H_2 Production/Oxidation. *Acc. Chem. Res*. **2009**, *42*, 1974-1982.

82. Kunjapur, A. M.; Eldridge, R. B. Photobioreactor Design for Commercial Biofuel Production from Microalgae. *Ind. Eng. Chem. Res*. **2010**, *49*, 3516-3526.

83. Wasielewski, M. R. Photoinduced Electron Transfer in Supramolecular Systems for Artificial Photosynthesis. *Chem. Rev*. **1992**, *92*, 435-461.

84. Barber, J. Photosynthetic Energy Conversion: Natural and Artificial. *Chem. Soc. Rev*. **2009**, *38*, 185-196.

85. Osterloh, F. E. Inorganic Nanostructures for Photoelectrochemical and Photocatalytic Water Splitting. *Chem. Soc. Rev*. **2013**, *42*, 2294-2320.

86. Kärkäs, M. D.; Verho, O.; Johnston, E. V.; Åkermark, B. Artificial Photosynthesis: Molecular Systems for Catalytic Water Oxidation. *Chem. Rev*. **2014**, *114*, 11863-12001.

87. Tien, H. T. Photoelectric Effects in Thin and Bilayer Lipid Membranes in Aqueous Media. *J. Phys. Chem*. **1968**, *72*, 4512-4519.

88. Mangel, M. Properties of Liposomes That Contain Chloroplast Pigments: Photosensitivity and Efficiency of Energy Conversion. *Biochim. Biophys. Acta- Bioenergetics*. **1976**, *430*, 459-466.

89. Oostergetel, G. T.; van Amerongen, H.; Boekema E. J. The Chlorosome: A Prototype for Efficient Light Harvesting in Photosynthesis. *Photosyn. Res*. **2010**, *104*, 245-255.

90. Dostál, J.; Pšenčík, J.; Zigmantas, D. In Situ Mapping of the Energy Flow Through the Entire Photosynthetic Apparatus. *Nat. Chem*. **2016**, *8*, 705–710.

91. Gruszecki, W. I.; Grudzinski, W.; Banaszek-Glos, A.; Matula, M.; Kernen, P.; Krupa, Z.; Sielewiesiuk, J. Xanthophyll Pigments in Light-Harvesting Complex II in Monomolecular Layers: Localisation, Energy Transfer and Orientation. *Biochim. Biophys. Acta-Bioenergetics*. **1999**, *1412*, 173-183.

92. Sumino, A.; Dewa, T.; Kondo, M.; Morii, T.; Hashimoto, H.; Gardiner, Richard J. Cogdell, A. T.; Nango, M. Selective Assembly of Photosynthetic Antenna Proteins into a Domain-Structured Lipid Bilayer for the Construction of Artificial Photosynthetic Antenna Systems: Structural Analysis of the Assembly Using Surface Plasmon Resonance and Atomic Force Microscopy. *Langmuir* **2011**, *27*, 1092-1099.

93. Zapf, T.; Tan, C. D.; Reinelt, T.; Huber, C.; Shaohua, D.; Geifman-Shochat, S.; Paulsen, H.; Sinner, E. K. Synthesis and Functional Reconstitution of Light-Harvesting Complex II into Polymeric Membrane Architectures. *Angew. Chem. Int. Ed*. **2015**, *54*, 14664-14668.

94. Saboe, P. O.; Lubner, C. E.; McCool, N. S.; Vargas-Barbosa N. M.; Yan, H.; Chan, S.; Ferlez, B.; Bazan, G. C.; Golbeck, J. H.; Kumar, M. Two-Dimensional Protein Crystals for Solar Energy Conversion. *Adv. Mater*. **2014**, *26*, 7064-7069.

95. Bhosale, S.; Sisson, A. L.; Talukdar, P.; Fürstenberg, A.; Banerji, N.; Vauthey, E.; Bollot, G.; Mareda, J.; Röger, C.; Würthner, F.; Sakai, N.; Matile, S. Photoproduction of Proton Gradients with p-Stacked Fluorophore Scaffolds in Lipid Bilayers. *Science* **2006**, *313*, 84-86.

96. Sahin, T.; Harris, M. A.; Vairaprakash, P.; Niedzwiedzki, D. M.; Subramanian, V.; Shreve, A. P.; Bocian, D. F.; Holten, D.; Lindsey J. S. Self-Assembled Light-Harvesting System from Chromophores in Lipid Vesicles. *J. Phys. Chem. B* **2015**, *119*, 10231-10243.

97. Woller, J. G.; Hannestad, J. K.; Albinsson, B. Self-Assembled Nanoscale DNA-Porphyrin Complex for Artificial Light Harvesting. *J. Am. Chem. Soc*. **2013**, *135*, 2759-2768.

98. Hwang, K.; Mauzerall, D. Photoinduced Electron Transport Across a Lipid Bilayer Mediated by C70. *Nature* **1993**, *361*, 138-140

99. Baral, S.; Fendler, J. H. Cadmium Sulfide Mediated Photoelectric Effects in Bilayer Lipid Membranes. *J. Am. Chem. Soc*. **1989**, *111*, 1604-1614.

100. Rakovich, A.; Sukhanova, A.; Bouchonville, N.; Lukashev, E.; Oleinikov, V.; Artemyev, M.; Lesnyak, V.; Gaponik, N.; Molinari, M.; Troyon, M.; Rakovich, Y. P.; Donegan, J. F.; Nabiev, I. Resonance Energy Transfer Improves the Biological Function of Bacteriorhodopsin within a Hybrid Material Built from Purple Membranes and Semiconductor Quantum Dots. *Nano Lett*. **2010**, *10*, 2640-2648.

101. Lukashev E. P.; Knox P. P.; Gorokhov V. V.; Grishanova N. P.; Seifullina N. K.; Krikunova M.; Lokstein H.; Paschenko V. Z. Purple-Bacterial Photosynthetic Reaction Centers and Quantum-Dot Hybrid-Assemblies in Lecithin Liposomes and Thin Films. *J. Photochem. Photobio. B* **2016**, *164*,73-82.

102. Kudo, A.; Miseki, Y. Heterogeneous Photocatalyst Materials for Water Splitting. *Chem. Soc. Rev*. **2009**, *38*, 253-278.

103. Troppmann, S.; König, B. Functionalized Membranes for Photocatalytic Hydrogen Production. *Chem. Eur. J*. **2014**, *20*, 14570-14574.

104. Hansen, M.; Li, F.; Sun, L.; König, B. Photocatalytic Water Oxidation at Soft Interfaces. *Chem. Sci*. **2014**, *5*, 2683-2687.

105. Limburg, B.; Wermink, J.; van Nielen, S. S.; Kortlever, R.; Koper, M. T. M.; Bouwman, E.; Bonnet, S. Kinetics of Photocatalytic Water Oxidation at Liposomes: Membrane Anchoring Stabilizes the Photosensitizer. *ACS Catal*. **2016**, *6*, 5968-5977.

106. Xie, H.; Jiang, K.; Zhan, W. A Modular Molecular Photovoltaic System Based on Phospholipid/Alkanethiol Hybrid Bilayers: Photocurrent Generation and Modulation. *Phys. Chem. Chem. Phys*. **2011**, *13*, 17712-17721.

107. Sperelakis, N. Cell Physiology Source Book: Essentials of Membrane Biophysics. Academic Press. **2011**.

108. Ma, Y.; Ghosh, S. K.; DiLena, D. A.; Bera, S.; Lurio, L. B.; Parikh, A. N.; Sinha, S. K. Cholesterol Partition and Condensing Effect in Phase-Separated Ternary Mixture Lipid Multilayers. *Biophys. J*. **2016**, *110*, 1355-1366.

109. van Meer, G.; Voelker, D. R.; Feigenson, G. W. Membrane Lipids: Where They are and How They Behave. *Nat. Rev. Mol. Cell Biol*. **2008**, *9*, 112-124.

110. Hancock, J. F. Lipid Rafts: Contentious Only from Simplistic Standpoints. *Nat. Rev. Mol. Cell Biol*. **2006**, *7*, 456-462.

111. Meinhardta, S.; Vink, R. L. C.; Schmid, F. Monolayer Curvature Stabilizes Nanoscale Raft Domains in Mixed Lipid Bilayers. *Proc. Natl. Acad. Sci. U. S. A*. **2013**, *110*, 4476-4481.

112. Dietrich, C.; Bagatolli, L. A.; Volovyk, Z. N.; Thompson, N. L.; Levi, M.; Jacobson, K.; Gratton, L. A. Lipid Rafts Reconstituted in Model Membranes. *Biophys. J*. **2001**, *80*, 1417-1428.

113. Samsonov, A. V.; Mihalyov, I.; Cohen, F. S. Characterization of Cholesterol-Sphingomyelin Domains and Their Dynamics in Bilayer Membranes. *Biophys. J*. **2001**, *81*, 1486-1500.

114. Veatch, S. L.; Keller, S. L. Lateral Organization in Lipid Membranes Containing Cholesterol. *Phys. Rev. Lett*. **2002**, *89*, 268101.

115. Veatch, S. L.; Keller, S. L. Separation of Liquid Phases in Giant Vesicles of Ternary Mixtures of Phospholipids and Cholesterol. *Biophys. J*. **2003**, *85*, 3074-3083.

116. Marsh, D. Cholesterol-Induced Fluid Membrane Domains: A Compendium of Lipid-Raft Ternary Phase Diagrams. *Biochim. Biophys. Acta*. **2009**, *1788*, 2114-2123.

117. Klymchenko, A. S.; Kreder, R. Fluorescent Probes for Lipid Rafts: From Model Membranes to Living Cells. *Chem. Biol*. **2014**, *21*, 97-113.

118. Walther, A.; Müller, A. H. E. Janus Particles: Synthesis, Self-Assembly, Physical Properties, and Applications. *Chem. Rev*. **2013**, *113*, 5194-5261.

119. Hu, J.; Zhou, S.; Sun, Y.; Fang, X.; Wu, L. Fabrication, Properties and Applications of Janus Particles. *Chem. Soc. Rev*. **2012**, *41*, 4356-4378.

120. Loget, G.; Kuhn, A. Bulk Synthesis of Janus Objects and Asymmetric Patchy Particles. *J. Mater. Chem*. **2012**, *22*, 15457-15474.

121. Granick, S.; Jiang, S.; Chen, Q. Janus Particles. *Phys. Today* **2009**, *62*, 68-69.

122. Di Leonardo, R. Active Colloids: Controlled Collective Motions. *Nat. Mater*. **2016**, *15*, 1057-1058.

123. Tang, J. L.; Schoenwald, K.; Potter, D.; White, D.; Sulchek, T. Bifunctional Janus Microparticles with Spatially Segregated Proteins. *Langmuir* **2012**, *28*, 10033-10039.

124. Pickering, S. U. CXCVI.-Emulsions. *J. Chem. Soc. Trans*. **1907**, *91*, 2001-2021.

125. Suzuki, D.; Tsuji, S.; Kawaguchi, H. Janus Microgels Prepared by Surfactant-Free Pickering Emulsion-Based Modification and Their Self-Assembly. *J. Am. Chem. Soc*. **2007**, *129*, 8088-8089.

126. Nie, Z.; Petukhova, A.; Kumacheva, E. Properties and Emerging Applications of Self-Assembled Structures Made from Inorganic Nanoparticles. *Nat. Nanotechnol.* **2010**, *5*, 15-25.

127. Phillips, M. J.; Voeltz, G. K. Structure and function of ER membrane contact sites with other organelles. *Nat. Rev. Mol. Cell Biol*. **2016**, *17*, 69-82.

128. Hong, L.; Cacciuto, A.; Luijten, E.; Granick, S. Clusters of Charged Janus Spheres. *Nano Lett*. **2006**, *6*, 2510-2514.

129. Hong, L.; Cacciuto, A.; Luijten, E.; Granick, S. Clusters of amphiphilic colloidal spheres. *Langmuir* **2008**, *24*, 621-625.

130. Maye, M. M.; Nykypanchuk, D.; Cuisinier, M.; van der Lelie, D.; Gang, Q. Stepwise Surface Encoding for High-Throughput Assembly of Nanoclusters. *Nat. Mater*. **2009**, *8*, 388-391.

Chapter 2

Mimicking Photosynthesis with Supercomplexed Lipid Nanoassemblies: Design, Performance, and Enhancement Role of Cholesterol*

2.1 Introduction

The grand scale and harmonious blend of efficiency and sustainability make natural photosynthesis an inexhaustible source for us to learn and develop new approaches to effective solar energy utilization. Although the components and architectures involved in the photosynthetic apparatus vary rather greatly among different species, a general operating scheme exists,[1-3] in which lipid membrane-bound proteins assemble various pigments and cofactors mostly noncovalently to carry out coordinated energy and charge transfer at specific locations. Through these supercomplexed cross-membrane networks, the harvested light energy is directionally funneled to the charge-separation sites, and the subsequent electron transfer is coupled, for example, in the case of green plants, to proton translocation across lipid membranes to build up proton motive force for biochemical fuel production. To construct robust biomimetic systems following these design principles, however, one immediately faces what may be called the protein paradox. On one hand, a protein-free system is desirable because photosynthetic proteins are fragile and unattainable synthetically, which unfortunately often leads to function loss and compromised performance. To start to address this fundamental issue, we report here a new

*This chapter is copied from a published paper (*Langmuir* **2016**, *32*, 7326-7338) with minor modification.

protein-free, hybrid mimetic strategy that relies on supercomplexed lipid nanoassemblies to organize small organic species for coordinated light harvesting, energy/electron transfer, and photo-to-electrochemical energy conversion. Owing to their biological significance and versatility in molecular assembling, several lipid structures including liposomes (vesicles)[4,5] and lipid bilayers[6,7] have been actively used to mimic various aspects of natural photosynthesis.[8] Herein, we demonstrate that these lipid building blocks can be further assembled into higher-order architectures to mimic several key processes in photosynthesis with promising efficiency.

One natural system that we have drawn particular inspiration from is green sulfur bacteria (GSB),[9,10] which are anoxygenic photosynthetic bacteria that have evolved a relatively simple architecture to survive extremely low light conditions. To maximally capture the limited photons available, GSB have developed the largest light-harvesting complex in nature, that is, the chlorosomes,[11,12] each typically containing >200,000 bacteriochlorophylls (BChls) and carotenoids self-assembled into multilamellar tubular aggregates that are wrapped in a monolayer of chlorosome proteins and lipids (Figure 2.1A). Within these aggregates, the BChls display a Q_y absorption maximum at 740-750 nm. A quasi-crystalline region called baseplate[13] (Figure 2.1B) forms within the monolayer sheath of the chlorosome, which further connects the chlorosome with another photosynthetic component, the Fenna−Matthews−Olson (FMO) protein[14] (Figure 1C), at the bottom. The baseplate primarily comprises protein CmsA and BChl a and has a λmax (Qy) at 790−800 nm, whereas BChls in the FMO complex exhibit peak absorption at ∼815 nm.[15] The FMO proteins are aqueous-exposed trimers that affix the reaction center (RC, Figure 1D) complex typically by a 2:1 stoichiometry.[16] Together, this four-tier architecture ensures the harvested light energy to be efficiently funneled through an energy transfer (ET) cascade:[10,11] chlorosomes →

baseplates→ FMO → RC, and only at the last stop is the light energy converted to electrochemical energy via charge separation and transfer.

Clearly, the success of a protein-free mimicking system depends on how well these sophisticated protein-enabled functions can be replaced or compensated, which, to the minimum, entails a structural scaffold that can organize all involved components into desired locations and facilitate directional energy and electron flows. In this work, we set to explore the potential of supercomplexed lipid nanostructures in filling these roles. Specifically, we have discovered a robust electronic communication between rhodamine and fullerene organized in these lipid nanoassemblies and cholesterol as a significant enhancer of the overall photoconversion efficiency. The structure, performance, and underlying enhancement mechanisms are investigated in detail.

2.2 Experimental Section

2.2.1 Chemicals

Lipids, including 1,2-dioleoyl-*sn*-glycero-3-phosphocholine (DOPC), 1,2-dioleoyl-3-trimethylammonium-propane (DOTAP), 1,2-dipalmitoyl-*sn*-glycero-3-phosphocholine (DPPC), 1,2-dipalmitoyl-*sn*-glycero-3-phospho-*rac*-(1-glycerol) sodium salt (DPPG), and 1,2-dipalmitoyl-*sn*-glycero-3-phosphoethanolamine-N-(lissamine rhodamine B sulfonyl) (ammonium salt) (Rho-DPPE), were purchased from Avanti Polar Lipids (Alabaster, AL). Paraformaldehyde and glutaraldehyde were obtained from Electron Microscopy Sciences (Hatfield, PA). Monomalonic fullerene C_{60} was synthesized according to a procedure described previously.[7] Other chemicals,

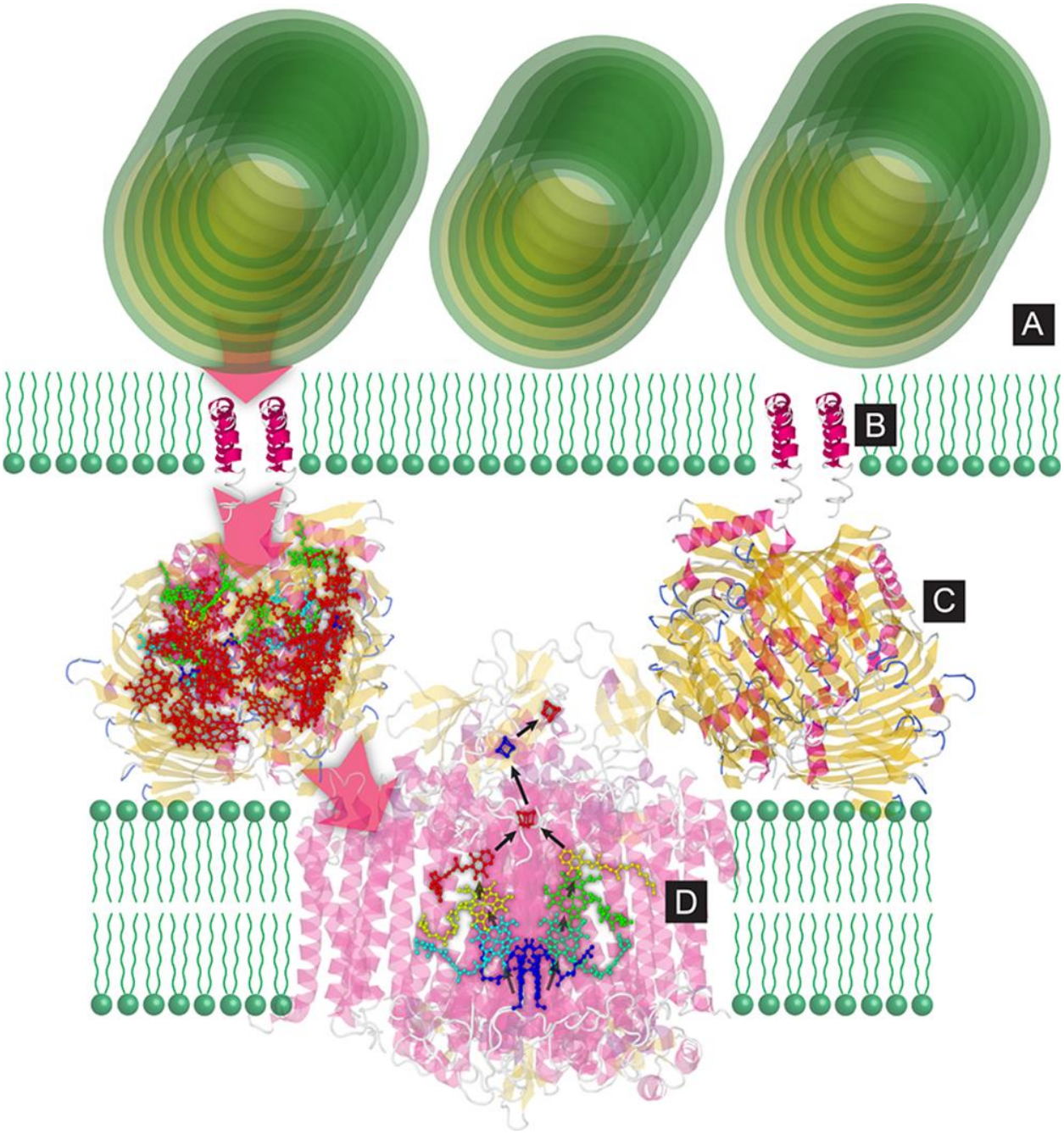

Figure 2.1 Organization of photosynthetic components in GSB. (A−D): the chlorosome (part), baseplate, FMO protein, and RC. Energy and electron flows are depicted by red and black arrows, respectively.

including cholesterol, 4-(2-hydroxyethyl) piperazine-1-ethanesulfonic acid (HEPES), (+)-sodium L-ascorbate, 1-dodecanethiol, D-(+)-glucose, glucose oxidase from Aspergillus niger, and catalase from bovine liver, were obtained from Sigma-Aldrich. All solutions employed in this work were prepared using 18.2 MΩ·cm deionized(DI) water (Millipore).

2.2.2 Formation of Two-Tier Lipid Nanoassemblies

The formation of a single lipid bilayer on glass or indium tin oxide (ITO)-coated substrates was achieved by lipid fusion using liposome solutions.[7] Before the exposure to liposome solutions, the substrates were first sonicated in acetone for 30 min and then boiled with base piranha solution ($NH_3 \cdot H_2O$/30% H_2O_2/DI water, 1:1:5, v/v) for another 30 min. These substrates were subsequently sonicated in DI water for 10 min, thoroughly rinsed with DI water, carefully dried with an argon stream, and then assembled in Teflon cells for further use.

The preparation of small unilamellar vesicles (SUVs) used throughout the entire study was carried out using an extrusion based method.[7] To start, appropriate quantities of lipids dissolved in chloroform were combined into a 50 mL round-bottom flask and thoroughly dried by rotary evaporation. The resulting thin lipid film on the flask wall was then rehydrated with HEPES buffer (10 mM HEPES, 100 mM NaCl, pH 7.70) by 1 h sonication at a temperature at least 10 °C above the phase transition temperatures (T_m) of the involved lipids. Such lipid suspensions were then extruded consecutively through polycarbonate membranes with 400 and 80 nm pores (Nuclepore, Whatman), again above their T_m. The final concentration of the as-prepared liposomes is typically ~2.5 mM. For the preparation of liposomes containing fullerene, membranes of 400 and 200 nm pore sizes were used instead.

To form a lipid bilayer on glass or ITO-coated glass substrates, a 300 μL thus-prepared liposome solution composed of 5% C_{60}, 20% DOTAP, and 75% DOPC (in mole fraction) was gently laid on a freshly cleaned substrate and incubated for 2 h. After that, the unbound liposome was removed by thorough buffer exchange (10 mM HEPES, 100 mM NaCl, pH 7.70). To assemble an additional layer of liposomes onto the above-described cationic lipid bilayer, 200 μL of anionic liposomes (Rho-DPPE/DPPG/DPPC, 5/15/80, or, Rho-DPPE/DPPG/cholesterol/DPPC, 5/15/30/50, in mole fraction) was added into the Teflon cell housing the lipid bilayer and incubated for 1 h. The unattached liposomes were similarly removed from the cell by exchanging with HEPES buffer.

To ensure reproducibility, all subsequent measurements of these two-layer lipid nanoassemblies were conducted on the same day of their preparation.

2.2.3 Fluorescence Microscopy

Fluorescence images of lipid samples deposited on glass substrates were collected on a Nikon A1+/MP confocal scanning laser (561 nm) microscope (Nikon Instruments, Inc., Melville, NY) together with a 595 ± 25 nm emission filter.

2.2.4 Spectroscopy

Absorption spectra of liposome samples containing Rho-DPPE were acquired on a UV-Vis spectrophotometer (Cary 50 Bio, Varian). Steady-state fluorescence spectroscopy data of the two-tier lipid nanoassemblies formed on glass substrates were recorded using a PI Acton spectrometer (SpectraPro SP 2356, Acton, NJ) connected to the side port of an epifluorescence microscope (Nikon TE-2000 U, Japan). The fluorescence signal was recorded using a charge-

coupled device (CCD) camera (PI Acton PIXIS: 400B, Acton, NJ) attached to the spectrometer. The excitation was provided by a mercury lamp (X-Cite 120, EXFO, Ontario, Canada) filtered at 475 ±20 nm; and a long-pass filter with a cutoff wavelength of 561 nm was used for emission. The obtained spectra are not corrected for distortions due to spectral nonuniformity associated with the filters and CCD camera, which are expected to be small.

Fluorescence lifetimes of rhodamines either suspended in buffer solutions or assembled in the two-tier lipid nanoassemblies were measured using a time-correlated single-photon counting system, which comprises a synchronizer/analyzer (PicoHarp 300, PicoQuant, Germany), a picosecond pulsed diode laser (PDL 800-B, wavelength: 405 nm), and a single-photon counting module (PDM Series, Micro Photon Devices, Italy) with timing resolution lower than 50 ps full width at half maximum. In the former case, a quartz fluorometer cell (Sub Micro type, Starna Cells, CA) was used to hold liposome solutions; the final rhodamine concentration in all samples was controlled to be ~0.5 μM. To be able to capture fluorescence signals emitted directly from the lipid nanoassemblies, this system was further coupled to a fluorescence microscope (Nikon TE-2000U), in which both the laser head and the photon counting module were directly mounted onto the microscope and optically aligned. All lipid samples were formed on glass substrates (Corning, Micro Slide 2947), in which all bottom lipid bilayers contain DOPC/DOTAP in an 80/20 mixing ratio with/without five additional fractions of C_{60}. Throughout the measurements, the laser head was operated at a repetition rate of 10 MHz. According to the manufacturer, this laser produces a minimum pulse width of 59 ps and a power of 29 pJ/pulse. All lifetime data were fitted by the exponential-tail fit method included in the fitting software package, FluoFit (PicoQuant, Germany). Oxygen was removed from all media by purging argon for at least 30 min right before the fluorescence measurements.

Transient absorption (TA) spectra were recorded with a pump−probe spectrometer based on a regenerative amplified titanium-sapphire laser system (Coherent Legend, 800 nm, 150 fs, 2.5 mJ/pulse, and 1 kHz repetition rate). Liposome samples with a total lipid concentration of ~2.5 mM in HEPES buffer (10 mM HEPES, 100 mM NaCl, pH 7.70) were excited using a pump pulse with a center wavelength of 515 nm obtained by sum frequency generation of the signal from an optical parametric amplifier (Opera, Coherent) and a small portion of (~7%) 800 nm output in a BBO crystal. The absorption variations were probed with a white light continuum from 430 to 750 nm generated by attenuating and focusing an 800 nm pulse into a 1 mm thick sapphire window. The pump and probe beam diameters at the sample were 300 and 150 μm, respectively. The probe beam after passing the sample was collimated and focused into a fiber optics-coupled multichannel spectrometer with complementary metaloxide semiconductor (CMOS) sensors and detected at a frequency of 1 kHz. The pump beam was chopped with a synchronized chopper to 500 Hz. The changes in absorbance for the pumped and unpumped samples were calculated. Cuvettes of 1 mm path length were used for all spectroscopy measurements. The instrument response function (IRF) of this system was measured to be ~150 fs by measuring solvent responses under the same experimental conditions.

2.2.5 Atomic Force Microscopy (AFM)

The AFM images were obtained either in tapping mode in air on a Veeco atomic force microscope (Dimension 3000) or in a fluid using a Bruker MultiMode 8 atomic force microscope (Bruker, USA) operated in the PeakForce quantitative nanomechanical mapping (PeakForce QNM) mode. In the former measurements, etched Si tips (FM-20, Nanoworld) with a force constant of 2.8 N/m and resonance frequency of 75 kHz were used. The tip scanning was operated

at 2 Hz. In-fluid measurements were carried out with two silicon nitride probes (Models: ScanAsyst Fluid, Bruker, 0.7 N/m, 20 nm tip radius; DNP S10, Bruker, 0.24-0.35 N/m, 10 nm tip radius) at a scan rate of 1 Hz and a resolution of 512 pixels × 512 pixels.

To prepare lipid assemblies suitable for in-air AFM scanning, a modified assembling procedure was followed. First, an alkanethiol self-assembled monolayer (SAM)/lipid hybrid bilayer17 formed on 10 nm gold-coated glass slides (Sigma-Aldrich) was used as the base layer. To start, these slides were treated with a piranha solution (concentrated H_2SO_4 to 30% H_2O_2, 3/1, v/v) for 3 min, thoroughly rinsed with DI water, dried under argon, and were then incubated in 1 mM 1- dodecanethiol in ethanol overnight. The excess thiol was removed by rinsing the substrate with ethanol and DI water and finally dried with argon. To form the hybrid bilayer, a liposome solution (DOTAP/DOPC, 2/8 in mole fraction) of suitable concentration was added onto the SAM and incubated for 2 h. The unbound liposomes were removed. To afford the final two-layer lipid structure, an anionic liposome (10% DOPC/20% DPPG/70% DPPC, in mole fraction) was added onto the hybrid bilayer and incubated for 1 h. The unattached liposomes were once again removed by thorough buffer exchange. To further stabilize the final lipid assemblies, thus-prepared samples were fixed in a mixture of 4% paraformaldehyde and 1% glutaraldehyde in DI water for 1 h. The fixative solution was subsequently exchanged out by DI water. Right before an AFM measurement, the remaining water covering the lipid complexes was gently blotted away with a paper towel.

Lipid samples probed in a fluid were prepared on glass substrates, similar to the procedure described above. Briefly, glass cover slides (Corning, USA) were first sonicated in acetone for 5 min, rinsed with DI water, and then boiled in the base piranha solution ($NH_3 \cdot H_2O$/30% H_2O_2/DI water, 1:1:5, v/v) for 30 min. After being rinsed with DI water again and dried with nitrogen, these

glass substrates were mounted onto the magnetic sample support disks of the microscope with a double-sided adhesive tape. From there, the first cationic lipid bilayer on glass was prepared by adding a suitable amount of DOTAP/DOPC liposome solution (2/8, in mole fraction) onto the glass substrate followed by a 2 h incubation. After the removal of the unbound liposomes, the resulting lipid bilayer was further incubated in the second, anionic liposome solution (Rho-DPPE/DPPG/DPPC, 5/15/80, in mole fraction) for 1 h. The unbound liposomes were similarly removed by buffer exchange. Thus-prepared lipid structures were transferred onto the microscope scanning stage and assembled with a fluid cell (Bruker) to give a sealed and aqueous-immersed scanning environment.

The control AFM measurement shown in Figure 2.10C was carried out by dewetting[18] the as-deposited lipid assemblies. To do this, lipid samples were briefly exposed to air by draining the HEPES buffer solution covering the samples from the fluid cells, which were immediately refilled with the same buffer to rehydrate the samples. Thus-treated lipid samples were then similarly probed by AFM in a fluid as described above.

2.2.6 Scanning Electron Microscopy (SEM)

To image the thus-formed lipid nanoassemblies by SEM, the exact same approach as used to prepare samples for in air AFM imaging was employed to prepare such a superstructure on gold substrates. After fixation by using a mixture of 4% paraformaldehyde and 1% glutaraldehyde in DI water for 1 h, the fixative solution was subsequently exchanged out by DI water. After that, the residue water covering the lipid complexes was gently blotted away with a paper towel. The substrates were then coated with sputtered gold using low-vacuum sputter coater. Scanning electron microscopy (SEM) images were acquired with a Zeiss scanning electron microscope.

2.2.7 Photoelectrochemical Measurements

The photoelectrochemical measurements were carried out in three-electrode Teflon photoelectrochemical cells consisting an ITO substrate covered with lipid nanoassemblies as the working electrode, a Pt wire as the counter electrode, and Ag/AgCl (in saturated KCl) as the reference electrode. All photocurrents were generated and collected under cell open-circuit potential conditions without an extra potential bias. For photocurrent generation, 50 mM ascorbate in HEPES buffer (10 mM HEPES, 100 mM NaCl, pH 7.70) was employed as the sacrificial electron donor. Oxygen in the cell was depleted by an enzymatic method reported elsewhere.7,19 To obtain photoaction spectra, photocells containing different lipid structures were illuminated with a 150 W xenon lamp (Ushio, Japan) whose wavelength selection was realized using a computer-controlled fluorescence spectrophotometer (RF-5301, Shimadzu, Japan). The resulting photocurrent was recorded on a PC controlled potentiostat (CHI 910B, CH Instruments). The photoaction spectra reported in the main text have been corrected for nonuniform spectral distribution of excitation in 5 nm intervals using a silicon photometer (PM120, Thorlabs). The photon-to-electron quantum conversion efficiency (QE) was calculated at a maximum absorption wavelength of Rho-DPPE (λ_m = 575 nm) using the equation, $\Phi = (i/e)/[(W\lambda_m/hc)(1 - 10^{-A})]$, where i is the measured photocurrent, e is the elementary charge, W is the light power at λ_m, h is Planck's constant, c is the light speed, and A is the absorbance of Rho-DPPE at λ_m in the final lipid assemblies.

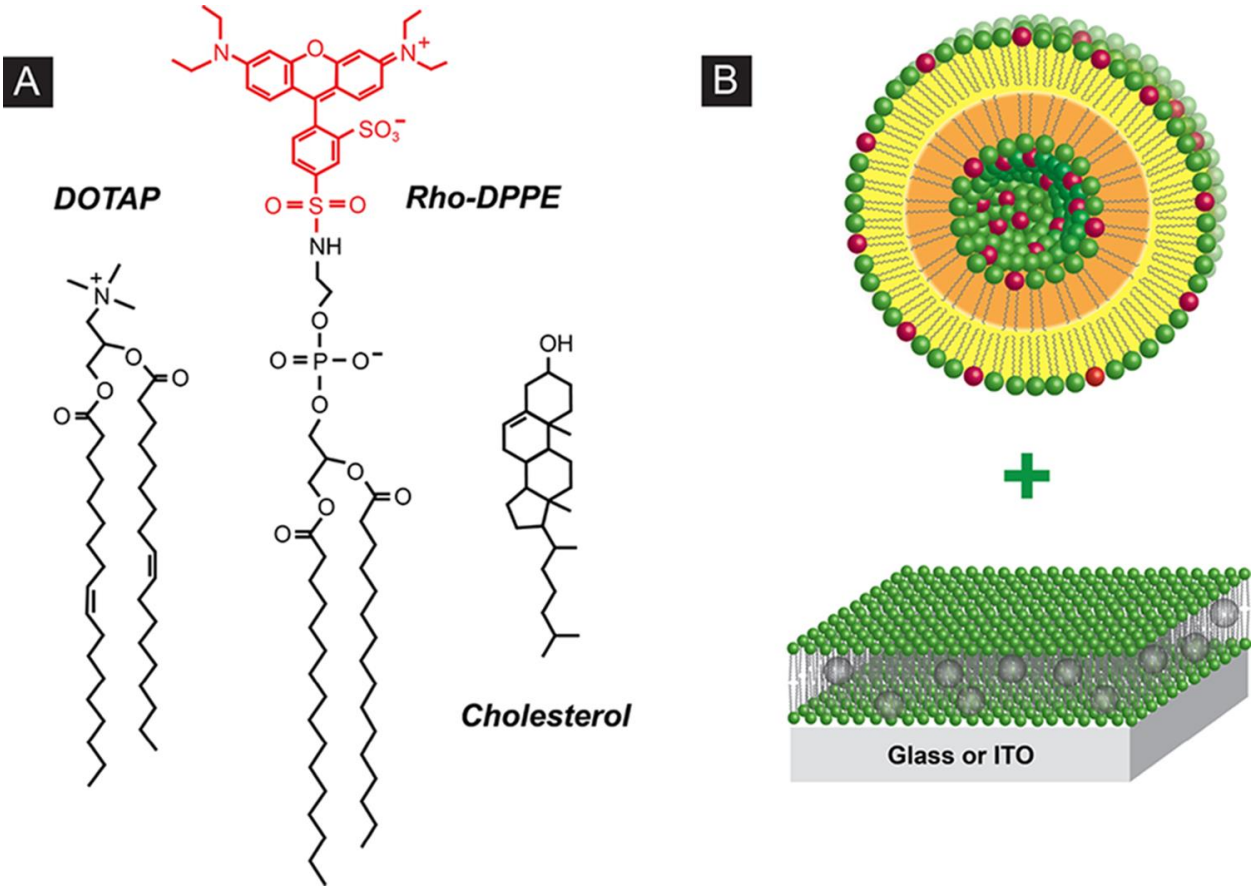

Figure 2.2 Main lipid components employed (A) in the formation of lipid-assembled photosynthetic mimics, which feature rhodamine and fullerene C_{60} assembled in a liposome-on-lipid bilayer two-tier nanoassembly (B) bound electrostatically.

2.3 Results and Discussion

2.3.1 System Design

To capture the essence of the layered organization and energy flow in GSB, we designed a two-tier lipid nanoassembly, in which a layer of anionic unilamellar liposomes (average size: ~80 nm) is electrostatically held on a positively charged lipid bilayer (Figure 2.2B). At the beginning of this investigation, lipids comprising all-saturated C16 chains, such as DPPC and 1,2-dipalmitoyl-sn-glycero-3-phosphoglycerol (DPPG), were used to form the liposomes at the top.

For the bottom lipid bilayer, unsaturated DOPC and cationic DOTAP were used. To provide light-harvesting capability to the lipid assembly, 5 mol % Lissamine rhodamine B conjugated to the phosphoethanolamine lipid (Rho-DPPE) was also incorporated into the top liposomes. Considering the ideal case in which lipids and dyes were symmetrically distributed between two identical leaflets of a spherical liposome, a loading of $\sim 3 \times 10^3$ rhodamines per liposome can be estimated.[20] Finally, to facilitate directional charge separation and electron transfer, 5% fullerene C_{60} molecules as electron acceptors were further assembled into the underlying lipid bilayer.[7] These supercomplexed lipid nanoassemblies were formed on either glass or ITO surfaces, and in the latter case, photocurrents can be directly generated and followed.

2.3.2 AFM and SEM of Lipid Deposits

Electrostatic deposition of charged liposomes on solid-supported lipid bilayers has been investigated previously,[21-23] and the fact that no single final deposited structure emerges from these studies points to the complexity of such processes. Depending on the type of lipid, charge density, and other experimental variables (e.g., deposition time) employed, oppositely charged liposomes and bilayers may interact differently or to a different degree, giving rise to one or several distinct end features: intact liposomes on a lipid bilayer, lipid multilayers, and partial lipid exchange between the supported lipid bilayer and free liposomes.[21-23] Although the first two cases produce morphological changes that can be identified by AFM, the detection of the third case requires other techniques such as fluorescence microscopy (next section).

As our initial attempt to unravel the morphology of electrostatically held lipid complexes, we used AFM to probe such assemblies in air. To maintain and reinforce the structure thus formed in solution, the samples were first fixed with paraformaldehyde and glutaraldehyde before being

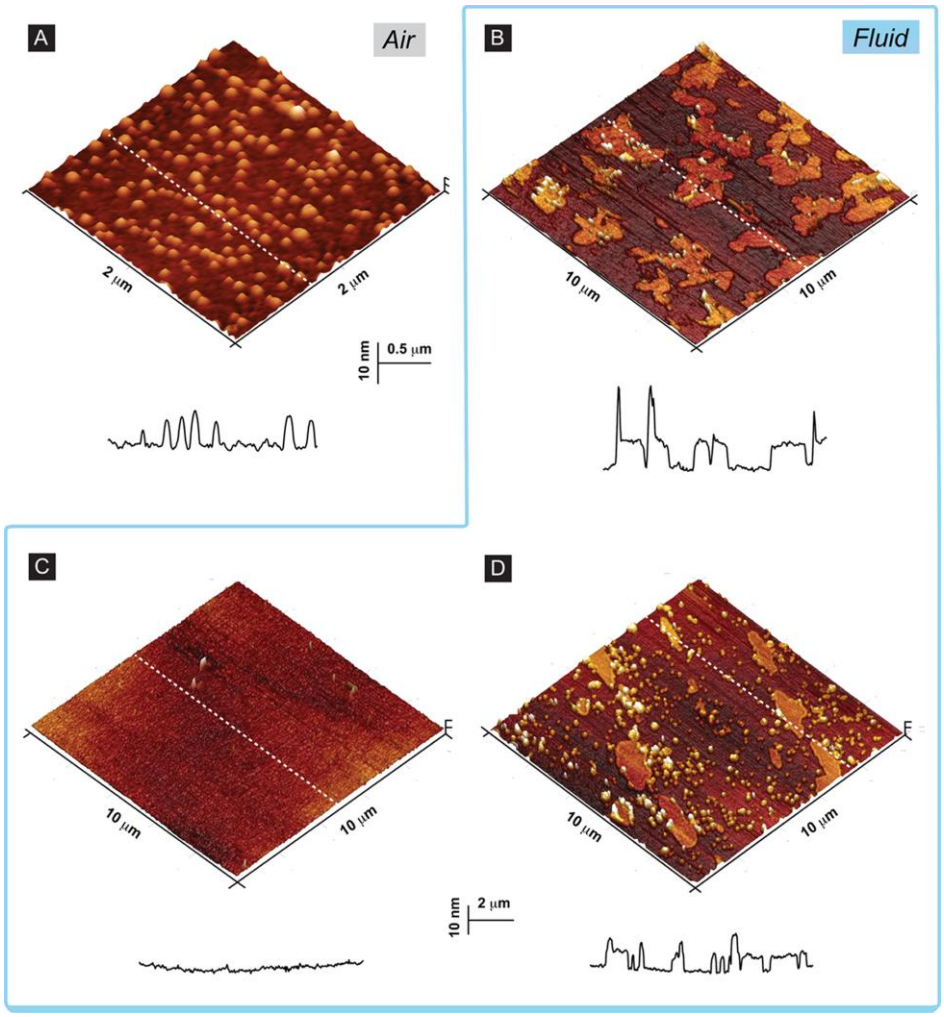

Figure 2.3 Structure of liposomes electrostatically deposited on lipid bilayers as probed by AFM. The image in (A) was obtained by scanning chemically fixed lipid assemblies in air on gold, whereas images (B)-(D) were lipid assemblies supported on glass and immersed in fluid (10 mM HEPES, 100 mM NaCl, pH 7.70). The height profiles shown at the bottom are obtained from line scans marked by the dashed lines in the corresponding images. Lipids employed to prepare liposomes: (A) DOPC/DPPG/DPPC (1/2/7 in mole fraction), (B) and (C) Rho-DPPE/DPPG/DPPC (5/15/80), and (D) DPPG/DPPC (2/8). The bottom lipid bilayer contains DOTAP/DOPC (2/8) in all cases. See the Experimental Section for more details.

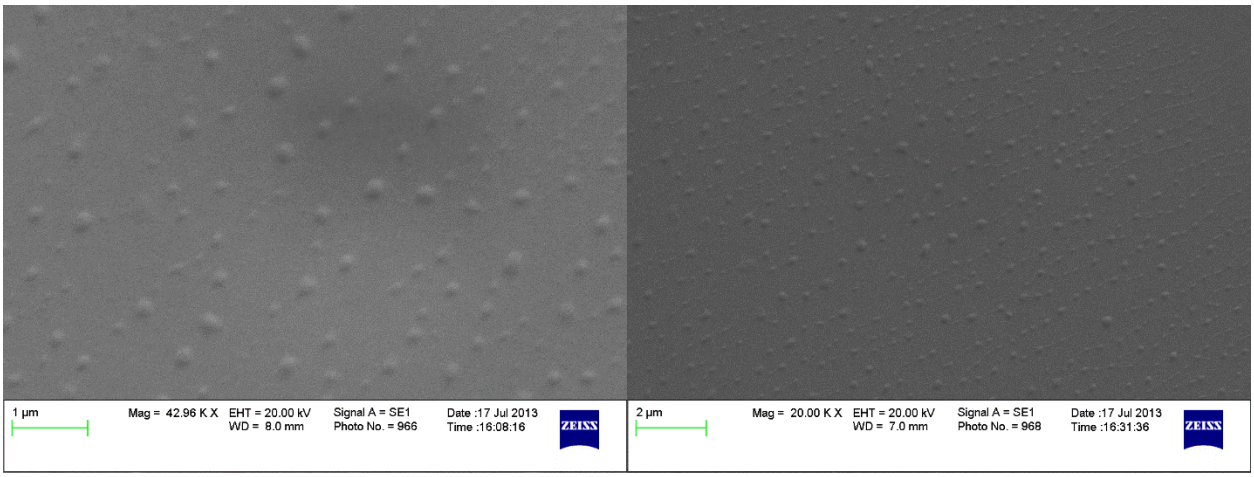

Figure 2.4 Structure of liposomes electrostatically deposited on lipid bilayers as probed by SEM with different magnifications (left: 42,960×; right: 20,000×). Lipids employed to prepare liposomes: DOPC/DPPG/DPPC (1/2/7 in mole fraction). The bottom hybrid lipid bilayer contains a C12 SAM and DOTAP/DOPC (2/8) monolayer. See the Experimental Section for more details.

exposed to air (see the Experimental Section). Besides the consideration on the relative ease of handling dry samples by AFM, the fixation step structurally locks everything in place and thus stops the deposited features from undergoing further morphological evolution. One such snapshot is shown in Figure 2.3A, revealing that individual liposomes can be deposited on a lipid bilayer in high density following our procedure. Although the measured average diameter of the liposomes is in line with that expected of the preparation, the height of these deposited features is much smaller: 5-15 nm. This deformation of spherical liposomes upon deposition and exposure to air very likely results from the alteration of forces, for example, electrostatic and hydration forces, experienced by each particle and in addition reflects the mechanical strength and conformability of cross-linked lipid bilayers. This in air AFM images is consistent with the images acquired by SEM, shown in Fig. 2.4.

We next moved to AFM measurements of aqueous immersed lipid assemblies. Because these samples are prepared under conditions close to those employed in photocurrent generation (see the Experimental Section), that is, lipid composition and the microenvironment in which the lipid deposits are surrounded, images obtained here unveil the morphology of the latter more accurately. To our initial surprise, these measurements yielded features quite different from those collected in air. One representative image, shown in Figure 2.3B, discloses irregular-shaped lipid micropatches of 8-9 nm thickness, whose edges are occasionally decorated with particles sticking out 10-20 nm farther. These features indicate that the electrostatic interaction between the two lipid subunits causes large-scale liposome rupturing and spreading on the lipid bilayer, resulting in lipid multilayer formation and liposome adsorption. From time to time, smooth and almost featureless images were also obtained (Figure 2.3C), which may result from (1) the uneven distribution of lipid deposits and the limited area sampled by the AFM and (/or) (2) the rigid AFM tip pushing and distorting relatively soft lipid structures during scanning. It should also be noted that Figure 2.3B,C was obtained with liposomes containing an identical composition as that used in the photocurrent generation, including 5% Rho-DPPE. When the dye was omitted in the preparation, the most frequently encountered images recorded both individual liposome deposition and lipid spreading/fusion (Figure 2.3D). The height of micropatches obtained in this case is ~4 nm, which should correspond to a single lipid bilayer. This is very different from Figure 2.3B, where the micropatches are twice as thick on average, pointing to a plausible role of 5% Rho-DPPE in modifying the final structure. Taken together, these results provide us the first confirmation in this study that electrostatic interaction can be used to organize multiple lipid nanostructures into layered architectures.

2.3.3 Fluorescence Imaging

Imaging thus-formed lipid assemblies with confocal fluorescence microscopy further reveals that this protocol affords high-density liposome deposition across a large surface area (Fig. 2.5). Here, the most abundant fluorescent spots are formed by micron-sized lipid deposits, which should correspond to those micropatches resolved by AFM. Besides these prominent features, importantly, there exists a relatively uniform fluorescent background in all obtained images. As it is evident from Figure 2.5B, this fluorescence intensity is distinctly higher compared to the control dark background, where the lipid deposits are specifically removed by scratching. Because the AFM resolves only one major feature above the ground floor (i.e., micropatches) and the fluorescent Rho-DPPE is initially incorporated only into the liposomes to be deposited, this background fluorescence strongly suggests that lipid exchange has occurred between oppositely charged liposomes and the lipid bilayer during deposition.

2.3.4 Steady-State and Time-Resolved Fluorescence Spectroscopy

To assess the energy flow among rhodamine dyes and their electronic communication with fullerenes embedded in the lipid bilayer, we next characterized these layered lipid nanoassemblies using steady-state as well as time-resolved fluorescence spectroscopy. From steady-state fluorescence emission spectra, it was first found that the presence of 5% C_{60} in the bottom layer led to a 75% quenching of fluorescence emission from 5% Rho-DPPE in the DPPC/DPPG liposomes deposited atop (spectra in black and green, Figure 2.6 inset).

Using time-resolved fluorescence spectroscopy, we further determined that the rhodamine sample without C_{60} coassembled and displayed two lifetimes at 0.73 and 2.41 ns, with amplitude weights of 62 and 38%, respectively. The lifetime of the long-lived component is close to the

lifetime observed from the same dye/lipid conjugate via homogenous emission,[24] whereas the short-lived component most likely arises from self-quenching[25,26] among the high-concentration and randomly distributed rhodamines existing in the gel-phase liposomes. Indeed, when the same sample was probed in the form of liposome suspensions instead of surface-deposited films, a single fluorescence lifetime of 0.79 ns was resolved. This result indicates that rhodamines exist in a relatively homogenous microenvironment in aqueous-dispersed liposomes and the dye loading in liposomes is high enough to induce global self-quenching. This lifetime is clearly of the same origin as the short component observed from the deposited sample, whereas their difference should result from changes in the liposome morphology or rhodamine concentration upon deposition. Furthermore, considering these fluorescence decay behaviors together with fluorescence imaging data, it seems reasonable to assign the long decay component (2.41 ns) to be fluorescence emission by rhodamine dyes transferred from liposomes to the bottom lipid bilayer or recovered free emission due to dilution at the top layer. On the other hand, the addition of 5% C_{60} in the underlying lipid bilayer caused the otherwise similarly deposited rhodamines to fluoresce at lifetimes of 0.60 and 2.48 ns. Assuming that photoinduced electron transfer (PeT) between rhodamine and fullerene is the only additional pathway competing with fluorescence emission, a PeT rate constant of 6.1×10^8 s^{-1} can be obtained from $k_{PeT} = 1/\tau_{F(C60)} - 1/\tau_F$, where $1/\tau_{F(C60)}$ and $1/\tau_F$ are the measured fluorescence lifetime of rhodamine with and without fullerene, respectively. This rate constant compares well with those obtained from more frequently investigated porphyrin−fullerene conjugate complexes,[27,28] thus verifying rhodamine dyes as a capable alternative electron-transfer partner to fullerene. Together, these spectroscopic results evidence that an efficient electronic communication pathway exists between the assembled dye and fullerene populations, which are brought to close proximity by the electrostatically appressed lipid nanoassemblies.

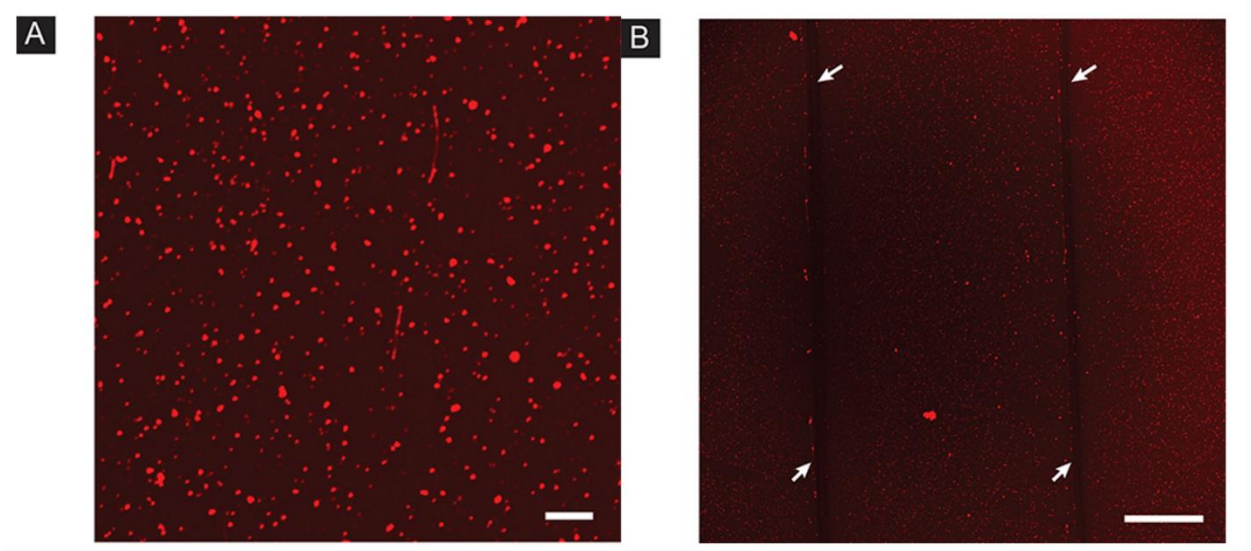

Figure 2.5 Fluorescence micrographs of rhodamine-labeled liposomes electrostatically deposited on an oppositely charged lipid bilayer supported on glass. Liposomes used: (A) Rho-DPPE/DPPG/DPPC (5/15/80) and (B) Rho-DPPE/DPPG/cholesterol/DPPC (5/15/30/50). White arrows in (B) point out the two passes where lipids were removed by scratching. The scale bars are (A) 10 and (B) 100 μm.

2.3.5 TA Spectroscopy Characterization of Liposome Suspensions

The photodynamics of excited rhodamines in liposome suspensions were further probed by TA spectroscopy. As shown in Figure 2.7A, the TA spectra of rhodamine dyes in the liposome suspension display a negative absorbance band at 585 nm upon 150 fs pulse excitation, which corresponds to the ground-state bleaching and subsequent stimulated emission of excited rhodamine monomers. Concurrently, the TA spectra also display a positive absorbance band with a maximum at 450 nm, which should result from absorption by the excited-state rhodamines. Both of these spectral features have been previously observed for rhodamine dyes in solution or

adsorbed on nanoparticles.[29] By fitting the kinetics of these features by exponential functions, one can further determine the excited state lifetime: 701 ps (at 585 nm) and 747 ps (at 450 nm).

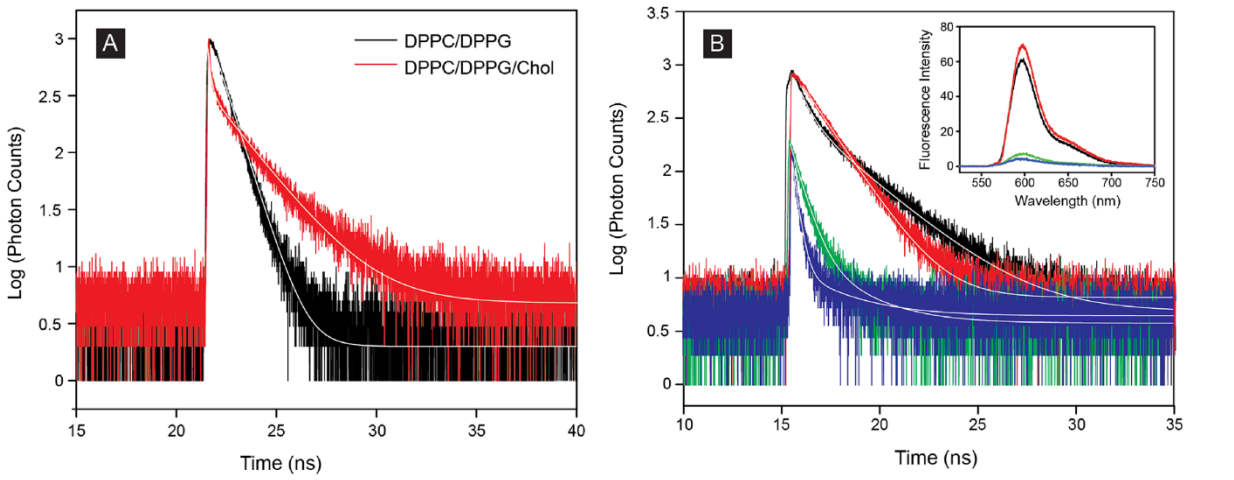

Figure 2.6 Steady-state and time-resolved fluorescence emission spectra of rhodamine assembled in liposome suspensions (A) and the two layer lipid nanostructures (B). In (A), the liposomes, containing either DPPC/DPPG/Rho-DPPE (80/15/5) or DPPC/DPPG/ cholesterol/Rho-DPPE (50/15/30/5), are dispersed in HEPES buffer, and the final rhodamine concentration is ~0.5 μM. All samples in (B) contain 5% Rho-DPPE and 15% DPPG in the top liposome layer. The complexes in addition contain 80% DPPC (black), 50% DPPC + 30% cholesterol (red), 80% DPPC + 5% C_{60} (in the bottom layer, traces in green), and 50% DPPC + 30% cholesterol + 5% C_{60} (blue). Exponential fitting curves associated with these decay profiles are shown by solid white lines embedded. The inset shows the corresponding steady-state fluorescence emission spectra of the four lipid deposits, which are color coded the same way. See the Experimental Section for more details.

2.3.6 Photocurrent Generation

As a direct test of the overall energy/electron transfer efficiency among all assembled components, these lipid supercomplexes were also wired to transparent ITO[7,30] electrodes to produce photocurrent (see the Experimental Section). As shown in Figure 2.8, for the photocell containing 5% Rho-DPPE in the top liposome layer and 5% fullerene C_{60} in the lipid underlayer, the photoelectrochemical action spectrum tracks closely the electronic absorption of rhodamine, suggesting that rhodamine is primarily responsible for the light harvesting and an efficient PeT process exists between rhodamine and fullerene. The internal photon-to-electron QE is a very encouraging value of 7.8%. By contrast, photocurrents from cells containing 5% rhodamine alone are negligible, which indicates that effective charge separation can be achieved only when a suitable electron acceptor such as fullerene is also present in the assembly.

2.3.7 Performance Enhancement by Cholesterol

Further optimization of photoconversion efficiency has uncovered an intriguing role of the lipid matrix in influencing the distribution and organization of dyes in liposomes, which can significantly impact the ET dynamics and thus the performance of these lipid-assembled systems. Strikingly, when 30% cholesterol was added into the liposomes to replace DPPC, whereas other components were kept unchanged, the otherwise similarly configured photocell produced a QE of 14.2% (red trace, Figure 2.8 inset).

To rule out the possibility that this enhanced performance is caused by some trivial mechanisms, for example, the addition of cholesterol in the top layer, facilitating fullerenes initially assembled underneath to enter the top layer and thus improving their electron transfer with rhodamines thereby, we also carried out additional control experiments. We found that, when the

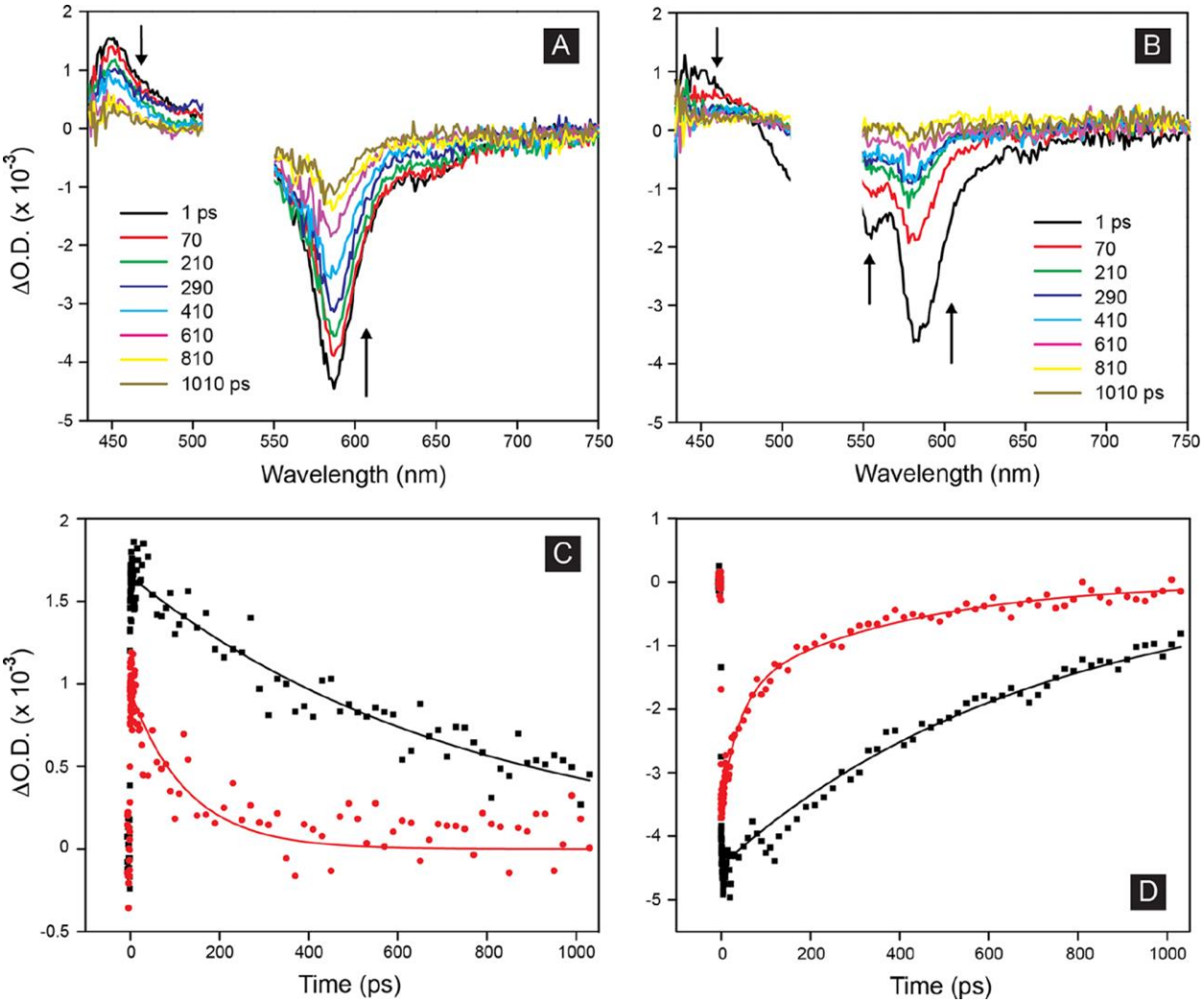

Figure 2.7 TA spectra of rhodamine in the liposome samples without (A) or with (B) cholesterol coassembled. Both samples contain 5% Rho-DPPE and 15% DPPG with the remaining portion(s) made up of 80% DPPC (A) or 50% DPPC + 30% cholesterol (B). The time-evolved optical density profiles at 450 (C) and 580 nm (D) of the cholesterol-containing and cholesterol-free samples are shown by red circles and black squares, respectively; the solid lines of the same color are the exponential fits of the experimental data.

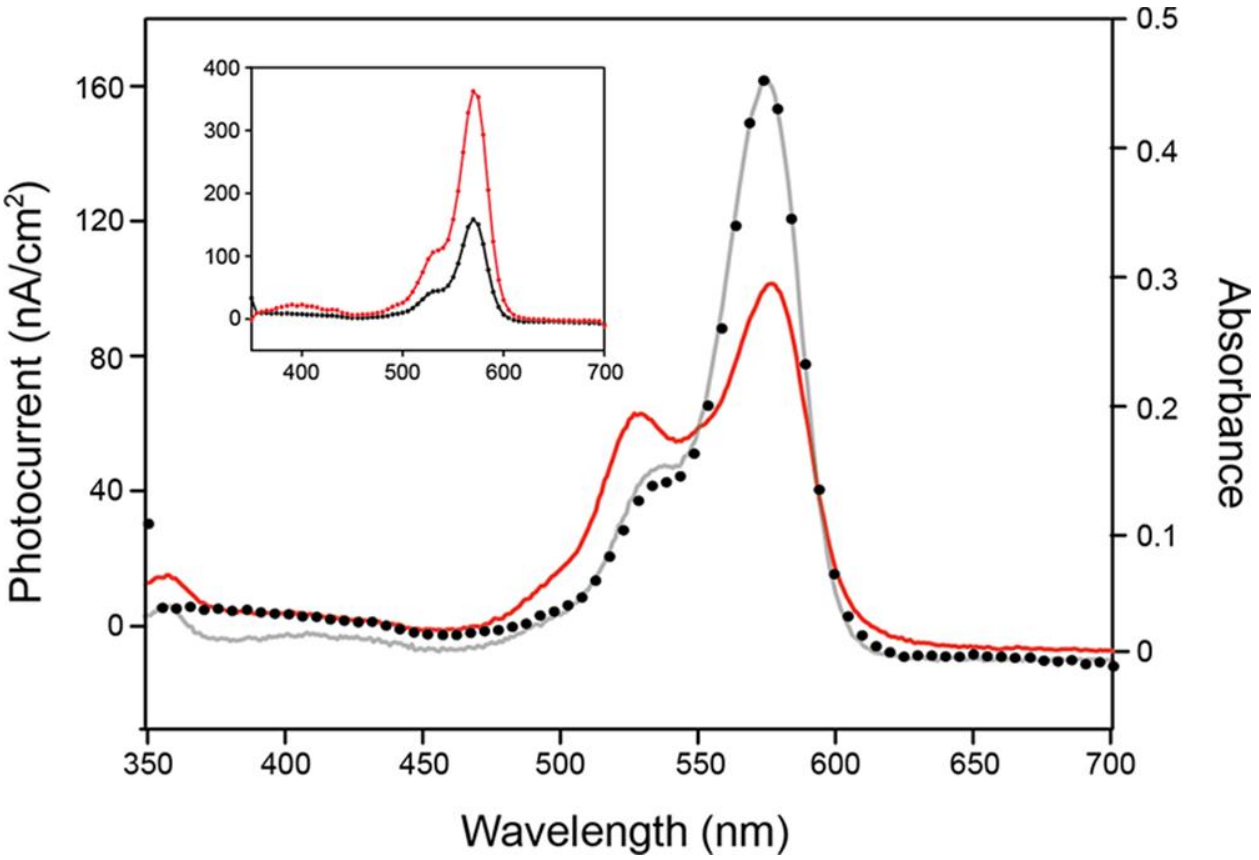

Figure 2.8 Absorption spectra of 5 mol % Rho-DPPE in liposomes in the presence (in red) or absence (in gray) of 30 mol % cholesterol. The rhodamine concentration in both samples is approximately 5 μM. The trace shown in solid circle is the corresponding photoaction spectrum of the cholesterol-free sample. Inset: photoaction spectra of lipid-assembled rhodamines/fullerenes with (in red) or without (in black) cholesterol; coordinates are identical to the main plot.

same amount of fullerenes was directly assembled into the liposomes (i.e., together with rhodamine and cholesterol) instead of the underlying lipid bilayer, the obtained QE was only 7.3%. This result, therefore, rejects the possibility of relocation of fullerenes (caused by cholesterol) as the main mechanism of the observed enhancement. The significant difference in efficiency between these two cells highlights the delicacy of organizing an electron donor/acceptor into

desired positions to achieve optimal performance and in addition suggests that rhodamine and fullerene remain largely associated with their lipid hosts during the photocurrent generation process. The latter conclusion was also reached in our previous study, where the same amphiphilic fullerene as used here was found to be able to maintain its position within individual leaflets (i.e., upper vs bottom half) comprising the same lipid bilayer.[31]

2.3.8 Cholesterol-Containing Systems: Fluorescence Imaging and AFM Characterization

To understand the underlying enhancement mechanisms, we next examined the liposome suspensions as well as liposome-on-bilayer assemblies containing cholesterol using AFM and various spectroscopic techniques. By comparing these with cholesterol-free samples, we hope to identify morphological and spectroscopic fingerprints that can be associated with the presence of this species in the lipid complexes.

Under the confocal fluorescence microscope, the electrostatically bound liposome (with 30% cholesterol)/lipid bilayer assemblies appear similar to their cholesterol-free counterparts, featuring micron-sized lipid deposits dispersed in a common fluorescence background (Figure 2.9A). This similarity is not unexpected as cholesterol, a neutral species, would not directly participate in the interaction process between oppositely charged lipids. On the other hand, our AFM measurements on cholesterol-containing deposits almost exclusively return images with no apparent features similar to Figure 2.3C. Only once out of about a dozen attempts were we able to resolve additional features on top of the flat background, which in this particular case suggests a deposition process based on intact individual liposomes (Figure 2.9B). Besides factors already mentioned, such as the uneven distribution of lipid deposits and the limited areas probed by the AFM, the elusiveness of well-resolved cholesterol-containing structures may be because of the

fact that cholesterol can significantly increase the fluidity[32] of the liposome lipid matrix, which is composed of lipids with all-saturated C16 chains. As such, these softened lipid deposits tend to be pushed aside by the AFM tip more easily during scanning and therefore are not captured in the final images. In a separate control experiment, finally, we also confirmed that these featureless samples are nevertheless covered by a lipid bilayer (Figure 2.9C).

2.3.9 Cholesterol-Containing Systems: Spectroscopic Characterization

Further spectroscopic characterization of rhodamine dyes in liposomes coassembled with cholesterol reveals several important new features. The first piece is from the ground-state absorption spectroscopy, where rhodamine dyes in the cholesterol-containing liposomes display a significantly intensified shoulder peak at the expense of the main 0-0 transition (red trace, Figure 2.8). An 8 nm shift toward the shorter wavelength can also be clearly discerned. In TA spectroscopy, the same sample displays an additional negative absorption band at 555 nm, which is absent for the liposome sample containing the same amount of rhodamine but no cholesterol (Figure 2.7B). The influence of cholesterol on the photodynamics of coassembled rhodamines is clearly evident by following the decay/recovery of these absorption maxima over time (Figure 2.7C, D). At 585 nm, a lifetime of 701 ps for rhodamines in cholesterol-free liposomes was found, whereas two time constants of 41 and 391 ps were obtained for the same dye in cholesterol-coassembled liposomes. Likewise, the lifetimes of the rhodamine dimers as judged by the absorbance change at 555 nm are found to be 302 ps. A similar trend is also obtained by fitting the data at 450 nm: 747 ps (no cholesterol) vs a much shorter 127 ps when cholesterol is coassembled. On the other hand, by probing the same liposome samples with time-resolved fluorescence spectroscopy, we identified a single fluorescence lifetime of 0.79 ns for the cholesterol-free sample

and two lifetimes at 0.21 and 2.05 ns for the cholesterol included sample. These time constants are in general agreement with those found by the TA spectroscopy, whereas the discrepancies are likely caused by the different time resolution and experimental setup, for example, the probed time window and photoexcitation conditions, between the two techniques.

Table 2.1 Excited-state lifetimes of rhodamines assembled in liposomes as probed by time-correlated fluorescence single-photon counting (TCSPC) and TA spectroscopy

Lipid composition	Fluorescence lifetime (ns)[a]	Excited-state lifetime (ps)[b]		
		585 nm	450 nm	555 nm
Rho-DPPE/DPPC/ DPPG: 5/80/15	0.79 ± 0.02	701 ± 18	747 ± 25	
Rho-DPPE/DPPC/DPPG/ Chol: 5/50/15/30	2.05 ± 0.06 (41%), 0.21 ± 0.07 (59%)	41 ± 5; 391 ± 29	127 ± 13	302 ± 12

[a]Data obtained from TCSPC measurements. [b]Data obtained from TA measurements. See also Figures 2.6 and 2.7.

When these cholesterol-containing liposomes are further deposited on a solid-supported lipid bilayer via electrostatic interactions, the photodynamics displayed by the coassembled rhodamines changed once again. Here, a single-component fluorescence lifetime of 1.60 ns was observed when the bilayer contained no electron-accepting fullerenes, whereas for the lipid complex with fullerene incorporated, the lifetime of the fluorophore was drastically shortened to 0.41 ns (amplitude weighted average of two components). From these data, one can again estimate the rate constant of the competing PeT process, 1.9×10^9 s^{-1}, which is more than two times faster

compared to that of the cholesterol-free supercomplex. All photoelectrochemical and spectroscopic data associated with these two lipid complexes are summarized in Tables 2.1 and 2.2.

Table 2.2 Spectroscopic and photoelectrochemical characteristics of rhodamines assembled in various lipid supercomplexes

Lipid composition in the top liposome layer[a]	Fluorescence lifetime (ns)[b]	k_{PeT} (s^{-1})	Photoconversion QE (%)
Rho-DPPE/DPPC/DPPG: 5/80/15	0.73 ± 0.09 (62%), 2.41 ± 0.11 (38%)[c]		
	0.60 ± 0.03 (92%), 2.48 ± 0.24 (8%)[d]	6.1×10^8	7.8 (±0.6)[e]
Rho-DPPE/DPPC/DPPG/ Chol: 5/50/15/30	1.60 ± 0.08[c]		
	0.26 ± 0.03 (90%), 1.75 ± 0.38 (10%)[d]	1.9×10^9	14.2 (±0.6)

[a]All bottom lipid bilayers contain DOPC/DOTAP in an 80/20 mixing ratio with/without five additional fractions of C_{60}. [b]Data obtained from TCSPC measurements. [c]Measured with dye alone. [d]With C_{60} coassembled. [e]Standard deviation, n = 3.

2.3.10 Cholesterol-Containing Systems: Discussion on Enhancement Mechanisms

How could the simple addition of cholesterol boost the photoconversion efficiency by >80% in these lipid supercomplexes? To answer this question, it is necessary to first delineate the relevant biophysical functions of this important molecule in biomembranes. A ubiquitous

functional and structural component in biomembranes, cholesterol may contribute to the enhanced performance through several closely related mechanisms.[32-34]

Table 2.3 Fluorescence lifetime decay of rhodamine as a function of dye loading in cholesterol-free liposomes

Lipid composition	Fluorescence lifetime (ns)
Rho-DPPE/DPPG/DPPC: 1/19/80	2.70 ± 0.04
Rho-DPPE/DPPG/DPPC: 5/15/80	1.36 ± 0.10
Rho-DPPE/DPPC: 20/80	1.17 ± 0.02
Rho-DPPE/DPPC: 40/60[a]	0.62 ± 0.08

[a] Lipid aggregate formation observed in this case.

Structurally, cholesterol features a rigid four-member fused ring connecting a hydroxyl group and a relatively flexible C6 hydrocarbon chain at its distal ends (Figure 2.2A). This arrangement renders the overall molecule amphiphilic[35] and an end-to-end length of about 2 nm when fully extended,[36] that is, about half of the thickness of a typical lipid bilayer. When juxtaposed with phospholipids, cholesterol forms hydrogen bonding with the latter[37,38] (i.e., between its OH group and the *sn*-2 carbonyl/phosphate oxygen of the latter), and its hydrocarbon portion is further associated with the acyl chains of the phospholipids via hydrophobic/hydrophobic interactions in both leaflets of the bilayer. Thanks to these specific interactions, cholesterol tends to insert into a lipid bilayer with a preferential orientation and at a fixed depth and in so doing can occupy biomembranes in very high concentrations, for example, ~50% in red blood cells.[33] Compared to typical phospholipids, moreover, cholesterol is compact in size and dissimilar in geometry, that is, a small hydrophilic OH headgroup relative to its

hydrocarbon backbone. Broadly speaking, it is this unique combination of complexing ability and structural mismatch with phospholipids that renders cholesterol the universal molecular wedge/filler inside lipid membranes. As such, it modifies the ordering, packing density, and distribution of neighboring phospholipids, thereby impacting the physical and mechanical characteristics of the lipid membrane at a macroscopic level.[33,34] Naturally, such modification effects come about in a lipid-, concentration- and temperature-dependent fashion. If the lipid bilayer is fluidic and disordered at room temperature to start with, for example, based on lipids with unsaturated acyl chains such as DOPC (18:1, two identical C18 chains with one double-bond each, phase-transition temperature, T_m, at -17 °C), adding cholesterol will increase the order of lipid organization, condense the lipid matrix, and thus lower the fluidity of the resulting membrane.[39,40] On the contrary, for a bilayer existing in the ordered gel phase at room temperature, for example, DPPC (16:0, T_m = 41 °C), incorporating cholesterol will not only increase the lipid ordering further but also help to break up the rigid lipid network, thus producing a more fluidic lipid bilayer.[41,42] In both cases, such ordering/condensing effects kick in first locally at low cholesterol concentrations, which effectively generate heterogeneity within the lipid matrix and hence phase separation.[43–45] Conceivably, as cholesterol interacts with different lipids (with various headgroups and acyl chains) differently and such interactions are also concentration dependent, the phase behavior of multicomponent lipid matrices can be quite complex.[46]

Back to our system and consider the rhodamine-assembled liposome suspensions first. Due mainly to the common 16:0 chains, Rho-DPPE lipids distribute homogeneously in the gel phase DPPC/DPPG matrix[47] at room temperature.[51] At a high dye loading of 5%, rhodamines in the same liposome host are placed within a direct electronic-coupling distance with their neighbors. However, because all three lipids still maintain freedom to rotate about the bilayer normal,[33] there

exists no apparent order in relative orientation among rhodamines, and as a result, such a coupling only leads to destructive self-quenching via ET between excited- and ground-state dyes. This is first evidenced by a single fluorescence lifetime (0.79 ns) that is much shorter than that of free-emitting individual dyes, for example, ~2.4 ns. When 30% cholesterol is included in the DPPC/DPPG (50/15%) liposomes, the pure gel-phase matrix of the latter is partially replaced by a new liquid-ordered phase modulated by cholesterol, resulting in two-phase coexistence. [52,53]

Of the two, the coassembled rhodamine prefers the new phase, which may be driven by its direct participation in the hydrogen-bonding network. In a fluorescence lifetime imaging microscopy study of DPPC/cholesterol vesicles, de Almeida et al. previously identified a preferential partition of rhodamine conjugated to dioleoylphosphatidylethanolamine (DOPE, 18:1) into the liquid-ordered phase over the gel phase.[54] Without the double bonds disrupting the association among lipid hydrocarbon chains in the present system, this preferential partition is expected to be even stronger. This produces two net effects: clustering of dyes in the cholesterol rich domain and a concentration decrease of dyes remaining associated with the gel phase (Figure 2.10). Situated in different microenvironments, the photodynamics of these two rhodamine populations diverge. For those dyes existing in the gel phase, a lower concentration means greater dye-to-dye separation and less coupling and self-quenching; therefore, their fluorescence lifetime recovers and approaches that of undisturbed emission from individual dyes. In comparison, the situation is more complex for those rhodamines in the liquid ordered phase. Here, the dyes are not only crowded (hence a shortened dye-to-dye distance) but, because the presence of cholesterol further reduces the tilting of lipids versus the bilayer normal and hence the cross-sectional area occupied per lipid,[33,34,42-44] it also modifies the relative orientation of transition dipoles among rhodamines. As a result, these dyes respond to the light excitation collectively, producing exciton

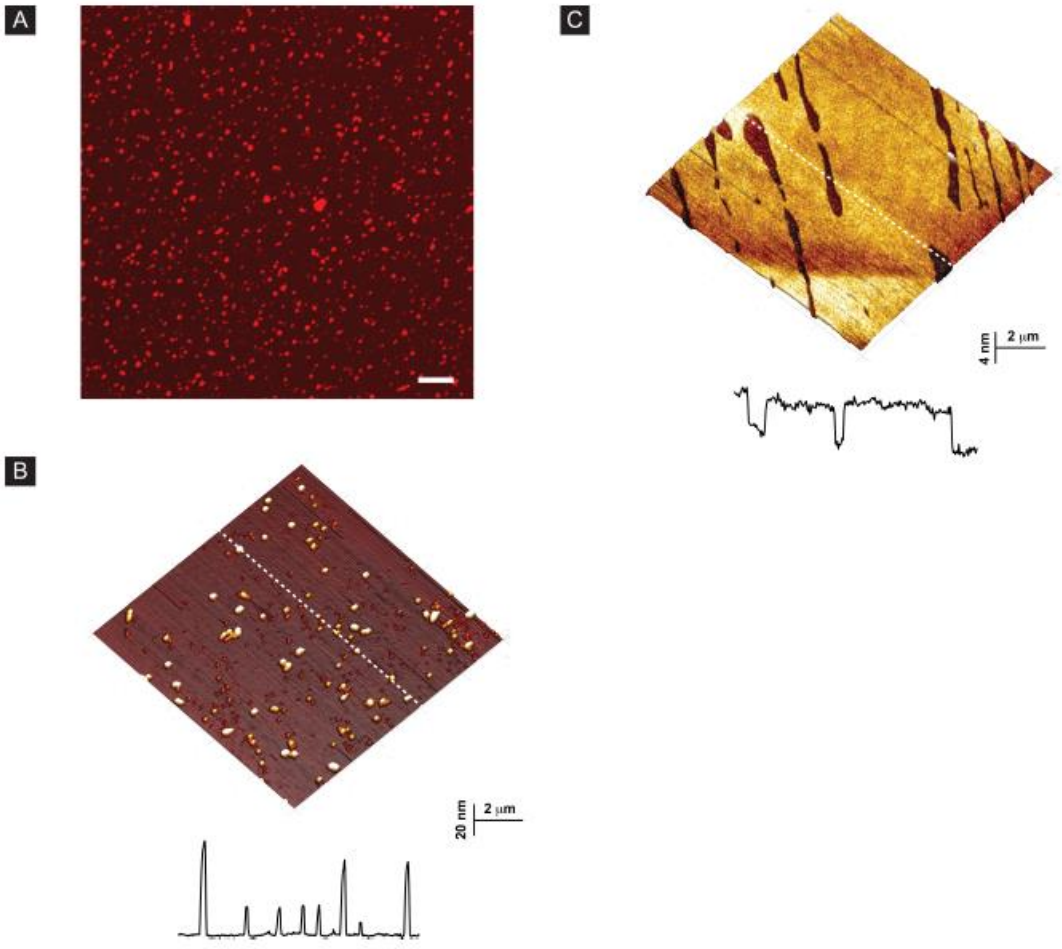

Figure 2.9 Fluorescence imaging (A) and AFM (B and C) characterization of cholesterol incorporated liposomes electrostatically deposited on lipid bilayers. All samples were prepared by incubating anionic liposomes (Rho-DPPE/DPPG/cholesterol/DPPC, 5/15/30/50, mole fraction) with a DOTAP/DOPC (20/80) bilayer supported on glass for 1 h. Scale bars in (A) is 10 μm. Image (C) was obtained after de-wetting the as-prepared lipid deposits. See the Experimental Section for more details.

states that display very different photodynamics compared to those of individual dye molecules.

The spectroscopic evidence presented above directly points to exciton formation in dye aggregates when cholesterol is coassembled in these lipid nanoassemblies. In particular, the shoulder peak observed in both steady-state and TA spectra only when cholesterol is present can be attributed to rhodamine dimer formation, which has been observed previously in several types of rhodamine dye aggregates.[55-57] Combining this feature with the blue-shifted 0-0 absorption band, it can be further deduced that the cholesterol-coassembled rhodamines belong to the weakly coupled exciton characteristic of H aggregates,[58,59] that is, with the dye transition dipoles arranged in parallel. Considering the facts that the transition dipole of rhodamine oscillates along the long axis of the molecule defined by the xanthene backbone[51,60] and a large distance (i.e., >4 nm) separates dyes occupying the opposite leaflets of the liposomal bilayer, this effective dimerization most likely results from an enhanced alignment of rhodamines within the same leaflet as cholesterol orders the neighboring lipids and limits their rotation therein. Consistent with this two-population analysis, the rhodamine/cholesterol-coassembled liposomes fluoresce in two lifetimes: 2.05 and 0.21 ns. The latter component may result from the faster ET between rhodamine monomers and dimers. Here, it is important to note that such a short fluorescence/excited-state lifetime cannot be obtained simply by crowding the rhodamines without cholesterol. As shown in Table 2.3, when the dye concentration in liposomes was systematically increased, a monotonous decrease in the fluorescence lifetime was obtained, again because of greater self-quenching at higher concentrations. Additional evidence is the lack of formation of aggregates along with the increasing concentration of rhodamines from 0.5 mol% to 20 mol% in liposomes, as in the case of cholesterol-including liposomes, as indicated by absorption spectra (Figure 2.11). Of all concentrations examined, however, the rhodamines fluoresce in a single population. Even at an

extremely high dye loading of 40%, the obtained lifetime remains significantly longer than that of cholesterol-containing samples, pointing once again to the critical roles of this species.

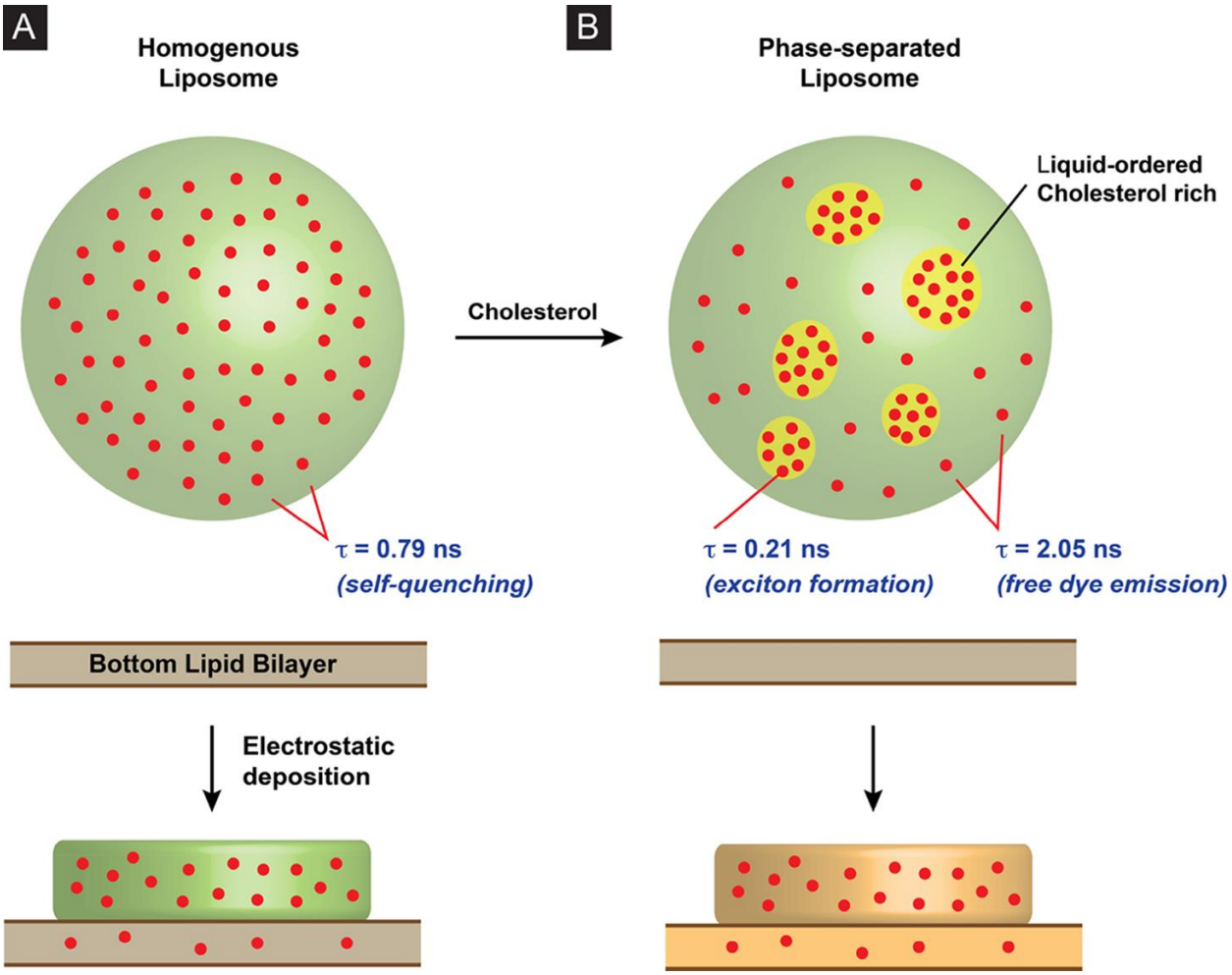

Figure 2.10 Cartoon depiction of cholesterol-induced phase separation (gel vs liquid-ordered phase) in liposomes and the clustering of rhodamine dyes in the cholesterol-rich liquid-ordered phase. Objects are color coded in terms of lipid composition; red dots represent individual rhodamine molecules. These drawings grant no information regarding the dye cluster size, distribution, or number of dyes per cluster in liposomes.

Complexing these liposomes with a solid-supported lipid bilayer further modifies the organization and lipid microenvironment in which the rhodamines reside and hence their photodynamics. As clearly evident from Figures 2.3 and 2.5, the electrostatic interaction between these two lipid assemblies causes the liposomes to rupture and spread on the oppositely charged bilayer, producing multilayer lipid micropatches. Accompanying this morphological transition, there is also lipid transfer, which can occur as soon as the liposomes start landing on the solid-supported bilayer. For the rhodamines assembled in DPPC/DPPG liposomes, this transfer process

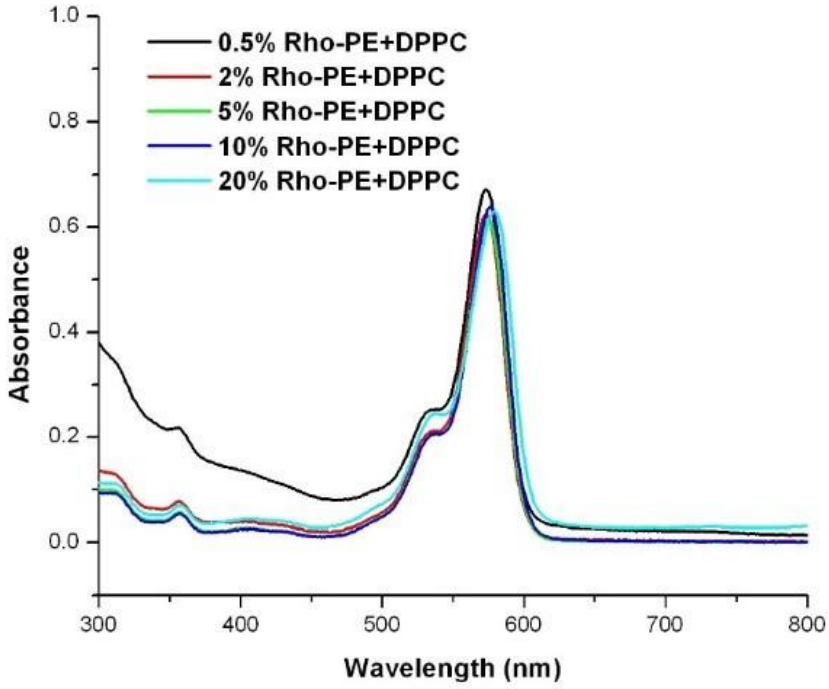

Figure 2.11 UV-Vis absorption spectra of Rho-DPPE with different concentration from 0.5 mol% to 20 mol% in liposomes in the absence of cholesterol. The final concentrations of Rho-DPPE are 5 μM for UV-Vis spectroscopic measurements.

brings a new population of dyes into the bottom bilayer, which fluoresces relatively undisturbed, that is, 2.41 ns. For those dyes that remain associated with the original host, the fluorescence lifetime is almost unchanged: 0.73 vs 0.79 ns in suspended liposomes. In striking contrast, when liposomes containing 30% cholesterol were similarly deposited, only a single fluorescence lifetime of 1.60 ns was found. Because the fluorescence imaging identifies two dye locations (Figures 2.5B and 2.9A), that is, in the bilayer and micropatches, similar to cholesterol-free assemblies, this single-component emission suggests improved electronic communication among rhodamines as a result of their rearrangement upon lipid deposition. As mentioned above, cholesterol can order and condense both fluidic/disordered and gel/ordered lipid bilayers, leveling the fluidity and mechanical strength of the resulting membranes. When cholesterol containing liposomes are being deposited on the solid supported bilayer, not only will cholesterol enter the bilayer, but it will also facilitate the transfer of all other species in both directions. This large-scale transfer and mixing of lipids effectively demolishes the phase segregation in the liposomes, resulting in homogenization of dyes throughout the assembled network (Figure 2.10). In comparison, such a transfer would be considerably weaker in the absence of cholesterol because of mismatches in phase and mechanical characteristics between the two lipid nanoassemblies.

Finally, when the electron-accepting fullerene is also incorporated, the photodynamics of rhodamine dyes coexisting in the system change yet again as a result of PeT between the two. This efficient process opens up another energy-dissipation channel to the photoexcited dyes, which produces a shortened fluorescence lifetime accompanied by a low-population (~10%) long-lived component in both cases (Table 2.2). Interestingly, the latter component is even slightly longer than that observed in the corresponding fullerene-free lipid complexes, which indicates that the PeT process engages the majority but not all of the dyes. In consequence, for those rhodamines

whose excited states elude direct electronic communication with fullerenes, their fluorescence emission recovers as the PeT relaxes their coupling with other dyes. One plausible assignment for such is the dye population located within liposomes decorating the edge of lipid micropatches (Figure 2.3B,D), which is separated the furthest from fullerenes embedded in the lipid bilayer underneath. Strikingly, with every other component/factor held identical, the lipid complex with 30% cholesterol displays a PeT rate constant two times faster than that of the corresponding cholesterol-free system, which underpins the higher photoconversion efficiency observed in the former (Table 2.2). This result once again supports the notion that cholesterol can significantly enhance the electronic communication among rhodamine dyes coassembled, inducing the latter to behave collectively within the same supramolecular network. Throughout this network, this exciton-based transfer mechanism supersedes Förster-type energy hopping among individual dyes,[61,62] facilitating a more efficient delivery of the harvested light energy to the charge-separation sites. Another potential contributor to the enhanced performance may be the condensed and more ordered medium, which would benefit the ET processes by lowering the extent of energy loss due to vibrations, that is, the electron-phonon coupling,[63,64] within the lipid matrix. A good number of recent investigations have highlighted the general occurrence of exciton formation[2,61] in photosynthetic complexes, which nature employs to fight off energy losses due to electron-phonon coupling and disorders in soft protein matrices. By this mechanism, for example, a higher level of coherence of excited states is achieved in the FMO protein,[65] and additional quantum-mechanical states are activated for ET and trapping in purple bacteria.[66]

It is also important to note that the differences observed in the absorption spectra are absent in their corresponding photoaction spectra. As shown in Figure 2.8 inset, the lipid deposits with/without cholesterol display essentially identical photoaction profiles, that is, the peak position

and relative intensity, despite that the photocurrent is more than tripled in the cholesterol-containing samples. These results indicate that, instead of the exciton states, it is the same first singlet excited state (S1) of individual rhodamines that is directly responsible for the charge separation in both complexes. To account for this seemingly surprising disparity, one needs to realize the fact that only those dyes situated within the bilayer are close enough to the bilayer-embedded fullerenes to directly participate in the electron transfer with the latter. Although exciton formation speeds up ET within the cholesterol-containing deposits, the harvested light energy has to be first funneled to and collected by these interfacial rhodamines, and the subsequent charge separation events take place primarily between individual electron donors and acceptors. Thus, similar to their natural counterpart, for example, BChl pigments in GSB (Figure 2.1), these lipid-assembled rhodamine dyes can carry out either ET or charge separation depending on their location and surrounding partners in the photosynthetic machinery.

2.4 Conclusions

Following nature's lead, we have developed multilayer lipid assembled supercomplexes to mimic key steps in photosynthesis. Efficient PeT is identified between rhodamine and fullerene, which adds this class of dyes into the repository of small-molecule organic photovoltaics. The remarkable possibility of using a lipid matrix to improve photoconversion efficiency is further demonstrated by cholesterol, whose addition triggers exciton formation that leads to faster ET in these lipid nanoassemblies. Our approach should be immediately useful in designing new models to study the photodynamics of dye aggregates under quasi-natural settings. Constructed right, these systems should even be able to host or interface with natural photosynthetic components to interrogate photoelectrochemical properties of the latter or to form hybrid photoconverting

devices. Possibilities to further enhance the functionality and performance of these lipid assembled supercomplexes are equally exciting. For instance, it should be possible to extend the current design by including multiple dyes to occupy different locations in the lipid matrix. Alternatively, additional lipid structures and layers can be introduced into these lipid assemblies for more efficient light harvesting and electronic excitation transfer. Some of these ideas are currently being explored in this laboratory.

References

1. Molecular Mechanisms of Photosynthesis; Blankenship, R. E., Ed.; Blackwell Science Ltd.: Oxford, U.K., 2002.
2. Cheng, Y.-C.; Fleming, G. R. Dynamics of Light Harvesting in Photosynthesis. *Annu. Rev. Phys. Chem*. **2009**, *60*, 241-262.
3. Scholes, G. D.; Fleming, G. R.; Olaya-Castro, A.; van Grondelle, R. Lessons from Nature About Solar Light Harvesting. *Nat. Chem*. **2011**, *3*, 763-774.
4. Calvin, M. Simulating Photosynthetic Quantum Conversion. *Acc. Chem. Res*. **1978**, *11*, 369-374.
5. Gust, D.; Moore, T. A.; Moore, A. L. Mimicking Photosynthetic Solar Energy Transduction. *Acc. Chem. Res*. **2001**, *34*, 40-48.
6. Iida, K.; Nango, M.; Matsuura, M.; Yamaguchi, M.; Sato, K.;Tanaka, K.; Akimoto, K.; Yamashita, K.; Tsuda, K.; Kurono, Y. Energy Transfer and Electron Transfer of Poly(Ethylene Glycol)-Linked Fluorinated Porphyrin Derivatives in Lipid Bilayers. *Langmuir* **1996**, *12*, 450-458.

7. Zhan, W.; Jiang, K. A Modular Photocurrent Generation System Based on Phospholipid-Assembled Fullerenes. *Langmuir* **2008**, *24*, 13258-13261.
8. Lymar, S. V.; Parmon, V. N.; Zamaraev, K. I. Photoinduced Electron Transfer Across Membranes. *Top. Curr. Chem*. **1991**, *159*, 1-65.
9. Olson, J. M. Chlorophyll Organization and Function in Green Photosynthetic Bacteria. *Photochem. Photobiol*. **1998**, *67*, 61-75.
10. Frigaard, N.-U.; Chew, A. G. M.; Li, H.; Maresca, J. A.; Bryant, D. A. Chlorobium tepidum: Insights into the Structure, Physiology, and Metabolism of a Green Sulfur Bacterium Drived from the Complete Genome Sequence. *Photosynth. Res*. **2003**, *78*, 93-117.
11. Holzwarth, A. R.; Griebenow, K.; Schaffner, K. Chlorosomes, Photosynthetic Antennae with Novel Self-Organized Pigment Structures. *J. Photochem. Photobiol. A.* **1992**, *65*, 61-71.
12. Oostergetel, G. T.; van Amerongen, H.; Boekema, E. J. The Chlorosome: A Prototype for Efficient Light Harvesting in Photosynthesis. *Photosynth. Res*. **2010**, *104*, 245-255.
13. Pedersen, M. Ø.; Linnanto, J.; Frigaard, N.-U.; Nielsen, N. C.; Miller, M. A Model of the Protein−Pigment Baseplate Complex in Chlorosomes of Photosynthetic Green Bacteria. *Photosynth. Res*. **2010**, *104*, 233-243.
14. Wen, J.; Zhang, H.; Gross, M. L.; Blankenship, R. E. Membrane Orientation of the FMO Antenna Protein from Chlorobaculum tepidum as Determined by Mass Spectrometry-Based Footprinting. *Proc. Natl. Acad. Sci. U. S. A.* **2009**, *106*, 6134-6139.
15. Tronrud, D. E.; Wen, J.; Gay, L.; Blankenship, R. E. The Structural Basis for the Difference in Absorbance Spectra for the FMO Antenna Protein from Various Green Sulfur Bacteria. *Photosynth. Res*. **2009**, *100*, 79-87.

16. Ben-Shem, A.; Frolow, F.; Nelson, N. Evolution of Photosystem I From Symmetry through Pseudosymmetry to Asymmetry. *FEBS Lett*. **2004**, *564*, 274-280.

17. Jiang, K.; Xie, H.; Zhan, W. Photocurrent Generation from $Ru(bpy)_3^{2+}$ Immobilized on Phospholipid/Alkanethiol Hybrid Bilayers. *Langmuir* **2009**, *25*, 11129-11136.

18. Attwood, S. J.; Choi, Y.; Leonenko, Z. Preparation of DOPC and DPPC Supported Planar Lipid Bilayers for Atomic Force Microscopy and Atomic Force Spectroscopy. *Int. J. Mol. Sci*. **2013**, *14*, 3514-3539.

19. Hwang, K. C.; Mauzerall, D. Photoinduced Electron Transport across a Lipid Bilayer Mediated by C70. *Nature* **1993**, *361*, 138-140.

20. The estimate is obtained as follows. Total lipid area per liposome is twice $4 \times \pi \times (40)^2$ nm^2, which is ~40 000 nm^2. This area corresponds to ~57 000 lipid molecules, approximated using the area occupied per DPPC in a bilayer, 0.7 nm^2. Factoring in the dye loading, 5%, then gives the number in the main text.

21. Liu, J.; Jiang, X.; Ashley, C.; Brinker, C. J. Electrostatically Mediated Liposome Fusion and Lipid Exchange with a Nanoparticle-Supported Bilayer for Control of Surface Charge, Drug Containment, and Delivery. *J. Am. Chem. Soc*. **2009**, *131*, 7567-7569.

22. Akita, H.; Kudo, A.; Minoura, A.; Yamaguti, M.; Khalil, I. A.; Moriguchi, R.; Masuda, T.; Danev, R.; Nagayama, K.; Kogure, K.; Harashima, H. Multi-Layered Nanoparticles for Penetrating the Endosome and Nuclear Membrane via a Step-Wise Membrane Fusion Process. *Biomaterials* **2009**, *30*, 2940-2949.

23. Solon, J.; Streicher, P.; Richter, R.; Brochard-Wyart, F.; Bassereau, P. Vesicles Surfing on a Lipid Bilayer: Self-Induced Haptotactic Motion. *Proc. Natl. Acad. Sci. U. S. A.* **2006**, *103*, 12382-12387.

24. Gadella, T. W. J., Jr.; Jovin, T. M.; Clegg, R. M. Fluorescence Lifetime Imaging Microscopy (FLIM): Spatial Resolution of Microstructures on the Nanosecond Time Scale. *Biophys. Chem.* **1993**, *48*, 221-239.

25. MacDonald, R. I. Characteristics of Self-quenching of the Fluorescence of Lipid-conjugated Rhodamine in Membranes. *J. Biol. Chem.* **1990**, *265*, 13533-13539.

26. Castro, B. M.; de Almeida, R. F. M.; Fedorov, A.; Prieto, M. The Photophysics of a Rhodamine Head Labeled Phospholipid in the Identification and Characterization of Membrane Lipid Phases. *Chem. Phys. Lipids* **2012**, *165*, 311-319.

27. Yamada, H.; Imahori, H.; Nishimura, Y.; Yamazaki, I.; Ahn, T. K.; Kim, S. K.; Kim, D.; Fukuzumi, S. Photovoltaic Properties of Self-Assembled Monolayers of Porphyrins and Porphyrin-Fullerene Dyads on ITO and Gold Surfaces. *J. Am. Chem. Soc.* **2003**, *125*, 9129-9139.

28. D'Souza, F.; Chitta, R.; Gadde, S.; Shafiqul Islam, D.-M.; Schumacher, A. L.; Zandler, M. E.; Araki, Y.; Ito, O. Design and Studies on Supramolecular Ferrocene-Porphyrin-Fullerene Constructs for Generating Long-Lived Charge Separated States. *J. Phys. Chem. B* **2006**, *110*, 25240-25250.

29. Huang, J.; Stockwell, D.; Boulesbaa, A.; Guo, J.; Lian, T. Comparison of Electron Injection Dynamics from Rhodamine B to In2O3, SnO2, and ZnO Nanocrystalline Thin Films. *J. Phys. Chem. C* **2008**, *112*, 5203-5212.

30. Salafsky, J.; Groves, J. T.; Boxer, S. G. Architecture and Function of Membrane Proteins in Planar Supported Bilayers: A Study with Photosynthetic Reaction Centers. *Biochemistry* **1996**, *35*, 14773-14781.

31. Zhan, W.; Jiang, K.; Smith, M. D.; Bostic, H. E.; Best, M. D.; Auad, M. L.; Ruppel, J. V.; Kim, C.; Zhang, X. P. Photocurrent Generation from Porphyrin/Fullerene Complexes Assembled in a Tethered Lipid Bilayer. *Langmuir* **2010**, *26*, 15671-15679.
32. Liposomes: A Practical Approach; New, R. R. C., Ed.; IRL Press: Oxford, U.K., **1990**.
33. Róg, T.; Pasenkiewicz-Gierula, M.; Vattulainen, I.; Karttunen, M. Ordering Effects of Cholesterol and Its Analogues. *Biochim. Biophys. Acta, Biomembr*. **2009**, *1788*, 97-121.
34. Hofsäβ, C.; Lindahl, E.; Edholm, O. Molecular Dynamics Simulations of Phospholipid Bilayers with Cholesterol. *Biophys. J*. **2003**, 84, 2192-2206.
35. Yeagle, P. L. Cholesterol and the Cell Membrane. *Biochim. Biophys. Acta, Rev. Bioenerg*. **1985**, *822*, 267-287.
36. Craven, B. M. Crystal Structure of Cholesterol Monohydrate. *Nature* **1976**, *260*, 727−729.
37. Sankaram, M. B.; Thompson, T. E. Modulation of Phospholipid Acyl Chain Order by Cholesterol. A Solid-State Deuterium NuclearMagnetic Resonance Study. *Biochemistry* **1990**, *29*, 10676-10684.
38. Reinl, H.; Brumm, T.; Bayerl, T. M. Changes of the Physical Properties of the Liquid-Ordered Phase with Temperature in Binary Mixtures of DPPC with Cholesterol. *Biophys. J*. **1992**, *61*, 1025-1035.
39. Ho, C.; Slater, S. J.; Stubbs, C. D. Hydration and Order in Lipid Bilayers. *Biochemistry* **1995**, *34*, 6188-6195.
40. Alwarawrah, M.; Dai, J.; Huang, J. A Molecular View of the Cholesterol Condensing Effect in DOPC Lipid Bilayers. *J. Phys. Chem. B* **2010**, *114*, 7516-7523.
41. McIntosh, T. J. The Effect of Cholesterol on the Structure of Phosphatidylcholine Bilayers. *Biochim. Biophys. Acta Biomembr*. **1978**, *513*, 43-58.

42. Chiu, S. W.; Jakobsson, E.; Mashl, R. J.; Scott, H. L. Cholesterol-Induced Modifications in Lipid Bilayers: A Simulation Study. *Biophys. J.* **2002**, *83*, 1842-1853.
43. Marsh, D. Cholesterol-Induced Fluid Membrane Domains: A Compendium of Lipid-Raft Ternary Phase Diagrams. *Biochim. Biophys. Acta Biomembr.* **2009**, *1788*, 2114-2123.
44. Vist, M. R.; Davis, J. H. Phase Equilibria of Cholesterol/Dipalmitoylphosphatidylcholine Mixtures: Deuterium Nuclear Magnetic Resonance and Differential Scanning Calorimetry. *Biochemistry* **1990**, *29*, 451-464.
45. Sankaram, M. B.; Thompson, T. E. Cholesterol-Induced Fluid-Phase Immiscibility in Membranes. *Proc. Natl. Acad. Sci. U. S. A.* **1991**, *88*, 8686-8690.
46. Veatch, S. L.; Keller, S. L. Seeing Spots: Complex Phase Behavior in Simple Membranes. *Biochim. Biophys. Acta Mol. Cell Res.* **2005**, *1746*, 172-185.
47. DPPG displays very similar phase behavior as DPPC when coexisting with the latter, e.g., refs 48-50.
48. Singh, H.; Emberley, J.; Morrow, M. R. Pressure Induces Interdigitation Differently in DPPC and DPPG. *Eur. Biophys. J.* **2008**, *37*, 783−792.
49. Blosser, M. C.; Starr, J. B.; Turtle, C. W.; Ashcraft, J.; Keller, S. L. Minimal Effect of Lipid Charge on Membrane Miscibility Phase Behavior in Three Ternary Systems. *Biophys. J.* **2013**, *104*, 2629-2638.
50. Mukai, M.; Regen, S. L. Exchangeable Mimics of DPPC and DPPG Exhibiting Similar Nearest-Neighbor Interactions in Fluid Bilayers. *Langmuir* **2015**, *31*, 12674-12678.
51. Bagatolli, L. A.; Gratton, E. Two Photon Fluorescence Microscopy of Coexisting Lipid Domains in Giant Unilamellar Vesicles of Binary Phospholipid Mixtures. *Biophys. J.* **2000**, *78*, 290−305.

52. Veatch, S. L.; Soubias, O.; Keller, S. L.; Gawrisch, K. Critical Fluctuations in Domain-Forming Lipid Mixtures. *Proc. Natl. Acad. Sci. U. S. A.* **2007**, *104*, 17650-17655.

53. Davis, J. H.; Clair, J. J.; Juhasz, J. Phase Equilibria in DOPC/DPPC-d_{62}/Cholesterol Mixtures. *Biophys. J*. **2009**, *96*, 521-539.

54. de Almeida, R. F. M.; Borst, J.; Fedorov, A.; Prieto, M.; Visser, A. J. W. G. Complexity of Lipid Domains and Rafts in Giant Unilamellar Vesicles Revealed by Combining Imaging and Microscopic and Macroscopic Time-Resolved Fluorescence. *Biophys. J*. **2007**, *93*, 539-553.

55. Kemnitz, K.; Yoshihara, K. Entropy-Driven Dimerization of Xanthene Dyes in Nonpolar Solution and Temperature-Dependent Fluorescence Decay of Dimers. *J. Phys. Chem*. **1991**, *95*, 6095-6104.

56. Burghardt, T. P.; Lyke, J. E.; Ajtai, K. Fluorescence Emission and Anisotropy from Rhodamine Dimers. *Biophys. Chem*. **1996**, *59*, 119-131.

57. Blackman, M. J.; Corrie, J. E. T.; Croney, J. C.; Kelly, G.;Eccleston, J. F.; Jameson, D. M. Structural and Biochemical Characterization of a Fluorogenic Rhodamine-Labeled Malarial Protease Substrate. *Biochemistry* **2002**, *41*, 12244-12252.

58. Kasha, M. Energy Transfer Mechanisms and the Molecular Exciton Model for Molecular Aggregates. *Radiat. Res*. **1963**, *20*, 55-70.

59. Spano, F. C. The Spectral Signatures of Frenkel Polarons in Hand J-Aggregates. *Acc. Chem. Res*. **2010**, *43*, 429-439.

60. Bogen, S.-T.; Karolin, J.; Molotkovsky, J. G.; Johansson, L. B.-Å. 1,32-Dihydroxy-Dotriacontane-bis(Rhodamine) 101 Ester. *J. Chem. Soc., Faraday Trans*. **1998**, *94*, 2435-2440.

61. Scholes, G. D. Designing Light-Harvesting Antenna Systems Based on Superradiant Molecular Aggregates. *Chem. Phys*. **2002**, *275*, 373-386.

62. Brandes, T. Coherent and Collective Quantum Optical Effects in Mesoscopic Systems. *Phys. Rep*. **2005**, *408*, 315-474.

63. Seifert, U. Configurations of Fluid Membranes and Vesicles. *Adv. Phys*. **1997**, *46*, 13-137.

64. Coropceanu, V.; Cornil, J.; da Silva Filho, D. A.; Olivier, Y.; Silbey, R.; Brédas, J.-L. Charge Transport in Organic Semiconductors. *Chem. Rev*. **2007**, *107*, 926-952.

65. Cho, M.; Vaswani, H. M.; Brixner, T.; Stenger, J.; Fleming, G. R. Exciton Analysis in 2D Electronic Spectroscopy. *J. Phys. Chem. B* **2005**, *109*, 10542-10556.

66. Cogdell, R. J.; Gall, A.; Köhler, J. The Architecture and Function of the Light-Harvesting Apparatus of Purple Bacteria: From Single Molecules to In Vivo Membranes. *Q. Rev. Biophys*. **2006**, *39*, 227-324.

Chapter 3

Mimicking Photosynthesis with Supercomplexed Lipid Nanoassemblies: Other Cases

3.1 Introduction

In this study, we continue our exploration of using lipid nanoassemblies to mimic photosynthesis. We adopted the same design detailed in Chapter 2, that is, two-tier lipid nanoassemblies in which anionic liposomes are electrostatically held on top of a solid supported cationic lipid bilayer.[1] However, instead of using DPPC as the main component, we investigated two lipid nanoassemblies that are mainly made up of POPC (1-palmitoyl-2-oleoyl-*sn*-glycero-3-phosphocholine) in the presence/absence of cholesterol, and DPPE (1,2-dipalmitoyl-*sn*-glycero-3-phosphoethanolamine) with incorporated cholesterol, respectively. The goal of this study is to understand the effect of l_d phase and l_d-l_o coexisting phases on the photo-conversion efficiency by using liposomes composed of POPC and cholesterol. Cholesterol-induced l_o domain formation in pure l_d phase has been reported elsewhere.[3-9] Besides, POPC containing one saturated and one unsaturated chain is considered a more biologically relevant lipid.[10] In addition, we are also interested in photo-electrochemical conversion in DPPE/Cholesterol system, since DPPE is a major component of plasma membranes, and interestingly they are asymmetrically distributed in the inner/outer leaflets.[11,12] Of particular interest is the previous finding that DPPE/cholesterol bilayers are reported to show domain coexistence.[12]

Herein, photocurrent generation from such two mimics are first presented and rationalized by using UV-Vis spectroscopy, steady-state fluorescence spectroscopy, time-correlated single photon counting, AFM, and transient absorption spectroscopy.

3.2 Experimental Section

3.2.1 Chemicals

Lipids, including 1,2-dioleoyl-*sn*-glycero-3-phosphocholine (DOPC), 1,2-dioleoyl-3-trimethylammonium-propane (DOTAP), 1-palmitoyl-2-oleoyl-*sn*-glycero-3-phosphocholine (POPC), 1-palmitoyl-2-oleoyl-*sn*-glycero-3-phospho-(1'-*rac*-glycerol) (sodium salt) (POPG), 1,2-dipalmitoyl-*sn*-glycero-3-phosphoethanolamine (DPPE), 1,2-dipalmitoyl-*sn*-glycero-3-phospho-rac-(1-glycerol) sodium salt (DPPG), 1,2-dioleoyl-*sn*-glycero-3-phosphoethanolamine-N-(lissamine rhodamine B sulfonyl) (ammonium salt) (Rho-DOPE), and 1,2-dipalmitoyl-*sn*-glycero-3-phosphoethanolamine-N-(lissamine rhodamine B sulfonyl) (ammonium salt) (Rho-DPPE), were purchased from Avanti Polar Lipids (Alabaster, AL). See Fig. 3.1 for chemical structures of main lipids used in this work. Monomalonic fullerene C_{60} was synthesized according to a procedure described previously.[13] Other chemicals, including cholesterol, 4-(2-hydroxyethyl) piperazine-1-ethanesulfonic acid (HEPES), (+)-sodium L-ascorbate, 1-dodecanethiol, D-(+)-glucose, glucose oxidase from Aspergillus niger, and catalase from bovine liver, were obtained from Sigma-Aldrich. All solutions employed in this work were prepared using 18.2 MΩ·cm deionized (DI) water (Millipore).

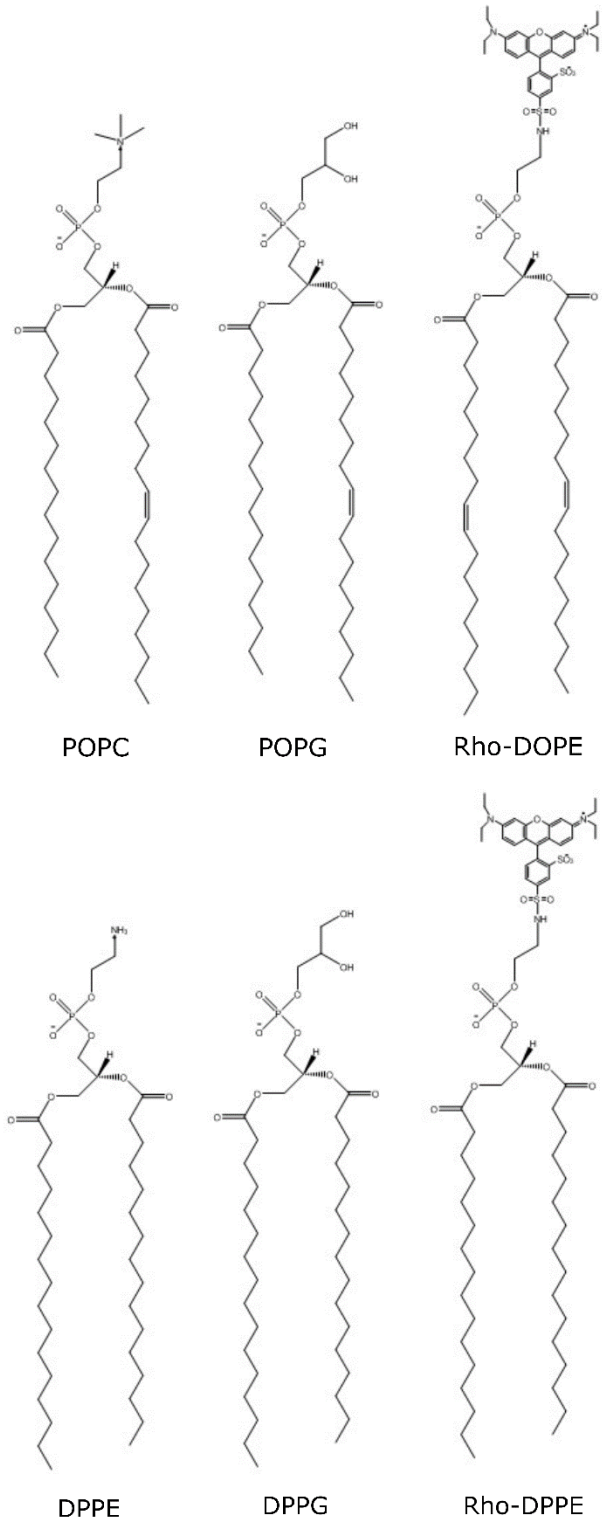

Figure 3.1 Chemical structures of main lipids used in this work.

3.2.2 Preparation of Two-Tier Lipid Nanoassemblies

The two-tier lipid nanoassemblies were prepared by following the procedure described in chapter 2. In brief, the formation of a single lipid bilayer (with/without fullerene embedded) on glass or indium tin oxide (ITO)-coated substrates was achieved by vesicle fusion using liposome solutions. Then anionic liposomes, prepared by an extrusion based method, were introduced into the Teflon cell housing the solid supported lipid bilayer and incubated for 1h. The unattached liposomes were similarly removed from the cell by exchanging with HEPES buffer.

3.2.3 Microscopy

Fluorescence images of lipid samples deposited on glass substrates were collected on a Nikon A1+/MP confocal scanning laser (561 nm) microscope (Nikon Instruments, Inc., Melville, NY) together with a 595 ± 25 nm emission filter.

The AFM images were obtained in a fluid using a Bruker MultiMode 8 atomic force microscope (Bruker, USA) operated in the PeakForce quantitative nanomechanical mapping (PeakForce QNM) mode. In-fluid measurements were carried out with silicon nitride probes (Model: DNP S10, Bruker, 0.24-0.35 N/m, 10 nm tip radius) at a scan rate of 1 Hz and a resolution of 512 pixels × 512 pixels.

3.2.4 Spectroscopy

Absorption spectra of liposome samples containing Rho-DOPE or Rho-DPPE were acquired on a UV-Vis spectrophotometer (Cary 50 Bio, Varian). Steady-state fluorescence spectroscopy data of the two-tier lipid nanoassemblies formed on glass substrates were recorded using a PI Acton spectrometer (SpectraPro SP 2356, Acton, NJ) connected to the side port of an

epifluorescence microscope (Nikon TE-2000 U, Japan). The fluorescence signal was recorded using a charge-coupled device (CCD) camera (PI Acton PIXIS: 400B, Acton, NJ) attached to the spectrometer. The excitation was provided by a mercury lamp (X-Cite 120, EXFO, Ontario, Canada) filtered at 475 ± 20 nm; and a long-pass filter with a cutoff wavelength of 561 nm was used for emission. The obtained spectra are not corrected for distortions due to spectral nonuniformity associated with the filters and CCD camera, which are expected to be small.

Fluorescence lifetimes of rhodamines either suspended in buffer solutions or assembled in the two-tier lipid nanoassemblies were measured using a time-correlated single-photon counting system, which comprises a synchronizer/analyzer (PicoHarp 300, PicoQuant, Germany), a picosecond pulsed diode laser (PDL 800-B, wavelength: 405 nm), and a single-photon counting module (PDM Series, Micro Photon Devices, Italy). In the former case, a quartz fluorometer cell (Sub Micro type, Starna Cells, CA) was used to hold liposome solutions; the final rhodamine concentration in all samples was controlled to be ~0.5 μM. To be able to capture fluorescence signals emitted directly from the lipid nanoassemblies, this system was further coupled to a fluorescence microscope (Nikon TE-2000U), in which both the laser head and the photon counting module were directly mounted onto the microscope and optically aligned. All lipid samples were formed on glass substrates (Corning, Micro Slide 2947), in which all bottom lipid bilayers contain DOPC/DOTAP in an 80/20 mixing ratio with/without 5 mol% C_{60}. Throughout the measurements, the laser head was operated at a repetition rate of 10 MHz. According to the manufacturer, this laser produces a minimum pulse width of 59 ps and a power of 29 pJ/pulse. All lifetime data were fitted by the exponential-tail fit method included in the fitting software package, FluoFit (PicoQuant, Germany). The equation used is $I(t) = \sum_{i=1}^{n} A_i e^{-\frac{t}{\tau_i}} + Bkgr._{DEC}$, in which A_i is the amplitude of the ith component, in counts, in the first fitting range channel; τ_i is the lifetime of the

i^{th} component; $Bkgr._{DEC}$ is the decay background, in counts. Oxygen was removed from all media by purging with argon for at least 30 min right before the fluorescence measurements.

Transient absorption (TA) spectra were recorded with a pump-probe spectrometer based on a regenerative amplified titanium-sapphire laser system (Coherent Legend, 800 nm, 150 fs, 2.5 mJ/pulse, and 1 kHz repetition rate). Liposome samples with a total lipid concentration of ~2.5 mM in HEPES buffer (10 mM HEPES, 100 mM NaCl, pH 7.70) were excited using a pump pulse with a center wavelength of 515 nm obtained by sum frequency generation of the signal from an optical parametric amplifier (Opera, Coherent) and a small portion of (~7%) 800 nm output in a BBO crystal. The absorption variations were probed with a white light continuum from 430 to 750 nm generated by attenuating and focusing an 800 nm pulse into a 1 mm thick sapphire window. The pump and probe beam diameters at the sample were 300 and 150 μm, respectively. The probe beam after passing through the sample was collimated and focused into a fiber optics-coupled multichannel spectrometer with complementary metaloxide semiconductor (CMOS) sensors and detected at a frequency of 1 kHz. The pump beam was chopped with a synchronized chopper to 500 Hz. The changes in absorbance for the pumped and unpumped samples were calculated. Cuvettes of 1 mm path length were used for all spectroscopy measurements. The instrument response function (IRF) of this system was measured to be ~150 fs by measuring solvent responses under the same experimental conditions.

3.2.5 Photocurrent Generation

The photoelectrochemical measurements were carried out in three-electrode Teflon photoelectrochemical cells as described in Chapter 2. Three-electrode system is used consisting an ITO substrate covered with lipid nanoassemblies as the working electrode, a Pt wire as the counter

electrode, and Ag/AgCl (in saturated KCl) as the reference electrode. All photocurrents were generated and collected under cell open-circuit potential conditions without an extra potential bias. For photocurrent generation, 50 mM ascorbate in HEPES buffer (10 mM HEPES, 100 mM NaCl, pH 7.70) was used as the sacrificial electron donor. Oxygen in the cell was removed by following the procedure described in Chapter 2. To obtain photoaction spectra, photocells containing different lipid structures were illuminated with a 150 W xenon lamp (Ushio, Japan) whose wavelength selection was achieved using a computer-controlled fluorescence spectrophotometer (RF-5301, Shimadzu, Japan). The photoaction spectra reported in the main text have been corrected for nonuniform spectral distribution of excitation in 5 nm intervals using a silicon photometer (PM120, Thorlabs).

3.3 Results and Discussion

3.3.1 POPC/Cholesterol System

POPC/cholesterol binary systems containing ~10-45 mol% cholesterol, display l_o/l_d coexistence, as determined by several methods including time-resolved fluorescence spectroscopy,[3-5] fluorescence anisotropy,[5,6] calorimetry,[6-8] NMR[9] together with simulation work[14]. In our hands, we found that no blue shift of 0-0 absorption band (~575 nm) was found from 5 mol% Rho-DOPE in liposomes containing 30 mol% cholesterol, compared to that without cholesterol, indicating no aggregation (Fig. 3.2). This is in line with the experimental results by Castro et al.[15] Rather differently in the DPPC case,[1] ~10 nm blue shift of the shoulder peak (~540 nm) clearly indicates formation of aggregates when 30 mol% of cholesterol is incorporated. Moreover, the relative absorbance ratio of 0-0 absorption peak and shoulder peak increases as the concentration of cholesterol is increased. From findings by our work[1] and others' work[14], changes

in the intensity ratio of shoulder peak to main peak have been employed as a sensitive fingerprint to probe rhodamine aggregate formation. Here, the moderately increased intensity of such a shoulder band likely suggests association of dyes, in other words, so-called dye clusters,[15] due to tight lipid packing (Fig. 3.3) and the condensing effect of cholesterol, albeit not triggering dye aggregation, possibly owing to random orientation of dipoles of rhodamine moieties. Since Rho-DOPEs prefer to partition into the l_d phase, we conjecture that they tend to group together to form clusters (Fig. 3.3), when forced into the l_o phase.

This interpretation can be further supported by fluorescence lifetimes of Rho-DOPE in liposomes acquired by using time-correlated single photon counting, as shown in Fig. 3.4. The fitted fluorescence lifetimes are listed in Table 3.1. Without cholesterol, the lifetime of Rho-DOPE in liposomes show single component of 1.98 ns, suggesting a random membrane distribution in a uniform l_d phase spanning the whole liposome. Compared to the DPPC case,[1] the lifetime also shows single but much shorter component, due to global self-quenching in gel phase, where the mean lipid molecular surface area is small and thus neighboring dyes are rather close. Nevertheless, no appreciable self-quenching of Rho-DOPE here was observed, simply because of larger mean lipid molecular surface area in lipid disordered phase, which to some extent separates neighboring Rho-DOPEs apart (Fig. 3.3).

When 30 mol% of cholesterol is incorporated into the POPC liposomes, however, two lifetime components are shown with only 3% population of 2.04 ns attributed to Rho-DOPE in l_d phase, which is consistent with the result (1.98 ns) in the case without cholesterol. Evidenced by their much shorter lifetime of 0.91ns, the major population of Rho-DOPEs is located in l_o phase, where the distance between neighboring Rho-DOPEs (as clusters) is greatly reduced and fluorescence lifetime is thus shortened.

When these liposomes are deposited on a solid supported lipid bilayer, Rho-DOPE presented rather different photophysical properties. The fluorescence lifetime (Table 3.2) of Rho-DOPE in liposomes without cholesterol are slightly longer than that from their corresponding liposome suspensions, suggesting there is likely a morphological change of liposomes after deposition. AFM images (Fig. 3.5) show the liposomes are deformed, aggregated, and compressed. Confocal fluorescence imaging (Fig. 3.6) further proves liposome fusion and aggregation.

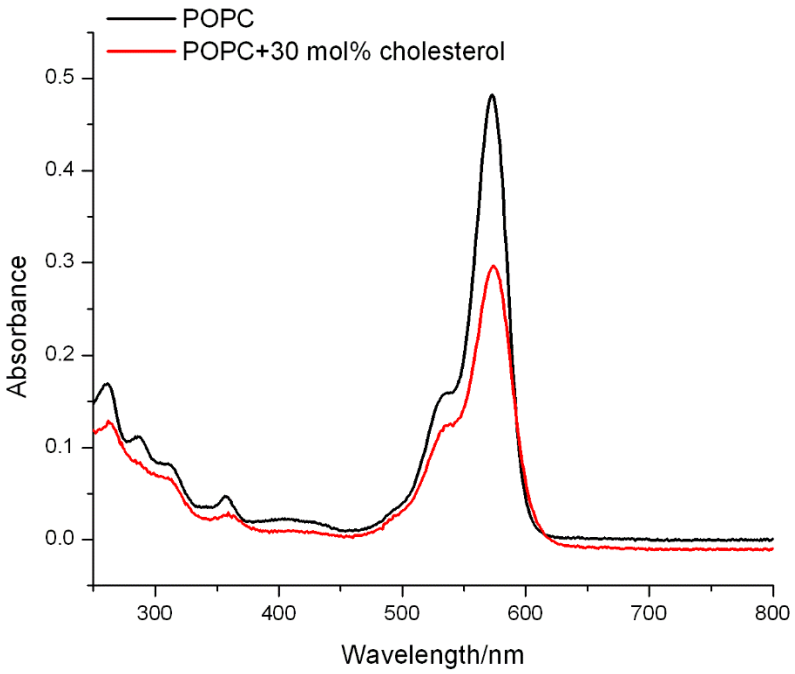

Figure 3.2 Absorption spectra of 5 mol% Rho-DOPE in liposomes in the presence (in red) or absence (in black) of 30 mol% cholesterol. The concentration of rhodamine in both samples is approximately 5 μM.

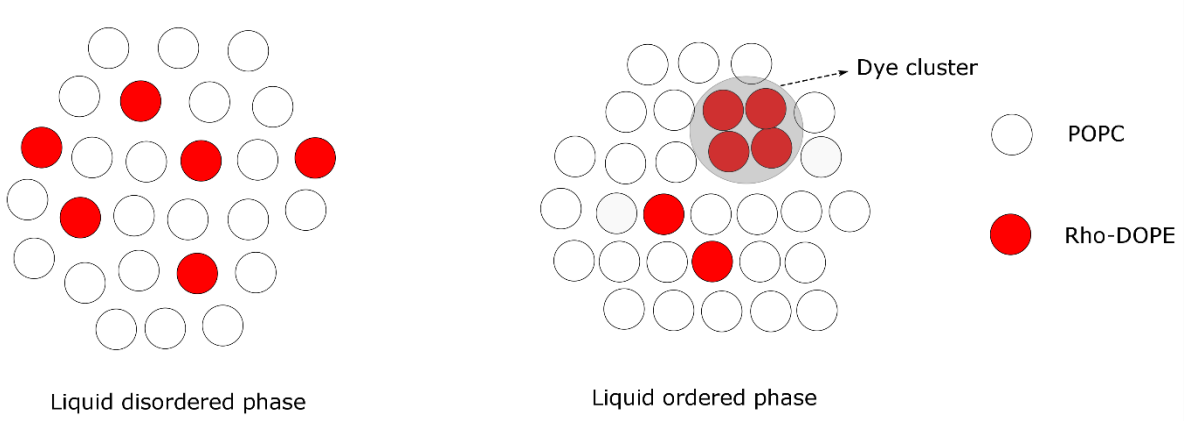

Figure 3.3 Top view of lipid packing in liposomes in liquid disordered (l_d) phase and liquid ordered (l_o) phase.

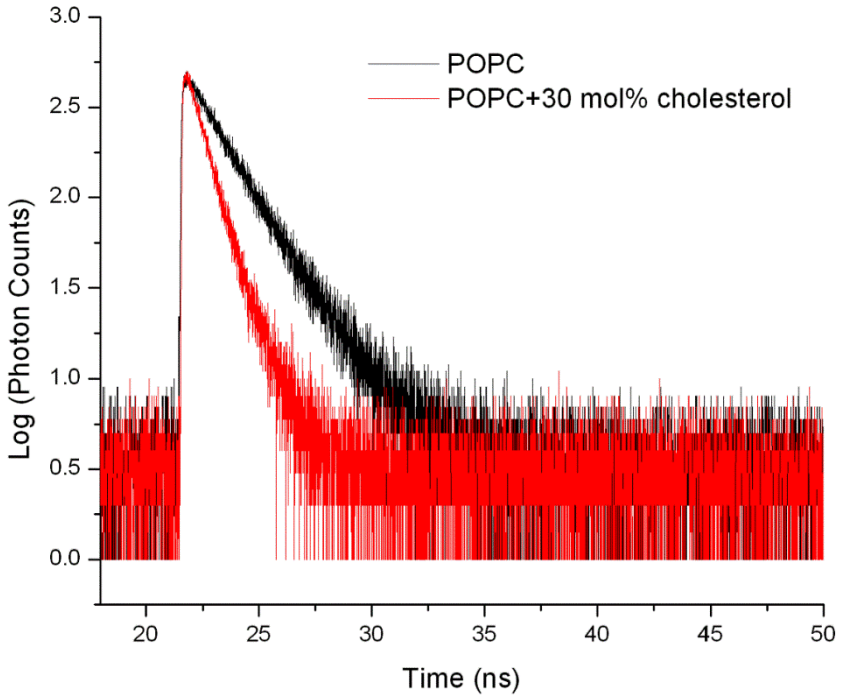

Figure 3.4 Time-resolved fluorescence decay of 5 mol% Rho-DOPE in liposome suspensions in the presence (in red) or absence (in black) of 30 mol% cholesterol. The concentration of rhodamine in both samples is approximately 0.5 μM.

Surprisingly, the fluorescence lifetime has only one component of 2.46 ns, longer than that of Rho-DOPE in l_d phase, when liposomes containing 30 mol% of cholesterol are electrostatically fixed on top of a lipid bilayer. Shorter component of ~1 ns is no longer observed. AFM and confocal images show individual liposomes with negligible fusion are evenly distributed on the substrate, indicative of cholesterol maintaining integrity of liposomes. This seeming discrepancy can be explained as electrostatic binding possibly disrupts the probe distribution, considering the probe, Rho-DOPE here, is negatively charged.

We then assembled these two-tier lipid nanoassemblies onto ITO electrodes so that photocurrent can be generated under continuous irradiation. As shown in Fig. 3.8, for the photocells comprising liposomes containing 5 mol% Rho-DOPE atop and underlying fullerene-coassembled lipid bilayer, the photoaction spectra markedly resemble the absorption spectra of their rhodamine moieties, which indicates rhodamine plays the primary role in capturing light energy and there exists an appreciable photo-induced electron transfer between rhodamine and fullerene, similar to the DPPC system reported in previous chapter. In the absence of cholesterol in the top liposomes, to our surprise, the photocurrent of ~35 nA is much lower than that from its DPPC counterpart (see Chapter 2 for details). However, it leads to an exciting photon-to-electron QE of 7.8%, comparable to that from the DPPC counterpart. This can be attributed to the much lower absorbance of rhodamine in POPC containing lipid nanoassemblies. When there is 30 mol% cholesterol in the liposomes, a much higher photocurrent of ~ 250 nA was observed with a photon-to-electron QE of 13.2%, slightly lower than that of its DPPC counterpart.

In order to understand the reason why a much higher QE was obtained in the presence of cholesterol, we investigated the fluorescence quenching of rhodamine by underlying fullerene by

steady-state fluorescence spectroscopy. As shown in Fig. 3.7A, we obtained a quenching efficiency of 62% and 91% for the nanoasemblies in the absence and presence of 30 mol% cholesterol, respectively. We then carried out a time-correlated single photon counting experiment. The fluorescence decay profile is shown in Fig. 3.7. An exponential tail fitting was done to extract the fluorescence lifetimes (Table 3.2). When C_{60} is coassembled in the underlying lipid bilayer, a shorter fluorescence lifetime of 1.54 ns is observed for the lipid nanoassemblies containing no

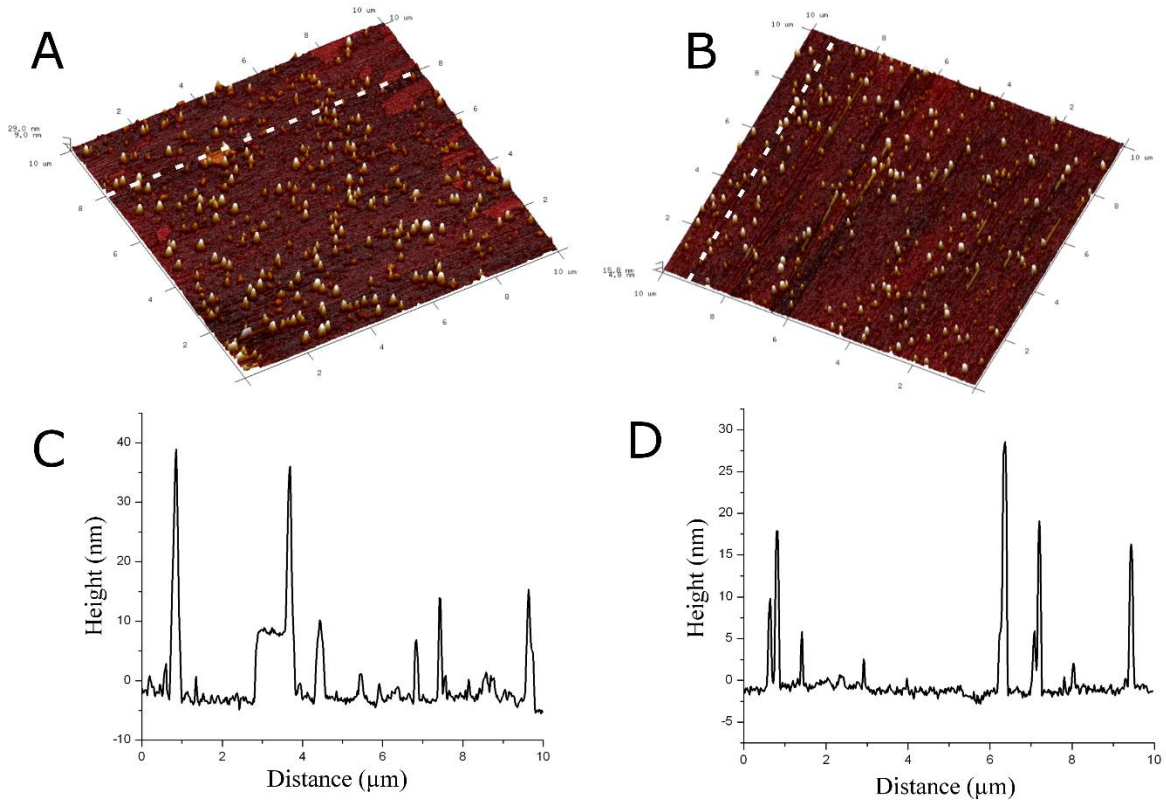

Figure 3.5 Structure of liposomes electrostatically deposited on lipid bilayers as probed by AFM. Liposomes employed: (A) Rho-DOPE/POPG/POPC (5/15/80) and (B) Rho-DOPE/POPG/cholesterol/POPC (5/15/30/50). Corresponding height profiles of lipid nanoassemblies marked by the dashed lines are shown in (C) and (D) See the Experimental Section for more details.

cholesterol. Assuming PeT between rhodamine and fullerene is the only additional pathway competing with fluorescence emission, we obtained a PeT rate constant of 2.1×10^8 s^{-1} by using equation $k_{PeT} = 1/\tau_{F(C60)} - 1/\tau_F$, where $1/\tau_{F(C60)}$ and $1/\tau_F$ are the measured fluorescence lifetime of rhodamine with and without fullerene, respectively. As to the nanoassemblies embedded with fullerene containing 30 mol% cholesterol, two components of fluorescence lifetime are seen. The longer component of 2.11 ns is consistent with that of free liposomes. However, it is slightly shorter than that from otherwise similar fullerene-free lipid nanoassembies, possibly because the morphology of liposomes is perturbed to a certain extent by the co-assembly of fullerene. Using the same equation, we obtained a much higher PeT rate constant of 5.3×10^8 s^{-1}.

Table 3.1 Fluorescence lifetimes of rhodamines assembled in liposomes as probed by time-correlated fluorescence single-photon counting (TCSPC)

Lipid composition (in mole fraction)	Fluorescence lifetime (ns)
Rho-DOPE/POPC/POPG: 5/80/15	1.98 ± 0.05
Rho-DOPE/POPC/POPG/Chol: 5/50/15/30	2.04 ± 0.1 (3%); 0.91 ± 0.006 (97%)

Comparing the PeT rate constants between DPPC and POPC cases, we found k_{PeT} values in DPPC cases are larger than those in POPC counterparts, yet producing rather similar photoconversion efficiency.

Table 3.2 Spectroscopic and photoelectrochemical characteristics of rhodamines assembled in various lipid supercomplexes

Lipid composition in top liposome layer[a]	Fluorescence lifetime (ns)[b]	k_{PeT} (s^{-1})	Photoconversion QE (%)
Rho-DOPE/POPC/POPG: 5/80/15	2.28 ± 0.005[c] 1.54 ± 0.02[d]	- 2.1×10^8	- 7.8 (± 0.3)[e]
Rho-DOPE/POPC/POPG/Chol: 5/50/15/30	2.46 ± 0.01[c] (2.11 ± 0.06 (21%); 0.79 ± 0.04 (79%))[d]	- 5.3×10^8	- 13.2 (± 3.2)[e]

[a]All bottom lipid bilayers contain DOPC/DOTAP in 80/20 mixing ratio in mole fraction with/without 5 additional fractions of C_{60}. [b]Data obtained from TCSPC measurements. [c]Measured with dye alone. [d]With C_{60} co-assembled. [e]Standard deviation, $n = 3$.

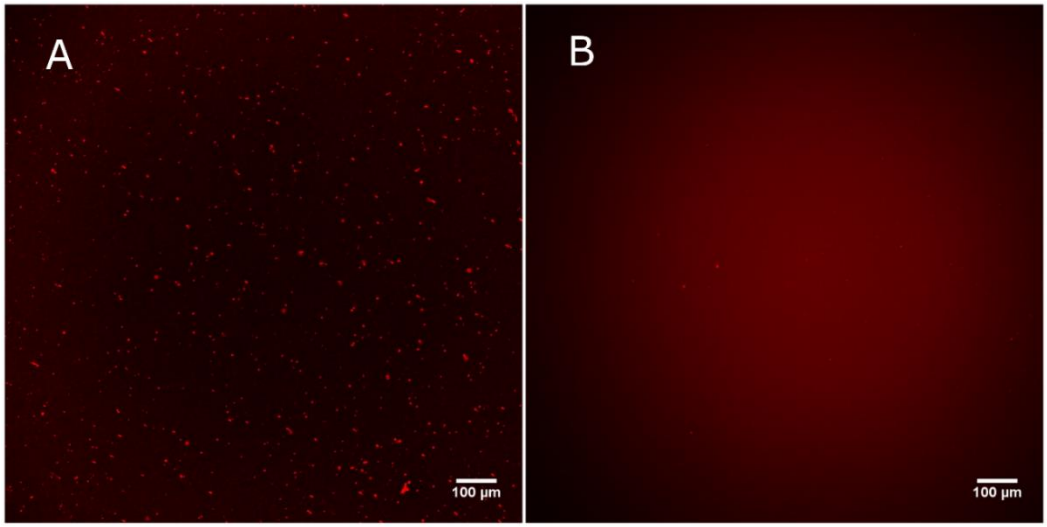

Figure 3.6 Fluorescence micrographs of rhodamine-labeled liposomes electrostatically deposited on oppositely charged lipid bilayer supported on glass. Liposomes used: (A) Rho-DOPE/POPG/POPC (5/15/80), and (B) Rho-DOPE/POPG/cholesterol/POPC (5/15/30/50).

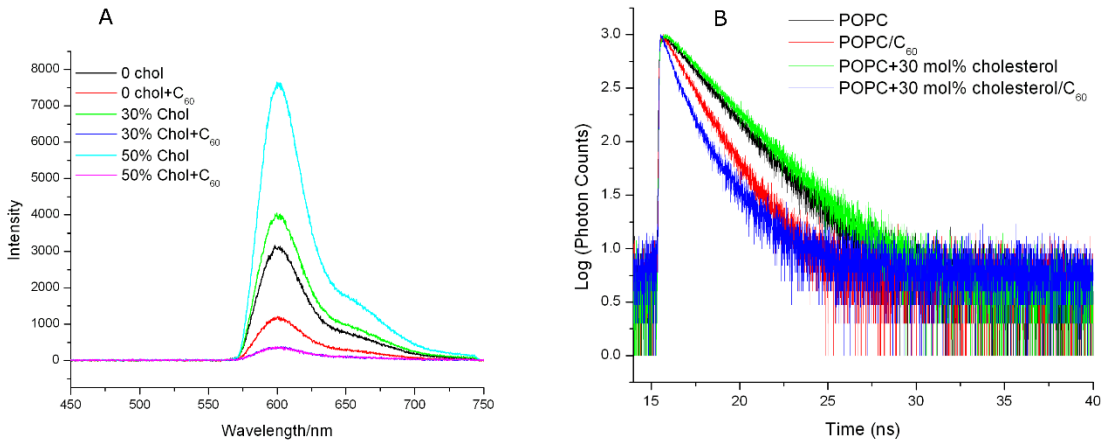

Figure 3.7 Steady-state (A) and time-resolved fluorescence emission spectra (B) from rhodamine assembled in the two-layer lipid nanostructures. All samples contain 5% Rho-DOPE and 15% POPG in the top liposome layer. The complexes in addition contain: 80% POPC (black), 80 % POPC + 5% C_{60} (red), 50% POPC + 30% cholesterol (green), 50% POPC + 30% cholesterol + 5% C_{60} (blue). See the Experimental Section for more details.

3.3.2 DPPE/Cholesterol System

Following the same procedure, we fabricated two-tier lipid nanoassemblies on ITO electrodes, which consist of anionic liposome layers atop and a cationic lipid bilayer at bottom. The liposomes comprise 5 mol% Rho-DPPE, 15 mol% DPPG, 50 mol% DPPE, and 30 mol% cholesterol, whereas the lipid bilayer comprises 15 mol% DOTAP and 80 mol% DOPC coassembled with 5 mol% fullerene. Under continuous irradiation, we acquired the photoaction spectrum (not shown), from which we observed much higher photocurrent produced with an exciting photoconversion quantum efficiency of 14±3.2%.

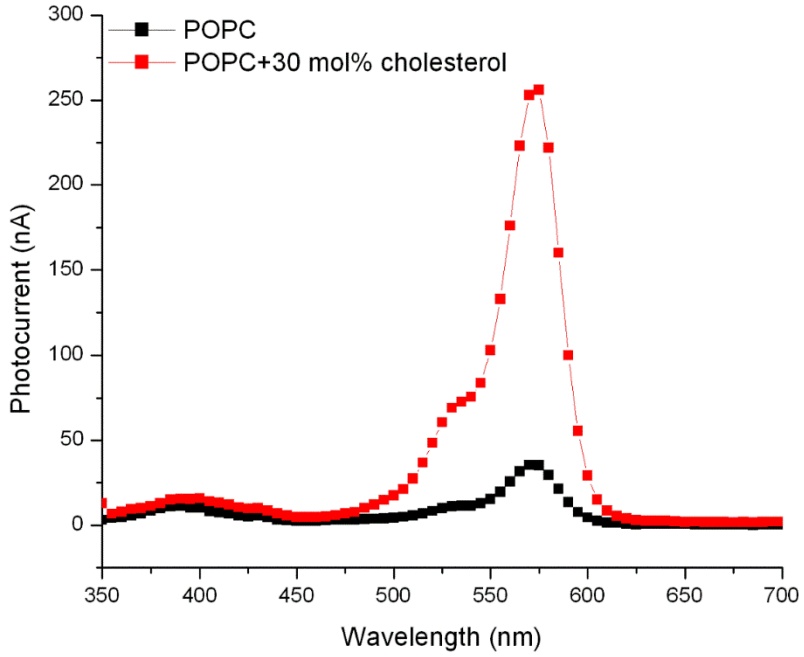

Figure 3.8 Normalized photoaction spectra from lipid-assembled rhodamines/fullerenes without cholesterol (in black) or with 30% cholesterol (in red).

To elucidate the underlying photophysics, we start with absorption spectroscopy. When there is no cholesterol in the liposomes, the absorption spectrum of rhodamine exhibits otherwise similar absorption bands as in DPPC liposomes (Fig. 3.9). Incorporating 15 mol% cholesterol, however, three bands surprisingly appear, including a 0-0 absorption band together with bands at 526 nm and 550 nm, respectively, clearly indicating a new state of dye aggregation. This is plausibly due to that cholesterol can condense DPPE bilayers.[12] These two bands at 526 nm and 550 nm can be presumably attributed to H-aggregrates of rhodamines.[1,15] When the percentage of cholesterol increases from 15 mol% to 30 mol%, the absorbances of H-aggregates decrease. Continuing to increase the concentration of cholesterol to 50 mol%, two bands attributed to H-aggregates of rhodamine disappear. Instead, a shoulder band at 532 nm shows, just as the one

shown in the DPPE liposomes without cholesterol. The only difference lies in different absorbance ratio of the two bands. Almost equal absorbance of two bands indicates existence of rhodamine aggregates in the liposomes containing 50 mol% cholesterol, but the degree of aggregation is much less. This change is in line with results suggested by time-of-flight secondary ion mass spectrometry,[12] where lateral heterogeneity exists with cholesterol lower than 50 mol%, but homogeneous phase appears at 50 mol% cholesterol.

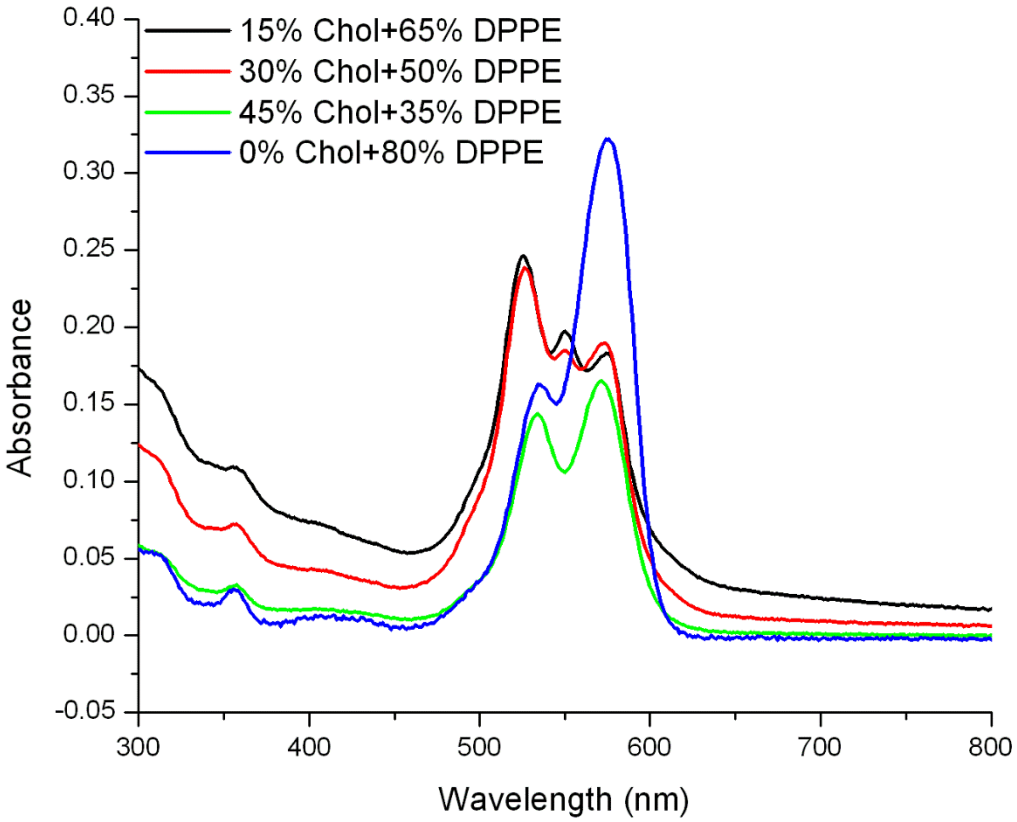

Figure 3.9 Absorption spectra from 5 mol% Rho-DOPE in liposomes containing 15 mol% DPPG and cholesterol and DPPE with different concentrations. The rhodamine concentration in these liposomes is approximately 5 μM.

A transient absorption spectrum (Fig. 3.10A) shows a negative band at 578 nm due to ground-state bleaching and stimulated emission, a negative band at 555 nm attributed to the H-aggregates, and a positive band at 450 nm due to excited state emission. Interestingly, the red shift of the band at 578 nm is less than that in DPPC case. By fitting the kinetic data (Fig. 3.10B), we found the lifetime of excited states has two components, one is about 20 ps, the other is approximately 500 ps (Table 3.1), suggesting rhodamines are distributed in two different environments. For the H-aggregate of rhodamine, the excited state lifetime also shows two components. The longer component is 440 ps, and the shorter one is 42 ps. In order to better appreciate the underlying photodynamics, further experiments such as steady-state and time-resolved fluorescence spectroscopy for lipid nanoassemblies remain to be done. Additionally, AFM should be of great help to provide morphological information.

Table 3.3 Excited-state lifetimes of rhodamines assembled in liposomes as probed by TA spectroscopy and photoconversion quantum yield from lipid nanoassemblies containing such liposomes.

Lipid composition	Excited-state lifetime (ps)			Q.E. (%)
	450 nm	555 nm	578 nm	
Rho-DPPE/DPPG/DPPE/cholesterol: 5/15/50/30, in mole fraction	17 ± 7; 667 ± 106	42 ± 8; 440 ± 49	25 ± 3; 409 ± 26	14 ± 3.2

3.4 Conclusions

In this work, we established another two different systems including POPC and DPPE to mimic natural photosynthesis. They represent different lipid bilayers in that POPC bilayer mostly

in l_d phase, and DPPE is rather complicated because of its relatively small headgroup and capability of formation of intermolecular bonding. Besides, we incorporated cholesterol into the lipid nanoassemblies to induce phase separation, considering that natural photosynthetic membranes are

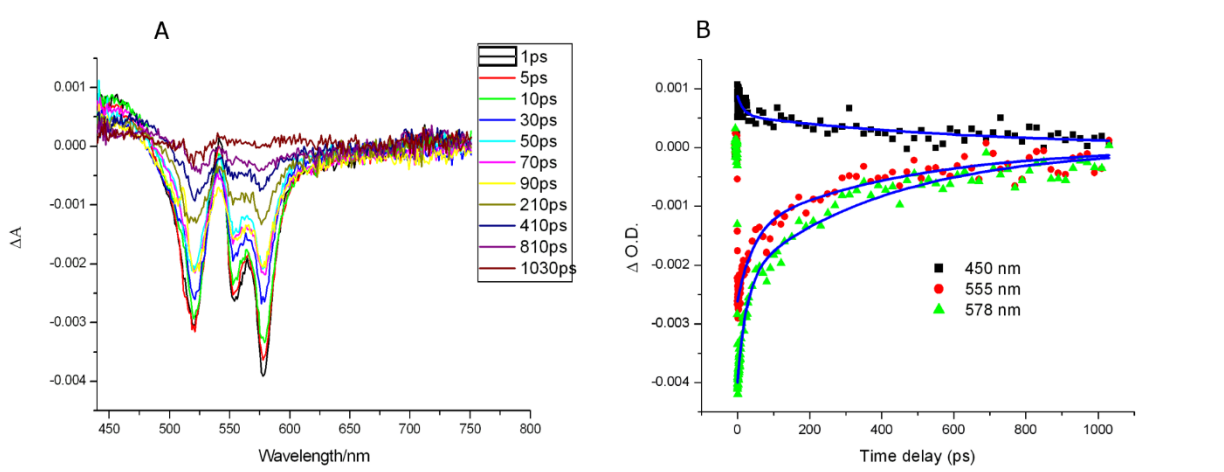

Figure 3.10 TA spectra (A) of rhodamine in the liposomes composed of 5 mol% Rho-DPPE, 15 mol% DPPG, 30 mol% cholesterol, and 50 mol% DPPE as a function of time delays (ps). The time-evolved optical density profiles (B) at 450 nm, 555 nm and 578 nm of the liposomes are shown by black squares, red circles, and green triangles, respectively; the solid blue lines are the corresponding exponential fits of the experimental data. The rhodamine concentration in these liposomes used is approximately 125 μM.

far from homogeneity. We studied the effect of such a phase separation on photoconversion, and found it greatly boosted the photoconversion efficiency. A series of spectroscopy and microscopy experiments were performed to elucidate underlying mechanisms. We found that rhodamine clusters and aggregates are formed by addition of cholesterol, and they may play a primary role in

light capture and facilitate photo-induced electron transfer. To fully understand the mechanism, however, more experiments remain to be done.

References

1. Wang, M.; Chen, J.; Lian, T.; Zhan, W. Mimicking Photosynthesis with Supercomplexed Lipid Nanoassemblies: Design, Performance, and Enhancement Role of Cholesterol. *Langmuir* **2016**, *32*, 7326-7338.
2. Hancock, J. F. Lipid Rafts: Contentious Only from Simplistic Standpoints. *Nat. Rev. Mol. Cell Biol*. **2006**, *7*, 456-462.
3. Mateo, C. R.; Acuna, A. U.; Brochon, J. C. Liquid-Crystalline Phases of Cholesterol/Lipid Bilayers as Revealed by the Fluorescence of Trans-Parinaric Acid. *Biophys. J*. **1995**, *68*, 978-987.
4. de Almeida, F. M.; Fedorov, A.; Prieto, M. Sphingomyelin/Phosphatidylcholine/Cholesterol Phase Diagram: Boundaries and Composition of Lipid Rafts. *Biophys. J*. **2003**, *85*, 2406-2416.
5. Mateo, C. R.; Brochon, J.-C.; Lillo, M. P.; Acuña, A. U. Liquid Crystalline Phases of Cholesterol/Lipid Bilayers as Revealed by the Fluorescence of Trans-Parinaric Acid. *Biophys. J*. **1993**, *65*, 2237-2247.
6. Halling, K. K.; Ramstedt, B.; Nyström, J. H.; Slotte, J. P.; Nyholm, T. K. M. Cholesterol Interactions with Fluid-Phase Phospholipids: Effect on the Lateral Organization of the Bilayer. *Biophys. J*. **2008**, *95*, 3861-3871.
7. Heerklotz, H.; Tsamaloukas, A. Gradual Change or Phase Transition: Characterizing Fluid Lipid-Cholesterol Membranes on the Basis of Thermal Volume Changes. *Biophys. J*. **2006**, *91*, 600-607.

8. Mabrey, S.; Sturtevant, J. M. Investigation of Phase Transitions of Lipids and Lipid Mixtures by High-sensitivity Differential Scanning Calorimetry. *Proc. Natl. Acad. Sci. U. S. A.* **1976**, *73*, 3862-3866.
9. Thewalt, J. L.; Bloom, M. Phosphatidylcholine: Cholesterol Phase Diagrams. *Biophys. J.* **1992**, *63*, 1176-1181.
10. Veatch, S. L.; Keller, S. L. Lateral Organization in Lipid Membranes Containing Cholesterol. *Phys. Rev. Letts.* **2002**, *89*, 268101.
11. Stidder, B; Fragneto, G.; Roser, S. J. Structure and stability of DPPE planar bilayers. *Soft Matter*, **2007**, *3*, 214-222.
12. McQuaw, C. M.; Sostarecz, A. G.; Zheng, L.; Ewing, A. G.; Winograd, N. Lateral Heterogeneity of Dipalmitoylphosphatidylethanolamine-Cholesterol Langmuir-Blodgett Films Investigated with Imaging Time-of-Flight Secondary Ion Mass Spectrometry and Atomic Force Microscopy. *Langmuir* **2005**, *21*, 807-813.
13. Zhan, W.; Jiang, K. A Modular Photocurrent Generation System Based on Phospholipid-Assembled Fullerenes. *Langmuir* **2008**, *24*, 13258-13261.
14. Favela-Rosales, F.; Carbajal-Tinoco, M. D.; Ortega-Blake, I. Liquid-Ordered Phase Formation in Cholesterol-POPC Bilayers: All-Atom Molecular Dynamics Simulations. *Biophys. J.* **2014**, *106*, 80a.
15. Castro, B. M.; de Almeida, R. F. M.; Fedorov, A.; Prieto, M. The Photophysics of a Rhodamine Head Labeled Phospholipid in the Identification and Characterization of Membrane Lipid Phases. *Chem. Phys. Lipids* **2012**, *165*, 311-319.

Chapter 4

Synthesis of Janus-like Liposomes

4.1 Introduction

Amongst model lipid membranes, giant liposomes are ideal cell mimics due to membrane curvature of live cells and equally importantly their comparable sizes, which allows for direct visualization and tracking of vesicles and their relevant biophysical phenomena such as cell adhesion and fusion, docking, protein-cell interaction at a single bilayer level.[1-4]

Triggered by the significance of giant liposomes, considerable research efforts have been devoted to developing general formation methods that can afford high-quality and high-yield giant liposomes at the same time. To date, several methods including gentle hydration,[5-8] electroformation,[8-11] emulsion-based methods[12,13] and gel-assisted swelling,[14,15] have been used to synthesize giant liposomes with different lipid compositions. Among these methods, the gentle hydration method involves first formation of a thin lipid film on a solid surface and subsequent exposure to buffer solution.[5] This method is time-consuming, and normally produces heterogenous vesicles. The emulsion-based method, on the other hand, forms an inverted emulsion first, and then a lipid monolayer spontaneously forms at the oil-water interface. The inverted emulsion droplets start settling due to density difference, and then pass through the oil-water interface where the second lipid monolayer is situated so that intact lipid vesicles are formed.[13] This method

renders high drug encapsulation efficiency[12] and the capability of synthesizing asymmetrical liposomes[13]. Nevertheless, it has the disadvantages of low yield, and tedious and problematic post-treatment to completely deplete oil in thus-formed liposomes. Electroformation is by far the most widely used method to synthesize giant liposomes comprising a wide variety of lipids. In this method, an alternating electrical field is applied between two electrodes (e.g. platinum and ITO), on one of which a thin layer of lipids is deposited .[8-11] Because of its use of electric field, the preparation of giant liposomes containing charged lipids can be problematic at times.[14] More recently, Mayer and coworkers[14] reported a gel-assisted swelling method to form various giant liposomes in solutions of physiologic ionic strength. Therein, a dried lipid film is first deposited on a thin layer of agarose gel, and subsequent hydration in aqueous solution results in swelling and rapid formation of giant liposomes in high yield. One major problem with this method is that agarose is associated with the liposome membranes and is even encapsulated into vesicles,[14] which modifies/changes the composition of resulting giant liposomes and hence complicates their further applications. Inspired by this work, Marques and coworkers used polyvinyl alcohol (PVA) gels instead, by which various giant liposomes can be prepared, even for those composed of lipids that typically pose a challenge for the formation of giant vesicles, and additionally polyvinyl alcohol does not associate with the resulting liposome membranes. [15]

Herein, we employ two methods, electroformation and gel-assisted swelling, in order to prepare Janus-like giant liposomes. Janus particles, possessing two distinct sides with contrasting functionality, have received much attention in recent years.[16-18] However, the unique formation of colloidal particles has not been systematically investigated with lipids. In this work, we report the synthesis of a wide variety of Janus-like giant liposomes. The anisotropy is introduced by cholesterol-induced phase separation.

4.2 Experimental Section

4.2.1 Chemicals

Lipids, including 1,2-dioleoyl-*sn*-glycero-3-phosphocholine (DOPC), 1,2-dioleoyl-3-trimethylammonium-propane (DOTAP), 1,2-dipalmitoyl-*sn*-glycero-3-phosphocholine (DPPC), 1,2-dipalmitoyl-*sn*-glycero-3-phospho-rac-(1-glycerol) sodium salt (DPPG), 1,2-dipalmitoyl-3-trimethylammonium-propane (chloride salt) (DPTAP), 1,2-dioleoyl-*sn*-glycero-3-phosphoethanolamine-N-(biotinyl) (sodium salt) (biotin-DOPE), 1,2-dioleoyl-*sn*-glycero-3-phosphoethanolamine-N-(lissamine rhodamine B sulfonyl) (ammonium salt) (Rho-DOPE), 23-(dipyrrometheneboron difluoride)-24-norcholesterol (BODIPY-Chol), 1-palmitoyl-2-(dipyrrometheneboron difluoride) undecanoyl-*sn*-glycero-3-phosphocholine (BODIPY-PC), were purchased from Avanti Polar Lipids (Alabaster, AL). See Fig. 4.1 for their chemical structure. Other chemicals, including agarose, polyvinyl alcohol, cholesterol, were obtained from Sigma-Aldrich. Phosphate buffer saline (PBS) was prepared by dissolving certain amount of NaCl (137 mM), KCl (2.7 mM), Na_2HPO_4 (10 mM), and KH_2PO_4 (1.8 mM) into DI water. 18.2 MΩ·cm deionized (DI) water (Millipore) was used throughout this work.

4.2.2 Synthesis of Giant Liposomes

For vesicle formation, lipid solutions with a total lipid concentration of 5 mM was prepared in chloroform (lipid mixtures containing DPPG was prepared in chloroform/methanol, 9/1, v/v). DOPC, DPPC, and cholesterol were used to form zwitterionic giant liposomes. Cationic giant liposomes were formed by mixing 10 mol % DOTAP or DPTAP with lipid mixture used for zwitterionic vesicle preparation. Anionic giant liposomes were prepared by incorporating 10 mol% DPPG instead. 0.2 mol% Rho-DOPE was used to label l_d phase, and 0.2 mol% BODIPY-Chol was

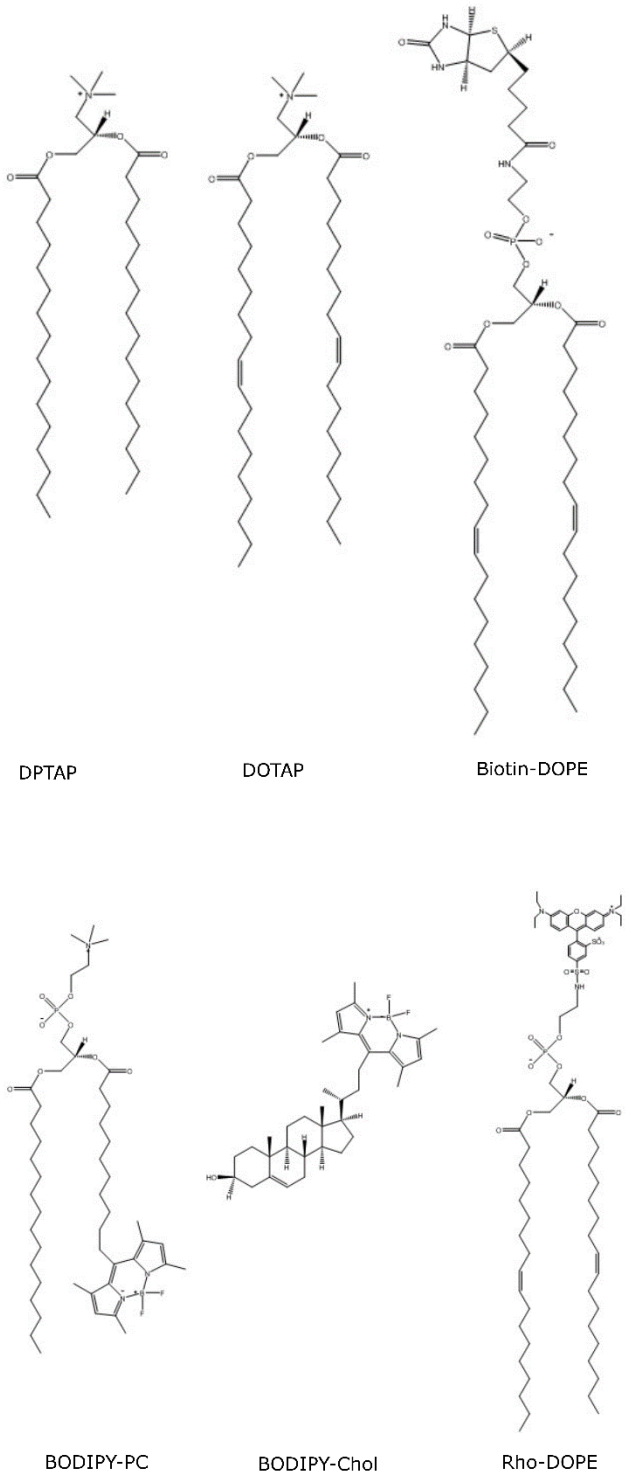

Figure 4.1 Chemical structures of main lipids used in this work.

used to track l_o phase. For biotinylated giant liposome preparation, 1 mol% Biotin-DOPE was incorporated into zwitterionic giant liposomes. In a few cases, we used BODIPY-PC to label l_d phase.[19]

4.2.2.1 Electroformation

To start, ITO-coated glass substrates were cleaned as described previously. 20 µL chloroform solution containing desired lipid mixtures (5 mM) and fluorescent probe, BODIPY-PC, was evenly spread onto an ITO coated substrate and dried under vacuum for at least 2 h to remove residual chloroform. This results in that a thin lipid layer was formed on the substrate, on top of which an O-ring (1 cm diameter) was then placed. Aqueous medium such as DI H_2O, sucrose, or phosphate buffer saline was pipetted into the reservoir defined by the O-ring. The hydrated sample was then carefully covered by a second ITO substrate with ITO coated side in contact with the solution, avoiding entrapment of air bubbles. Electroformation was performed at 60 ^oC, well above the phase transition temperatures of the lipids employed, under an AC current at 5 Hz and 3 V for 2 h. Thereafter the GUVs were allowed to cool down to room temperature and ready for fluorescence microscopy characterization. Thus-formed giant liposomes were harvested by aspiration through a pipette.

4.2.2.2 Agarose Gel-Assisted Swelling

The giant liposomes were prepared by following the procedure developed by Horger et al.[14] with minor modification. To start, 1% (w/w) agarose (Tg<31 ^oC, Tm<75^oC) was dissolved in DI H_2O by boiling the solution in a microwave oven. About 100 µL of this gel solution was then spread onto a clean glass substrate and dried on a hot plate at 40 ^oC for 2 h. 5 µL of desired lipid

solution in chloroform was brushed onto the dried agarose gel and dried under vacuum overnight. After that, hot DI water was used to hydrate the lipid film at 55 ^{o}C for 1 h. Similarly, thus-formed giant liposomes were harvested by applying aspiration through a pipette.

4.2.2.3 PVA Gel-Assisted Swelling

Giant liposomes of various compositions were prepared by following the procedure with minor modification developed by Weinberger et al.[15] Briefly, to start, 5% (w/w) polyvinyl alcohol (Mw=89,000-98,000) solution was prepared in DI water under continuous stirring in a water bath at ~80 ^{o}C. PVA gel was formed on a clean glass substrate (2×2 cm), similar to the procedure for preparing agarose gel. 5 µL of lipid mixtures was deposited on PVA gel and dried under vacuum overnight. DI water was then added to hydrate the lipid film at 45 ^{o}C for 1 h. After that, giant liposomes were allowed to cool down and then harvested by gentle pipetting.

4.2.3 Confocal fluorescence microscopy

Fluorescence images of giant liposomes were collected on a Nikon A1+/MP confocal scanning laser (488 nm and 561.4 nm) microscope (Nikon Instruments, Inc., Melville, NY) together with a 488 nm and a 561 nm long pass dichroic mirror, and a 525 ± 25 nm and a 595 ± 25 nm emission filter, respectively.

4.3 Results and Discussion

In this study, we wish to prepare various Janus-like giant liposomes including zwitterionic giant liposomes, anionic giant liposomes, cationic giant liposomes, biotinylated giant liposomes. Unlike single-phase liposomes, symmetry of Janus-like liposomes is broken and thus creating

anisotropy by cholesterol triggered phase separation, that is, l_o-l_d coexistence. The presence of l_o or l_d is identified by fluorescent membrane probes. Most of the time, we use Rho-DOPE to probe l_d phase, because Rho-DOPE presents a significant preference to partition into l_d phase with a partition coefficient $K_{p\ lo/ld}$ of 0.28.[20] We choose BODIPY-Chol to probe l_o phase, since it prefers to stay in l_o phase with a $K_{p\ lo/ld}$ of 4.[21] Equally important is that these two fluorescent probes emit fluorescence at different wavelengths (Fig. 4.1), so we can clearly visualize both lipid domains on individual liposomes simultaneously. In several cases, BODIPY-PC is used to label l_d domains due to its partition preference to l_d phase.

4.3.1 Zwitterionic Giant Liposomes

To start, we electroformed zwitterionic giant liposomes comprising 37.5 mol% DPPC, 37.5 mol% DOPC, and 37.5 mol% cholesterol doped with 0.5 mol% fluorescent probe, BODIPY-PC. As shown in Fig. 4.2A, vesicles are produced on the ITO substrate with clear phase separation on individual giant liposomes at room temperature. Most of regions on each vesicle are fluorescent that can be assigned to l_d phase, but several small circular domains are non-fluorescent, which is in l_o phase.

Using PVA gel assisted swelling method, we successfully synthesized a series of giant liposomes with different domains (Fig. 4.2B-D). These giant liposomes are dually labeled with Rho-DOPE for l_d phase and BODIPY-Chol for l_o phase, respectively. By changing the relative concentrations of the saturated lipid (DPPC) and unsaturated lipid (DOPC) as well as the concentration of cholesterol, we synthesized giant liposomes with different domains; in other words, we can precisely control the relative sizes of l_o and l_d domains. Here, we solely focus on the regions of liquid-liquid coexistence, i.e. l_o-l_d phase coexistence. The lipid domains observed in

these zwitterionic giant liposomes are in accordance with phase diagram plotted by Keller and coworker[22]. We observed that giant liposomes containing large fractions of DOPC are enriched in l_d phase (in red) but have much less l_o domains (in green) (Fig. 4.2B). As depicted in Fig. 4.3, we observed in confocal fluorescence images that increasing the concentration of DPPC and cholesterol increase the surface fraction of l_o domains.

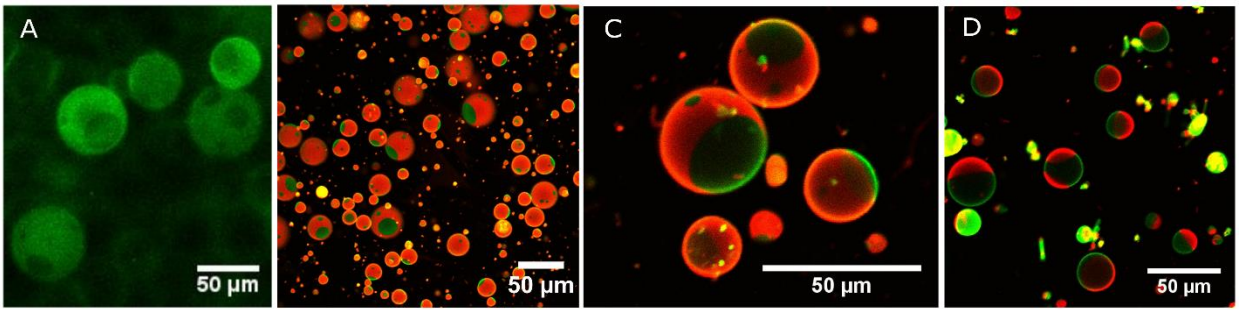

Figure 4.2 Fluorescence images of zwitterionic giant liposomes with different lipid compositions formed by using different methods. A) giant liposomes composed of 37.5 mol% DOPC, 37.5 mol% DPPG, 25 mol% cholesterol, and 0.5 mol% BODIPY-PC, prepared by electroformation; (B-D) giant liposomes labeled by 0.2 mol% Rho-DOPE and 0.2 mol% BODIPY-Chol, formed by the PVA gel-assisted swelling method: B) 53 mol% DOPC, 27 mol% DPPC, and 20 mol% cholesterol; C) 40 mol% DOPC, 40 mol% DPPC, and 20 mol% cholesterol; D) 23 mol% DOPC, 47 mol% DPPC, and 30 mol% cholesterol.

4.3.2 Anionic Giant Liposomes

Interestingly, electroformed anionic giant liposomes composed of ternary lipid mixtures are mostly multivesicular rather than univesicular, as shown in Figure 4.4A. This is also reported by Bucher et al.[23] and Rodriguez et al.[24], where giant liposomes containing pure POPG lipid or even only 2 mol% Rho-PE were electroformed. In contrast, by the agarose gel assisted swelling

method, the majority of the giant liposomes are univesicular and Janus-like with clear l_o/l_d phase separation (Figure 4.4B). Unfortunately, heterogenous multivesicular/multilamellar vesicles are also observed, which is in accordance with the previous findings.[14] GUVs formed from ternary lipid components using PVA gel are much more uniform and homogeneous (Figure 4.4C-E), which emphasizes the important role of PVA gel in assisting swelling and hydration of lipid film, i.e. the growth of liposomes promoted by forces normal to the lipid films.[15] Similar to zwitterionic GUVs formed by PVA gel assisted swelling, anionic Janus-like GUVs with different sizes of l_o/l_d domains are formed. In comparison to zwitterionic GUVs, incorporation of 10 mol% DPPG does not significantly change the phase separation.

4.3.3 Cationic Giant Liposomes

Following the agarose gel assisted swelling method, to begin with, two different lipid compositions (DPTAP/DPPC/DOPC/cholesterol, 10/38/32/20, in mole fraction, and DOTAP/DOPC/DPPC/cholesterol, 10/25/35/30, in mole fraction) were selected. Unfortunately, giant liposomes with rather low yield were produced when the lipid film is hydrated in DI H_2O. Hydrating such lipid films in phosphate buffer saline instead resulted in irregular shaped giant liposomes and low yield. We found that the presence of positively charged lipids (DPTAP or DOTAP) leads to a frequent adhesion of neighboring vesicles, which was also observed by Bucher et al.[23] Resulting aggregates rather than individual vesicles greatly limit their further applications on single liposome level.

PVA gel was thereafter exploited to synthesize cationic giant liposomes using the lipid mixtures with the same compositions (vide supra). Following the procedure developed by Marques and coworkers[15], our initial attempt was to hydrate the dried lipid film in phosphate buffer saline,

which is the most commonly used medium for preparing charged giant liposomes. This method is successful to form giant liposomes with high yield. Unfortunately, thus-generated giant liposomes are severely adhered to vesicles in proximity, plausibly due to charges on the bilayer surfaces being screened under high ionic strength so that the repulsion between adjacent vesicles is greatly undermined. Marques and coworkers [15] reported that formed vesicles are less prone to adhere to each other when PVA is prepared in sucrose solution or phosphate buffer saline. In our hands, adhesion between neighboring vesicles is not at all improved by dissolving PVA in 280 mM sucrose solution. Not only are vesicles seriously adhered to each other, what's worse, but also the sizes of vesicles greatly decrease when preparing PVA in phosphate buffer saline. Instead, giant liposomes are well formed with least adhesion and high yield when lipid film spread on a PVA gel prepared in DI H_2O is hydrated in DI H_2O (Fig. 4.5). It is presumably because electrostatic repulsion between vesicles keeps them apart under low ionic strength.

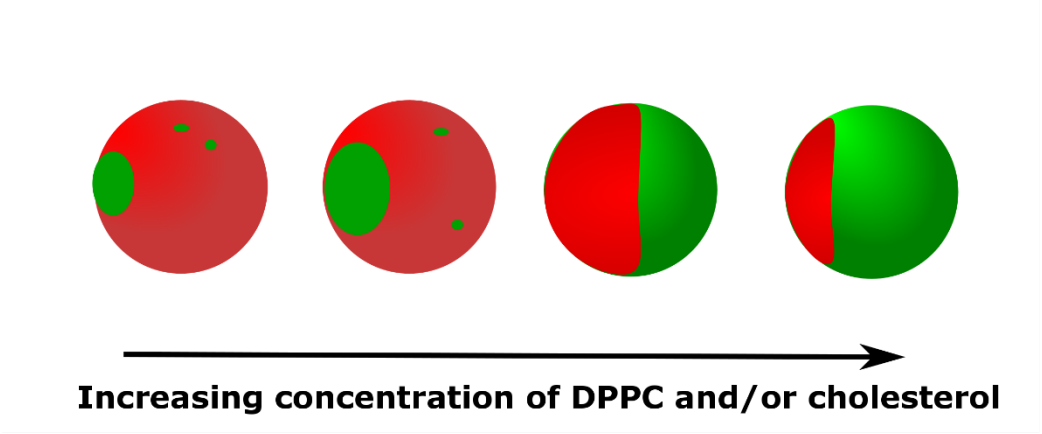

Figure 4.3 Schematic of phase separation in giant liposomes with the increased concentrations of DPPC and /or cholesterol. Regions in red represent l_d domains, and regions in green are l_o domains.

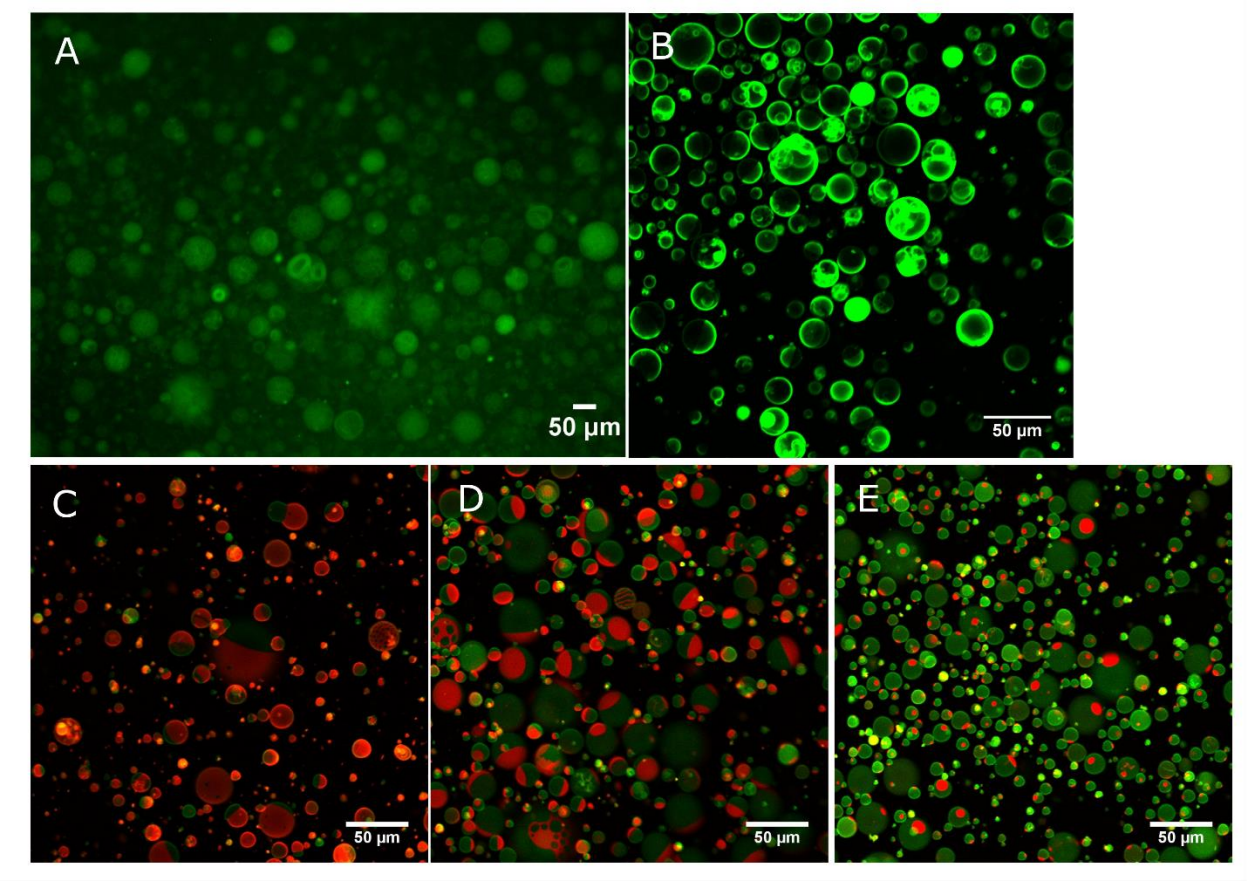

Figure 4.4 Fluorescence images of anionic giant liposomes with different lipid compositions formed by using different methods. (A) Giant liposomes composed of 35 mol% DOPC, 35 mol% DPPG, 30 mol% cholesterol, and 0.5 mol% BODIPY-PC, prepared by electroformation; (B) giant liposomes composed of 32 mol% DOPC, 38 mol% DPPC, 10 mol% DPPG, 20 mol% cholesterol, and 0.5 mol% BODIPY-PC formed by the agarose gel-assisted swelling method; (C-E) giant liposomes labeled by 0.2 mol% Rho-DOPE and 0.2 mol% BODIPY-Chol, formed by the PVA gel-assisted swelling method: (C) 40 mol% DOPC, 30 mol% DPPC, 10 mol% DPPG, and 20 mol% cholesterol; (D) 23 mol% DOPC, 37 mol% DPPC, 10 mol% DPPG, and 30 mol% cholesterol; (E) 12 mol% DOPC, 38 mol% DPPC, 10 mol% DPPG, and 40 mol% cholesterol.

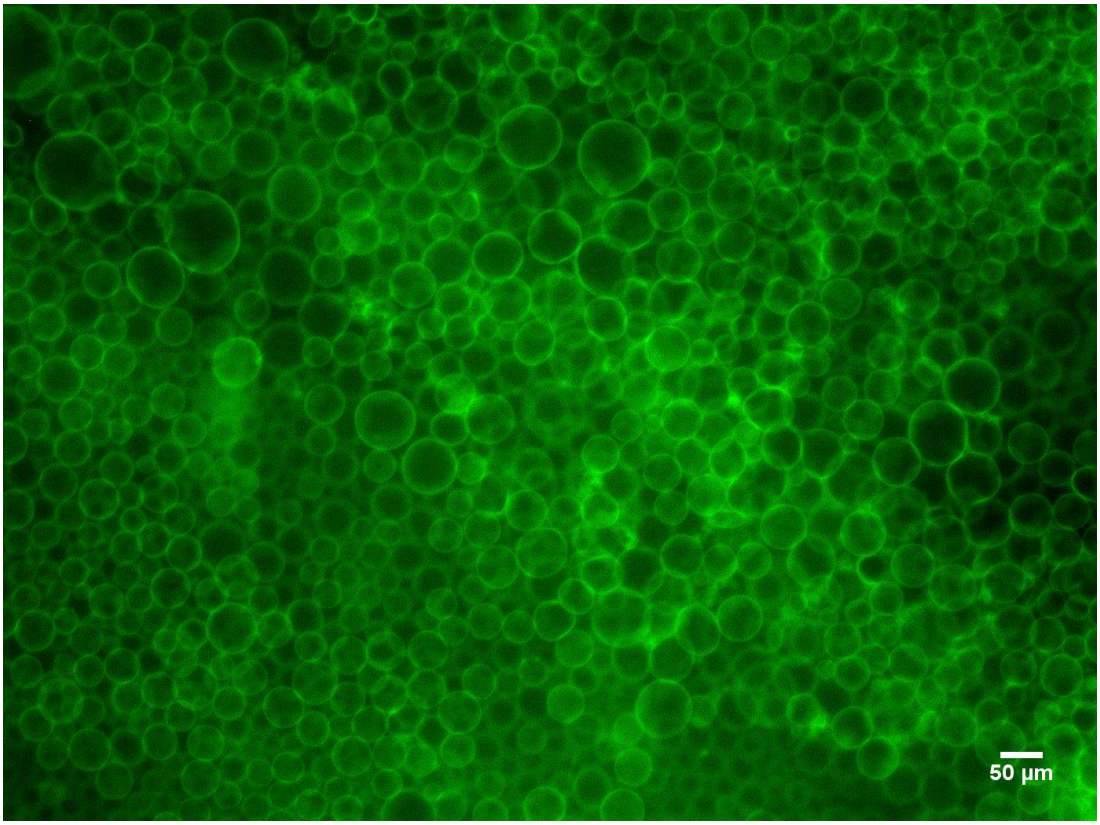

Figure 4.5 Fluorescence images of cationic giant liposomes formed by PVA gel swelling. Giant liposomes are composed of DPTAP-DPPC-DOPC-Chol-BODIPY-PC, 10%-22%-48%-20%-0.5%, in mole fraction.

4.3.4 Biotinylated Giant Liposomes

Incorporating 1 mol% Biotin-DOPE, we synthesized a series of Janus-like biotinylated giant liposomes with different domains by PVA gel swelling (Fig 4.6). No appreciable domain disruption or reorganization was observed after insertion of Biotin-DOPE.

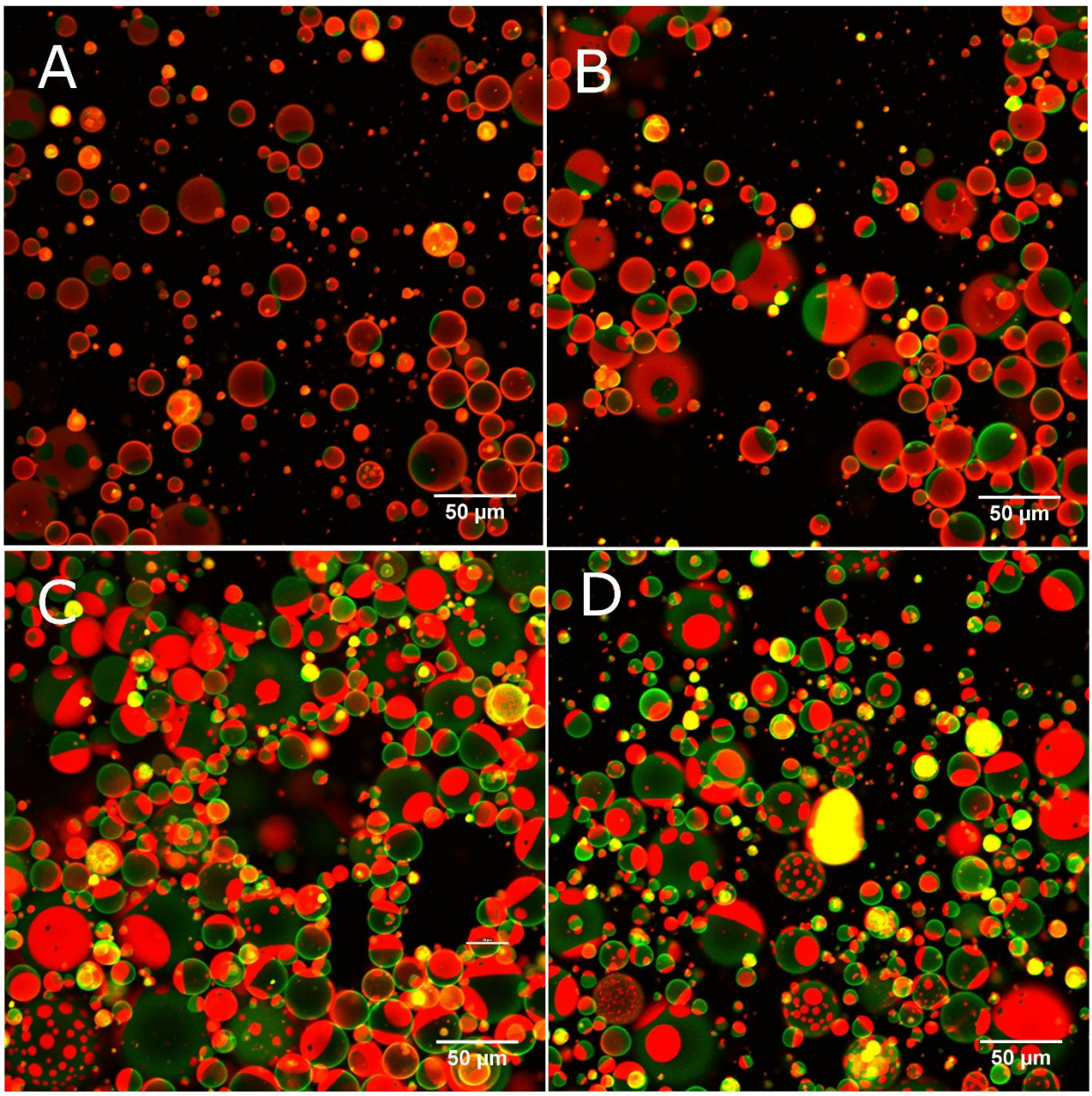

Figure 4.6 Fluorescence images of biotinylated giant liposomes containing 1 mol% Biotin-DOPE with different lipid compositions, dually labeled with 0.2 mol% Rho-DOPE and 0.2 mol% BODIPY-Chol: (A) 26.7 mol% DOPC-52.3 mol% DPPC-20 mol% cholesterol; (B) 39 mol% DOPC-40 mol% DPPC-20 mol% cholesterol; (C) 22.3 mol% DOPC-46.7 mol% DPPC-30 mol% cholesterol; (D) 16.5 mol% DOPC-52.5 mol% DPPC-30 mol% cholesterol.

4.3.5 Stability

Stability of giant liposomes were investigated by imaging the giant liposomes discussed above stored at 4^{o}C for at least 10 days using confocal microscopy. The individual giant liposomes remain intact and separate, and no appreciable change in shape and l_d/l_o domains were observed (data not shown). This indicates giant liposomes are rather stable when stored at 4^{o}C.

4.4 Conclusions

We successfully synthesized a wide of range of Janus-like giant liposomes including zwitterionic, cationic, anionic, and biotinylated giant liposomes using different methods. Overall, PVA gel swelling method produced giant liposomes with the best quality and highest yield for various kinds of giant liposomes. Additionally, for each kind of giant liposomes, we are able to precisely control the domain formation by changing the relative concentrations of the saturated lipids and unsaturated lipids as well as the concentration of cholesterol.

References

1. Menger, F. M.; Angelova, M. I. Giant Vesicles: Imitating the Cytological Processes of Cell Membranes. *Acc. Chem. Res*. **1998**, *31*, 789-797.
2. Dimova, R.; Aranda, S.; Bezlyepkina, N.; Nikolov, V.; Riske, K. A.; Lipowsky, R. A Practical Guide to Giant Vesicles. Probing the Membrane Nanoregime via Optical Microscopy. *J. Phys. Condens. Matter* **2006**, *18*, S1151-S1176.
3. Hotani, H.; Nomura, F.; Suzuki, Y. Giant Liposomes: from Membrane Dynamics to Cell Morphogenesis. *Curr. Opin. Colloid Interface Sci*. **1999**, *4*, 358-368.

4. Bagatolli, L. A. To See or Not to See: Lateral Organization of Biological Membranes and Fluorescence Microscopy. *Biochim. Biophys. Acta*. **2006**, *1758*,1541-1556.
5. Reeves, J. P.; Dowben, R. M. Formation and Properties of Thin-Walled Phospholipid Vesicles. *J. Cell. Physio*. **1969**, *73*, 49-60.
6. Akashi, K.; Miyata, H.; Itoh, H.; Kinosita, K. Preparation of Giant Liposomes in Physiological Conditions and Their Characterization under an Optical Microscope. *Biophys. J*. **1996**, *71*, 3242-3250.
7. Yamashita, Y.; Oka, M.; Tanaka, T.; Yamazaki, M. A New Method for the Preparation of Giant Liposomes in High Salt Concentrations and Growth of Protein Microcrystals in Them. *Biochim. Biophys. Acta* **2002**, *1561*, 129-134.
8. D'Onofrio, T. G.; Hatzor, A.; Counterman, A. E.; Heetderks, J. J.; Sandel, M. J.; Weiss, P. S. Controlling and Measuring the Interdependence of Local Properties in Biomembranes. *Langmuir* **2003**, *19*, 1618-1623.
9. Angelova, M. I.; Dimitrov, D. S. Liposome Electroformation. *Faraday Discuss Chem Soc*. **1986**, *81*, 303-311
10. Estes, D. J.; Mayer, M. Electroformation of Giant Liposomes from Spin-Coated Films of Lipids. *Colloids Surf. B* **2005**, *42*, 115-123.
11. Menger, F. M.; Seredyuk, V. A. Internally Catalyzed Separation of Adhered Lipid Membranes. *J. Am. Chem. Soc.* **2003**, *125*, 11800-11801.
12. Pautot, S.; Frisken, B. J.; Weitz, D. A. Production of Unilamellar Vesicles Using an Inverted Emulsion. *Langmuir* **2003**, *19*, 2870-2879.
13. Pautot, S.; Frisken, B. J.; Weitz, D. A. Engineering asymmetric vesicles. *Proc. Natl. Acad. Sci. U. S. A.* **2003**, *100*, 10718-10721.

14. Horger, K. S.; Estes, D. J.; Capone, R.; Mayer, M. Films of Agarose Enable Rapid Formation of Giant Liposomes in Solutions of Physiologic Ionic Strength. *J. Am. Chem. Soc*. **2009**, *131*, 1810-1819.

15. Weinberger, A.; Tsai, F.-C.; Koenderink, G. H.; Schmidt, T. H.; Itri, R.; Meier, W.; Schmatko, T.; Schröder, A.; Marques, C. Gel-Assisted Formation of Giant Unilamellar Vesicles. *Biophys. J*. **2013**, *105*, 154-164.

16. Walther, A.; Müller, A. H. E. Janus Particles: Synthesis, Self-Assembly, Physical Properties, and Applications. *Chem. Rev*. **2013**, *113*, 5194-5261.

17. Hu, J.; Zhou, S.; Sun, Y.; Fang, X.; Wu, L. Fabrication, Properties and Applications of Janus Particles. *Chem. Soc. Rev*. **2012,** *41*, 4356-4378.

18. Loget, G.; Kuhn, A. Bulk Synthesis of Janus Objects and Asymmetric Patchy Particles. *J. Mater. Chem*. **2012**, *22*, 15457-15474.

19. Klymchenko, A. S.; Kreder, R. Fluorescent Probes for Lipid Rafts: From Model Membranes to Living Cells. *Chem. Biol*. **2014**, *21*, 97-113.

20. Silva, L. C.; de Almeida, R. F. M.; Castro, B. M.; Fedorov, A.; Prieto, M. Ceramide-Domain Formation and Collapse in Lipid Rafts: Membrane Reorganization by an Apoptotic Lipid. *Biophys. J*. **2007**, *92*, 502-516.

21. Sezgin, E.; Levental, I.; Grzybek, M.; Schwarzmann, G.; Mueller, V.; Honigmann, A.; Belov, V. N.; Eggeling, C.; Coskun, Ü.; Simons, K.; Schwille, P. Partitioning, Diffusion, and Ligand Binding of Raft Lipid Analogs in Model and Cellular Plasma Membranes. *Biochim. Biophys. Acta* **2012**, *1818*, 1777-1784.

22. Veatch, S. L.; Keller, S. L. Separation of Liquid Phases in Giant Vesicles of Ternary Mixtures of Phospholipids and Cholesterol. *Biophys. J*. **2003**, *85*, 3074-3083.

23. Bucher, P.; Fischer, A.; Luisi, P. L.; Oberholzer, T.; Walde, P. Giant Vesicles as Biochemical Compartments: The Use of Microinjection Techniques. *Langmuir*. **1998**, *14*, 2712-2721.
24. Rodriguez, N.; Pincet, F.; Cribier, S. Giant Vesicles Formed by Gentle Hydration and Electroformation: A Comparison by Fluorescence Microscopy. *Colloids Surf. B* **2005**, *42*, 125-130.

Chapter 5

Self-Assembly of Biotinylated Janus-Like Liposomes

5.1 Introduction

Self-assembly is a process by which individual components spontaneously form ordered and well-defined hierarchical superstructures, differing from their starting materials in functionalities such as electronic, mechanic, magnetic, conducting, and optic properties.[1] In fact, an astounding range of complex/supercomplex structures in cells are formed by self-assembly, such as lipid membranes, intermembrane proteins, protein aggregates, and molecular machines.[2] Studies on self-assembly have been a fruitful research area over the past several decades.[3-7] The understanding of self-assembly processes is of paramount fundamental interest, not only for developing advanced materials, but for gaining insight into sophisticated biological functions of cells and organelles. The connection of specific organelles such as Golgi, peroxisomes, lipid droplets, etc. by membrane contact sites, for instance, is particularly important in cellular signaling, promotion of ion passage, and non-vesicular lipid trafficking.[8]

Janus particles, possessing two distinct sides with contrasting functionality, have attracted much attention in recent years.[9-11] They are promising building blocks for developing advanced functional materials. Because of their asymmetry and multi-domain surface, different functional groups can be grafted on each side for driving further self-assembly to form higher ordered

aggregates with interesting superstructures. A variety of chemistry have been to date explored on Janus particles such as amphiphilic particles, dipolar particles, and Janus particles with supramolecular binding motifs.[9]

Avidin-biotin interaction is well recognized to be one of the strongest known non-covalent bonds with dissociation constant (k_D) of 10^{-15} M.[12-14] Owing to its stable binding and small size of biotin label, it has been often used for biomolecule labeling[15], purification[16], immobilization[14,17-19] and patterning[20]. Avidin-biotin interaction has also been often used for immobilization of lipid vesicles for a wide variety of applications such as immunoassay[21,22], and single biomolecule detection[23].

In this work, we investigated the self-assembly of Janus-like biotinylated giant lipsomes whose symmetry is broken by cholesterol-triggered phase separation. Taking advantage of the latter, biotin moiety is confined exclusively in l_d domains. Using avidin-biotin chemistry, liposomes self-assemble into chain-like structures including dimer, trimer, and other higher ordered superstructures. To the best of our knowledge, this is the first time that cholesterol-triggered phase separation is employed to regioselectively anchor the biotin moieties, driving the self-assembly of liposomes.

5.2 Experimental Section

5.2.1 Chemicals

Lipids, including 1,2-dioleoyl-*sn*-glycero-3-phosphocholine (DOPC), 1,2-dipalmitoyl-*sn*-glycero-3-phosphocholine (DPPC), 1,2-dioleoyl-*sn*-glycero-3-phosphoethanolamine-N-(biotinyl) (sodium salt) (Biotin-DOPE), 1,2-dioleoyl-*sn*-glycero-3-phosphoethanolamine-N-(lissamine rhodamine B sulfonyl) (ammonium salt) (Rho-DOPE), and 23-(dipyrrometheneboron difluoride)-

24-norcholesterol (BODIPY-Chol), were purchased from Avanti Polar Lipids (Alabaster, AL). Other chemicals, including NeutrAvidin, Alexa Fluor® 488 conjugated avidin, polyvinyl alcohol, cholesterol, were obtained from Sigma-Aldrich. 18.2 MΩ·cm deionized (DI) water (Millipore) was used throughout this work.

5.2.2 Determination of Phase Preference of Biotinylated Lipids

Biotinylated giant liposomes were prepared as described in Chapter 4. Briefly, 1 mol% Biotin-DOPE is incorporated into zwitterionic giant liposomes, which are singly labeled by Rho-DOPE. To determine the l_d/l_o phase preference of Biotin-DOPE, confocal microscopy was performed before and after the giant liposomes were mixed with a fluorescently labeled avidin (Alexa 488 conjugated avidin) in a biotin/avidin mole ratio of 10 to 1.

5.2.3 Self-Assembly of Biotinylated Janus-Like Giant Liposomes

As-prepared biotinylated liposomes were mixed with an equal volume of NeutrAvidin in a mole ratio of 10 to 1. The total concentration of lipids in these liposomes is approximately 2.5 μM. To improve the chance of encounter and binding, the resulting mixture was subjected to vortexing and incubated at room temperature.

5.2.4 Confocal Fluorescence Microscopy

As-prepared giant liposomes and self-assemblies were transferred to a homemade cell for imaging, where a ~ 1 mm thin layer of PDMS with holes whose diameters are 3 mm is attached to the surface of coverslip (Corning). Fluorescence images of giant liposomes were collected on a

Nikon A1+/MP confocal scanning laser (488 nm and 561 nm) microscope (Nikon Instruments, Inc., Melville, NY) together with a 525 ± 25 nm and a 595 ± 25 nm emission filter, respectively.

5.3 Results and Discussion

5.3.1 Phase Preference of Biotin-DOPE

To qualitatively determine the phase preference of Biotin-DOPE, we synthesized giant liposomes of Biotin-DOPE/DOPC/DPPC/cholesterol (1/34/35/30, in mole fraction) composition, presenting l_d/l_o coexistence. Such liposomes are singly labeled with a l_d phase-preferred fluorescent membrane probe, Rho-DOPE, with a partition coefficient ($K_{p\ lo/ld}$) of 0.28[24]. The confocal image (Fig. 5.1A) shows clear phase separation on each vesicle, where the majority of vesicle surface is non-fluorescent (in dark), indicating a l_o phase, while the minority of surface area is fluorescent (in red), which is in l_d phase. We then mixed such liposomes with an appropriate amount of Alexa 488 conjugated avidin. We envision that Rho-DOPE prefers to partition into l_d phase because it has two double bonds in the acyl chains. Indeed, confocal images indicate Rho-DOPE is most preferably located in l_d phase under the concentration of avidin used herein. Upon incubation with Alexa 488 labeled avidin, no fluorescence (in green) was observed in l_o phase but in l_d phase, as can be seen from Fig. 5.1B.

5.3.2 Design

Taking advantage of cholesterol-triggered phase separation, we can regioselectively anchor biotin tag in l_d phase. We wish to investigate self-assembly of such biotinylated liposomes with different domains. As shown in Fig. 4.6 in Chapter 4, by increasing the concentration of cholesterol and DPPC, we observe a phase change in giant liposomes, from l_d phase-dominated to l_o phase-

dominated. A scheme in Fig. 5.2 shows how these biotinylated liposomes self-assemble into chain-like structures in two different scenarios. One scenario is for l_d phase-dominated giant liposomes, the other is for l_o phase-dominated giant liposomes. In brief, avidin binds two neighboring liposomes whose l_d phase (in red) is doped with Biotin-DOPE. Continuing to tether more liposomes, the aggregates grow and propagate to form chain-like structures.

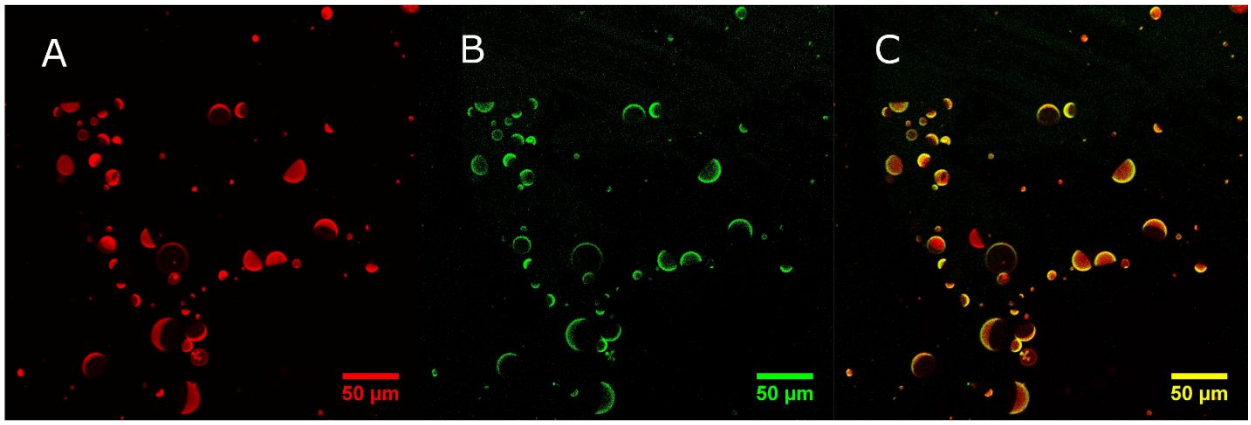

Figure 5.1 Confocal fluorescence images of giant liposomes containing 1 mol% of Biotin-DOPE incubated with Alexa 488-avidin for ~2 h. (A) green channel, (B) red channel, (C) merged images. The concentration of alexa 488 conjugated avidin is ~0.05 µM. Giant liposomes singly labeled with Rho-DOPE, are composed of 35 mol% DPPC, 34 mol% DOPC, and 30 mol% cholesterol.

5.3.3 Self-Assembly of Biotinylated Giant Liposomes

We investigated the self-assembly of biotinylated liposomes with in total four different lipid compositions. In this study, we used NeutrAvidin that has near-neutral isoelectric point and thus minimizes non-specific adsorption.[25] We intentionally used low concentration of NeutrAvidin to minimize the disruption and reorganization of lipid domains upon binding to avidin. It has been reported that Biotin-PE lipids are to some extent vertically displaced out of the membrane, upon

binding to avidin in a lipid membrane.[26] In fact, we mixed liposomes with avidin at a higher concentration (avidin/biotin, 1/1) and observed significant reorganization of lipid domains (image not shown).

5.3.3.1 l_d Phase-Dominated Giant Liposomes

Using l_d phase-dominated biotinylated liposomes, we produced chain-like dimer, trimer, tetramer and pentamer (Fig. 5.3). The confocal fluorescent images show the binding sites are unambiguously located in l_d phases on neighboring liposomes, confirming that biotin-avidin interaction drives the self-assembly of these liposomes. Due to the availability of l_d phase, branched structure is observed from time to time (Fig. 5.3D). Taking close inspection of Fig. 5.3, interestingly, the aggregates take a zig-zag configuration in which liposomes alternately face one another, as shown in Fig. 5.2A. Similar alignment of dipolar Janus rods was reported by Granick and coworkers [27], who believe this zig-zag configuration is most stable. No dipole but anisotropy exists in the present system, however. Another interesting phenomenon is that the binding takes place mostly in the l_d phase close to the boundary of l_d and l_o phases, plausibly indicating uneven distribution of biotin in l_d domain. Observation of uniform green fluorescence across the l_d domain upon avidin binding (Fig. 5.1B), however, rules out this possibility. Presumably in such an alignment can steric hindrance of biotin moieties be minimized, because Biotin-DOPE has larger headgroup (Fig. 4.1), which sticks out of bilayer membrane much further, compared to DOPC.

As control, we synthesized isotropic biotinylated liposomes, that is, Biotin-DOPE is homogeneously distributed across the whole vesicle. We performed the self-assembly using isotropic liposomes in the same fashion. We infrequently observed such chain-like structures. This emphasizes the significance of cholesterol-induced phase separation affording anisotropy of

liposomes, which allows for regio-selectively tagging functional groups, driving self-assembly of liposomes in a controlled way.

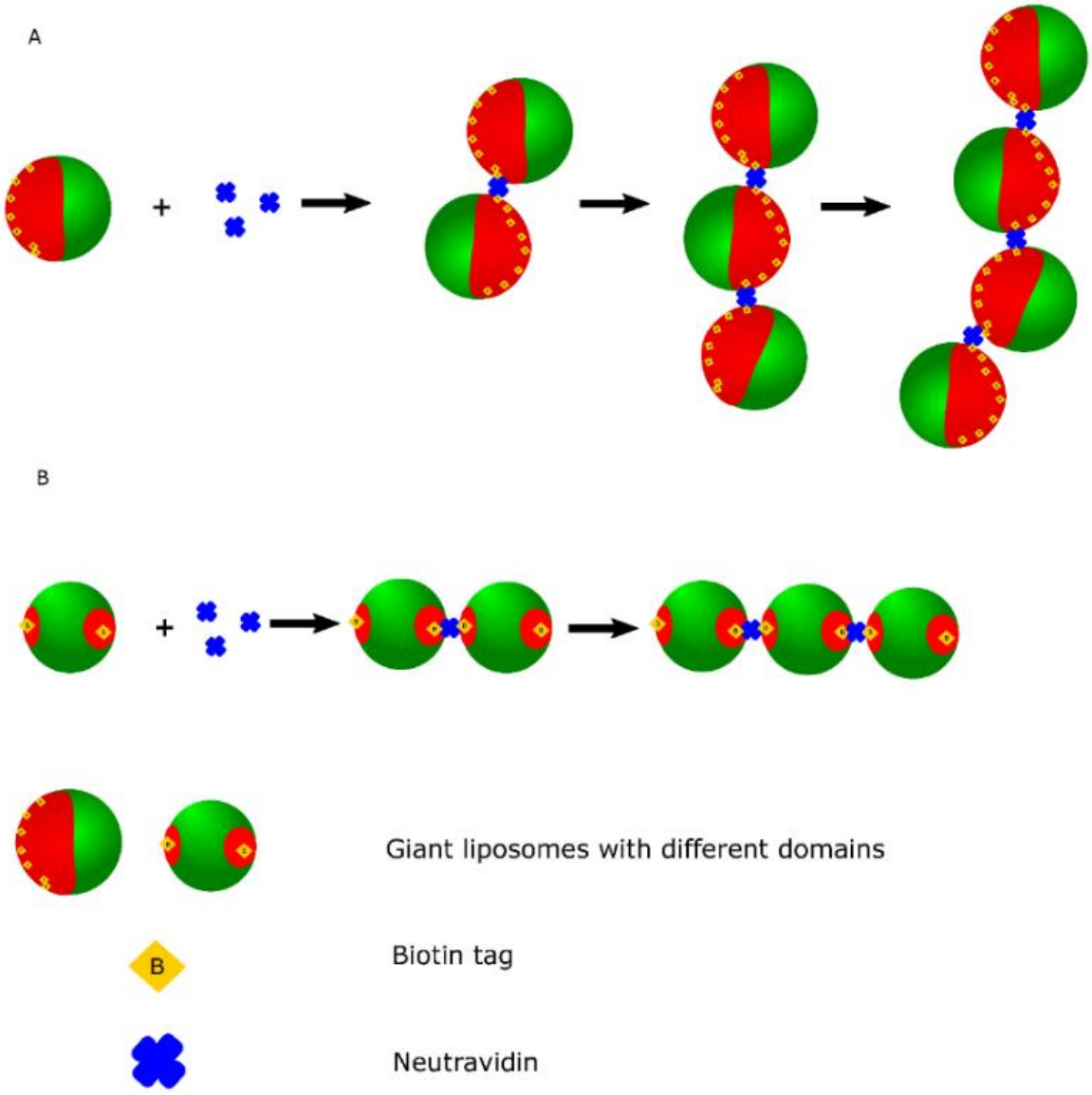

Figure 5.2 Self-assembly of Janus-like biotinylated liposomes with different domains: (A) l_d phase-dominated and Janus lipsomes (more or equal l_d phase (in red)), (B) l_o phase-dominated liposomes (more l_o phase (in green)).

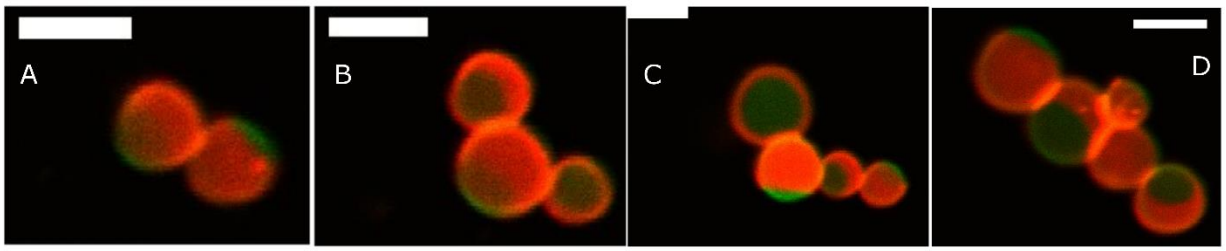

Figure 5.3 Chain-like structures by self-assembly of biotinylated giant liposomes visualized by confocal fluorescence microscopy: (A) dimer, (B) trimer, (C) tetramer, (D) pentamer. The liposomes contain 1 mol% Biotin-DOPE, 52.3 mol% DOPC, 26.7 mol% DPPC, and 20 mol% cholesterol, labeled with 0.2 mol% Rho-DOPE and 0.2 mol% BODIPY-Cholesterol. Scale bars=10 μm.

5.3.3.2 Janus Giant Liposomes

The giant liposomes used here are Janus liposomes, because the surface area of l_d and l_o phases is almost equal (Fig. 4.6B). Confocal images (Fig. 5.4) show rather similar dimer, trimer, tetramer and pentamer to those shown in Fig. 5.3. The binding occurs in the l_d phases between liposomes in proximity, again proving biotin-avidin chemistry triggers the self-assembly. Similarly, the aggregates take a zig-zag alignment and the binding occurs in l_d phases that are near the boundary of l_d and l_o phases. Depending on the size of liposomes, aggregates with different shape can be generated. Possibly liposomes with uniform size tend to self-assemble into linear aggregates (Fig. 5.4D bottom), while aggregates can be bent or zig-zag when liposomes have non-uniform size (Fig. 5.4C and D top).

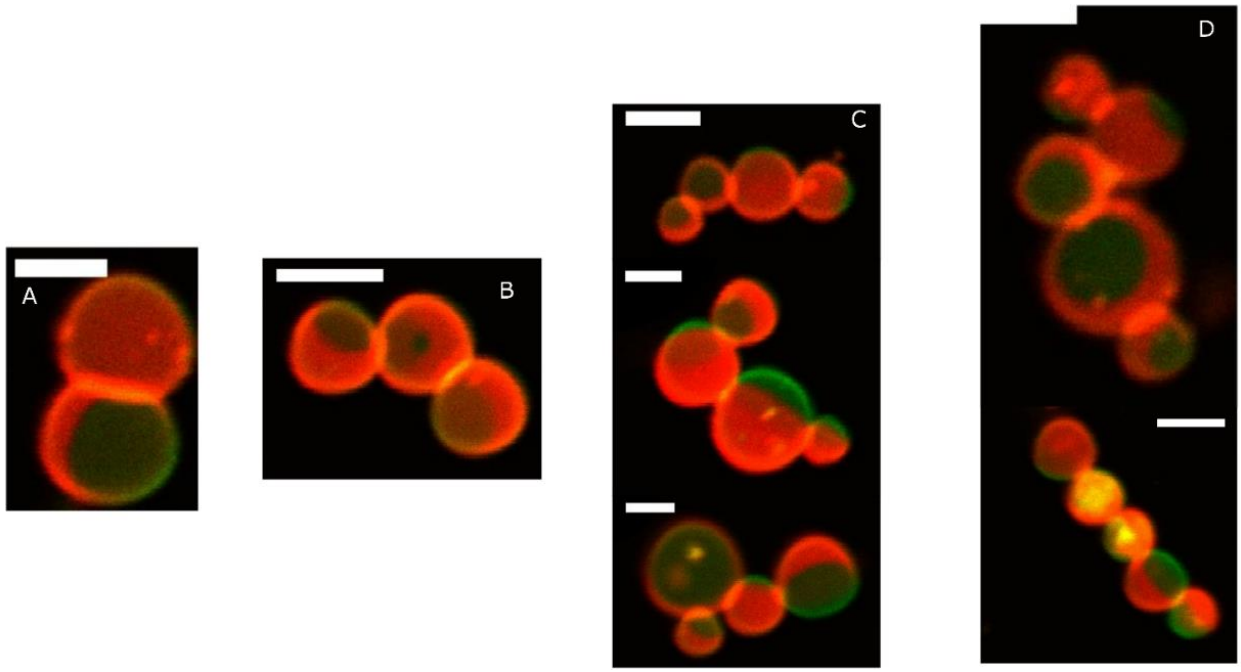

Figure 5.4 Chain-like structures by self-assembly of biotinylated giant liposomes visualized by confocal fluorescence microscopy: (A) dimer, (B) trimer, (C) tetramer, (D) pentamer. The giant liposomes contain 1 mol% Biotin-DOPE, 39 mol% DOPC, 40 mol% DPPC, and 20 mol% cholesterol, labeled with 0.2 mol% Rho-DOPE and 0.2 mol% BODIPY-Cholesterol. Scale bars=10 μm.

5.3.3.3 l_o Phase-Dominated Giant Liposomes

Along with the increase in the concentration of DPPC together with cholesterol, the giant liposomes have larger surface area of l_o phase than that of l_d phase, i.e. so-called l_o phase-dominated. Confocal images show most of the liposomes have one l_d domain. Dimer and trimer are formed by liposomes with single l_d domain (Fig. 5.5A and 5.5B top panel), taking a similar configuration shown in **5.3.3.1** and **5.3.3.2**. However, more than one l_d domains can be found on some vesicles (Fig. 4.6C, D). Dimers are formed from such biotinylated liposomes (Fig. 5.6A). These separated l_d domains on liposomes are binding sites for attaching liposomes in proximity to

form longer chain-like structures by biotin-avidin interaction. For example, a liposome with two l_d domains at its two ends binds another two liposomes to generate a linear trimer (Fig. 5.5B bottom panel). If these l_d domains have random location in liposomes, bent chain-like structures can be formed (Fig. 5.6B and 5.6C).

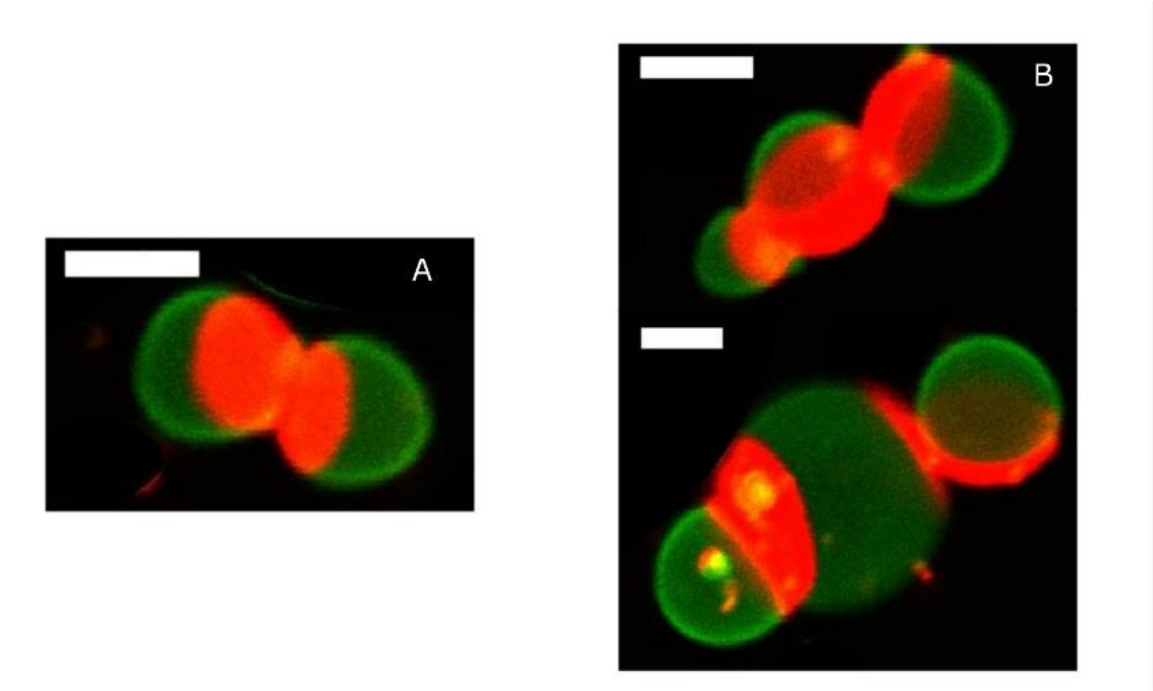

Figure 5.5 Chain-like structures by self-assembly of biotinylated giant liposomes visualized by confocal fluorescence microscopy: (A) dimer and (B) trimer. The liposomes contain 1 mol% Biotin-DOPE, 22.3 mol% DOPC, 46.7 mol% DPPC, and 30 mol% cholesterol, labeled with 0.2 mol% Rho-DOPE and 0.2 mol% BODIPY-Cholesterol. Scale bars=10 μm.

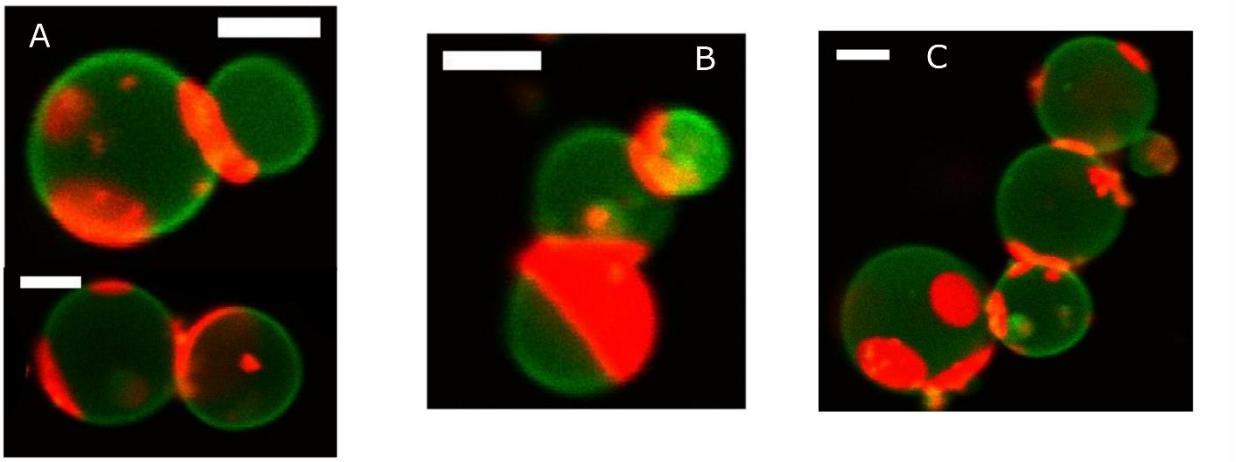

Figure 5.6 Chain-like structures by self-assembly of biotinylated giant liposomes visualized by confocal fluorescence microscopy: (A) dimer, (B) trimer, (C) tetramer. The liposomes contain 1 mol% Biotin-DOPE, 16.5 mol% DOPC, 52.5 mol% DPPC, and 30 mol% cholesterol, labeled with 0.2 mol% Rho-DOPE and 0.2 mol% BODIPY-Cholesterol. Scale bars=10 μm.

5.4 Conclusions

Taking advantage of cholesterol-induced phase separation, we can regio-selectively dope liposomes with biotin moieties. Using biotin-avidin interaction, biotinylated liposomes self-assemble into chain-like structures. Depending on the size of liposomes as well as lipid domains, linear or bent structures can be formed. Future work is focused on introducing another functionality exclusively into l_o domains. For instance, hydrophobic group can be introduced by post-modification of such phase-separated biotinylated liposomes. We wish to use the hydrophobic interaction together with avidin-biotin to drive the self-assembly of liposomes to form better controlled superstructures. Another future research direction is to study why these chain-like aggregates observed in this work take such interesting alignment. To this end, computer simulation should be of considerable help.

References

1. Nie, Z.; Petukhova, A.; Kumacheva, E. Properties and Emerging Applications of Self-Assembled Structures Made from Inorganic Nanoparticles. *Nat. Nanotechnol*. **2010**, *5*, 15-25.
2. Grzybowski, B. A.; Wilmer, C. E.; Kim, J.; Browne, K. P.; Bishop, K. J. M. Self-Assembly: from Crystals to Cells. *Soft Matter* **2009**, *5*, 1110-1128.
3. Lindsey, J. S. Self-Assembly in Synthetic Routes to Molecular Devices-Biological Principles and Chemical Perspectives-A Review. *New J. Chem*. **1991**, *15*, 153-180.
4. Elemans, J. A. A. W.; Rowan, A. E.; Nolte, R. J. M. Mastering Molecular Matter. Supramolecular Architectures by Hierarchical Self-Assembly. *J. Mater. Chem.* **2003**, *13*, 2661-2670
5. Elemans, J. A. A. W.; van Hameren, R.; Nolte, R. J. M.; Rowan, A. E. Molecular Materials by Self-Assembly of Porphyrins, Phthalocyanines, and Perylenes. *Adv. Mater*. **2006**, *18*, 1251-1266.
6. Zhao, X.; Pan, F.; Xu, H.; Yaseen, M.; Shan, H.; Hauser, C. A. E.; Zhang, S.; Lu, J. R. Molecular Self-Assembly and Applications of Designer Peptide Amphiphiles. *Chem. Soc. Rev*. **2010**, *39*, 3480-3498.
7. Mao, Z.; Xu, H.; Wang, D. Molecular Mimetic Self-Assembly of Colloidal Particles. *Adv. Funct. Mater*. 2010, 20, 1053-1074.
8. Phillips, M. J.; Voeltz, G. K. Structure and Function of ER Membrane Contact Sites with Other Organelles. *Nat. Rev. Mol. Cell Biol*. **2016**, *17*, 69-82.
9. Walther, A.; Müller, A. H. E. Janus Particles: Synthesis, Self-Assembly, Physical Properties, and Applications. *Chem. Rev*. **2013**, *113*, 5194-5261.

10. Hu, J.; Zhou, S.; Sun, Y.; Fang, X.; Wu, L. Fabrication, Properties and Applications of Janus Particles. *Chem. Soc. Rev*. **2012,** *41*, 4356-4378.

11. Loget, G.; Kuhn, A. Bulk Synthesis of Janus Objects and Asymmetric Patchy Particles. *J. Mater. Chem*. **2012**, *22*, 15457-15474.

12. Green, N. M. Avidin. 1. The Use of [14C]Biotin for Kinetic Studies and for Assay. *Biochem. J*. **1963**, *89*, 585-591.

13. Green, N. M. Avidin and Streptavidin. *Methods Enzymol*. **1990**, *184*, 51-67.

14. Wong, L, S.; Khan, F.; Micklefield, J. Selective Covalent Protein Immobilization: Strategies and Applications. *Chem. Rev*. **2009**, 109, 4025-4053.

15. Howarth, M.; Chinnapen, D. J-F.; Gerrow, K.; Dorrestein, P. C.; Grandy, M. R.; Kelleher, N. L.; El-Husseini, A.; Ting, A. Y. A Monovalent Streptavidin with a Single Femtomolar Biotin Binding Site. *Nat Methods* **2006**, *3*, 267-273.

16. Hofmann, K.; Wood, S. W.; Brinton, C. C.; Montibeller, J. A.; Finn, F. M. Iminobiotin Affinity Columns and Their Application to Retrieval of Streptavidin. *Proc. Natl. Acad. Sci. U. S. A.* **1980**, *77*, 4666-4668.

17. Green, N. M. Avidin. *Adv. Protein Chem*. **1975**, *29*, 85-133.

18. Bayer, E. A.; Wilchek, M. The Use of the Avidin-Biotin Complex as a Tool in Molecular Biology. *Methods Biochem. Anal*. **1980**, *26*, 1-45.

19. Laitinen, O. H.; Nordlund, H. R.; Hytönen, V. P.; Kulomaa, M. S. Brave New (Strept) Avidins in Biotechnology. *Trends Biotechnol*. **2007**, *25*, 269-277.

20. Chai, J.; Wong L. S.; Giam, L.; Mirkina, C. L. Single-Molecule Protein Arrays Enabled by Scanning Probe Block Copolymer Lithography. *Proc. Natl. Acad. Sci. U. S. A.* **2011**, *108*, 19521-19525.

21. Zhan, W.; Bard, A. J. Electrogenerated Chemiluminescence. 83. Immunoassay of Human C-Reactive Protein by Using $Ru(bpy)_3^{2+}$-Encapsulated Liposomes as Labels. *Anal. Chem*. **2007**, *79*, 459-463.

22. Ho, J. A.; Zeng, S.-C.; Tseng, W.-H.; Lin, Y.-J.; Chen, C.-H. Liposome-Based Immunostrip for the Rapid Detection of Salmonella. *Anal. Bioanal. Chem*. **2008**, *391*, 479-485.

23. Boukobza, E.; Sonnenfeld, A.; Haran, G. Immobilization in Surface-Tethered Lipid Vesicles as a New Tool for Single Biomolecule Spectroscopy. *J. Phys. Chem. B* **2001,** *105*, 12165-12170.

24. Silva, L. C.; de Almeida, R. F. M.; Castro, B. M.; Fedorov, A.; Prieto, M. Ceramide-Domain Formation and Collapse in Lipid Rafts: Membrane Reorganization by an Apoptotic Lipid. *Biophys. J*. **2007**, *92*, 502-516.

25. Vermette, P.; Gengenbach, T.; Divisekera, U.; Kambouris, P. A.; Griesser, H. J.; Meagher, L. Immobilization and Surface Characterization of NeutrAvidin Biotin-Binding Protein on Different Hydrogel Interlayers. *J. Colloid Interface Sci*. **2003**, *259*,13-26.

26. Swamy, M. J.; Marsh, D. Spin-Label Studies on the Anchoring and Lipid-Protein Interactions of Avidin with N-Biotinylphosphatidylethanolamines in Lipid Bilayer Membranes. *Biochemistry* **1997**, *36*, 7403-7407.

27. Yan, J.; Chaudhary, K.; Bae, S. C.; Lewis, J. A.; Granick, S. Colloidal Ribbons and Rings from Janus Magnetic Rods. *Nat. Commun*. **2013**, *4*, 1516.

Chapter 6

Self-Assembly of Charged Janus-like Liposomes

6.1 Introduction

Lipids have long been recognized as essential components in biomembranes for hosting proteins and maintaining the membrane barrier.[1] Besides their structure-related functions, recent studies have suggested that lipids enhance and regulate membrane associated reactions.[1,2] In particular, charged lipids are involved in modulating the structure and function of some transmembrane proteins.[3] Phosphatidylinositol, for example, plays significant parts in lipid signaling, cell signaling, and membrane trafficking.[4] Phosphatidylserine, on the other hand, is the key component functioning in apoptosis, and additionally plays a role in blood coagulation.[5] Other charged lipids, such as phosphatidylglycerols, are essential components of the photosynthetic membranes, from cyanobacteria to chloroplasts of eukaryotic cells.[6]

A useful approach toward understanding the roles played by charged lipids in biomembranes is to study their interaction and dynamics in model lipid systems. Among these, electrostatic interaction between oppositely charged liposomes has been often investigated over the past several decades.[7-15] It is of significant fundamental interest because it is such a useful way to investigate membrane fusion that plays a significant role in many cellular processes such as vesicle targeting, exocytosis, endocytosis, and lipid trafficking.[16] In addition, electrostatically

bringing oppositely charged liposomes together forms junctions, which are considered as intermembrane junction mimics.[15] Such junctions are essential to multicellular organisms because they provide cell-cell or cell-substrate adhesion, and additionally are responsible for intercellular communication by affording the sites for trafficking ions or molecules between cells.[17-19] Moreover, such interaction may provide means for drug delivery, particularly gene delivery,[9] which are often carried by cationic liposomes,[20] considering that cell membranes generally carry net negative surface charge.

Herein, we investigate the electrostatic interaction between oppositely charged liposomes and study their self-assembly. Exploiting cholesterol-triggered phase separation, we demonstrate regioselective introduction of charge into the Janus liposomes. Two mechanisms were explored to achieve self-assembly of liposomes. One is to make use of electrostatic interaction between oppositely charged Janus giant liposomes, and the other one is to take advantage of electrostatic interaction between oppositely charged Janus giant liposomes and SUVs. Confocal fluorescence microscopy is used to track thus-formed aggregates.

6.2 Experimental Section

6.2.1 Chemicals

Lipids, including 1,2-dioleoyl-*sn*-glycero-3-phosphocholine (DOPC), 1,2-dipalmitoyl-sn-glycero-3-phosphocholine (DPPC), 1,2-dipalmitoyl-*sn*-glycero-3-phospho-*rac*-(1-glycerol) sodium salt (DPPG), 1,2-dipalmitoyl-3-trimethylammonium-propane (chloride salt) (DPTAP), 1,2-dioleoyl-*sn*-glycero-3-phosphoethanolamine-N-(lissamine rhodamine B sulfonyl) (ammonium salt) (Rho-DOPE), 23-(dipyrromethene boron difluoride)-24-norcholesterol

(BODIPY-Chol), were purchased from Avanti (Alabaster, Alabama). Cholesterol was bought from Sigma-Aldrich.

6.2.2 Synthesis of Liposomes

In this study, we synthesized three kinds of liposomes, including anionic Janus giant liposomes, cationic Janus-like giant liposomes, and cationic SUVs.

6.2.2.1 Synthesis of Anionic Janus Giant Liposomes

Anionic Janus liposomes were synthesized using PVA gel swelling as described in Chapter 4. Here, liposomes comprise 10 mol% DPPG, 30 mol% DPPC, 40 mol% DOPC, 20 mol% cholesterol, labeled with Rho-DOPE.

6.2.2.2 Synthesis of Cationic Janus Giant Liposomes

Cationic Janus-like liposomes were synthesized by following the PVA gel swelling procedure in Chapter 4. Liposomes are composed of 10 mol% DPTAP, 30 mol% DPPC, 40 mol% DOPC, 20 mol% cholesterol, labeled with BODIPY-PC.

6.2.2.3 Synthesis of SUVs

SUVs were prepared by using an extrusion-based method as described in Chapter 2. SUVs are made up of 10 mol% DPTAP, 88 mol% DPPC, 2 mol% BODIPY-PC. The as-prepared SUVs in DI H_2O have a total lipid concentration of 2.5 mM and a size of approximately 100 nm.

6.2.3 Self-Assembly

6.2.3.1 Cationic Giant Liposomes Interact with Anionic Giant Liposomes

Self-assembly was performed by mixing equal volume of cationic giant liposomes and anionic giant liposomes, both at 5 μM. Thereafter, the mixtures were vortexed and incubated at room temperature for 2 h.

6.2.3.2 Anionic Giant Liposomes Interact with Cationic SUVs

Mixing anionic giant liposomes at 5 μM and cationic SUVs at 10 μM in an equal volume was carried out. Similarly, the mixtures were vortexed and incubated at room temperature for 2 h.

6.2.4 Confocal Microscopy

The giant liposomes and resulting self-assemblies were imaged by a Nikon A1+/MP confocal scanning laser (488 nm and 561.4 nm) microscope (Nikon Instruments, Inc., Melville, NY) together with a 488 nm and a 561 nm long-pass dichroic mirror, and a 525 ± 25 nm and a 595 ± 25 nm emission filter, respectively.

6.3 Results and Discussions

6.3.1 Confocal Images of Anionic Giant Liposomes and Cationic Giant Liposomes

Using the PVA gel swelling method, we successfully synthesized anionic Janus giant liposomes and cationic Janus-like giant liposomes, visualized by confocal imaging (Fig. 6.1). For anionic liposomes, we incorporated 10 mol% DPPG to render negative charge. As is seen from Fig. 6.1A, one hemisphere of each vesicle is fluorescent (in red), indicating a l_d domain, since liposomes are labeled with Rho-DOPE that prefers a l_d phase. The other hemisphere is non-

fluorescent, belonging to the l_o phase. After introducing DPPG into giant liposomes, the phase separation becomes rather complicated, as shown in phase diagram (Fig. 6.2) described by Hemino et al.[21] Depending on the concentration of DPPG, another s_o domain enriched in DPPG can appear, besides l_d and l_o domains. Under the low concentration (10 mol%) of DPPG in this study, however, only l_o and l_d domains exist, suggested by the phase diagram (Fig. 6.2). Indeed, only two phases including l_o and l_d are observed from the confocal fluorescent image (Fig. 4.4C), and no trace of such s_o domain characterized by a stripe shape and particularly non-fluorescent,[21] when giant liposomes are dually labeled with Rho-DOPE and BODIPY-Chol. Since DPPG has two saturated acyl chains, we reason that DPPG is most likely to partition into l_o domain rather than l_d domain, at a low concentration of 10 mol%. This observation is corroborated by two previous findings. Firstly, Regen and coworker found DPPG and DPPC have a similar preference to cholesterol in l_o phase.[22] Secondly, Keller and coworkers showed monovalent charged lipids such as DPPG have a minimal effect on lipid miscibility phase behavior.[23] Consequently, in this study, we believe non-fluorescent domain (l_o domain) is negatively charged, and l_d domain is neutral, which give rise to broken symmetry in liposome surface charge.

On the other hand, as for cationic giant liposomes, we incorporated 10 mol% DPTAP to introduce the positive charge. The phase separation in such liposomes is different from that of anionic ones. The phase separation in anionic giant liposomes is characterized by almost equal surface area of l_o and l_d domains, while the cationic counterpart is featured by that more than half region is occupied by l_d domain (Fig. 6.1B). This possibly indicates that, unlike DPPG, DPTAP influences phase separation behavior to some extent. Note that cationic giant liposomes are singly labeled with a l_d phase preferred probe, BODIPY-PC, and as such the non-fluorescent region corresponds to the l_o phase. Again, considering that DPTAP has two saturated acyl chains, we

believe it is prone to partition into l_o domain along with DPPC. This means the non-fluorescent region is positively charged.

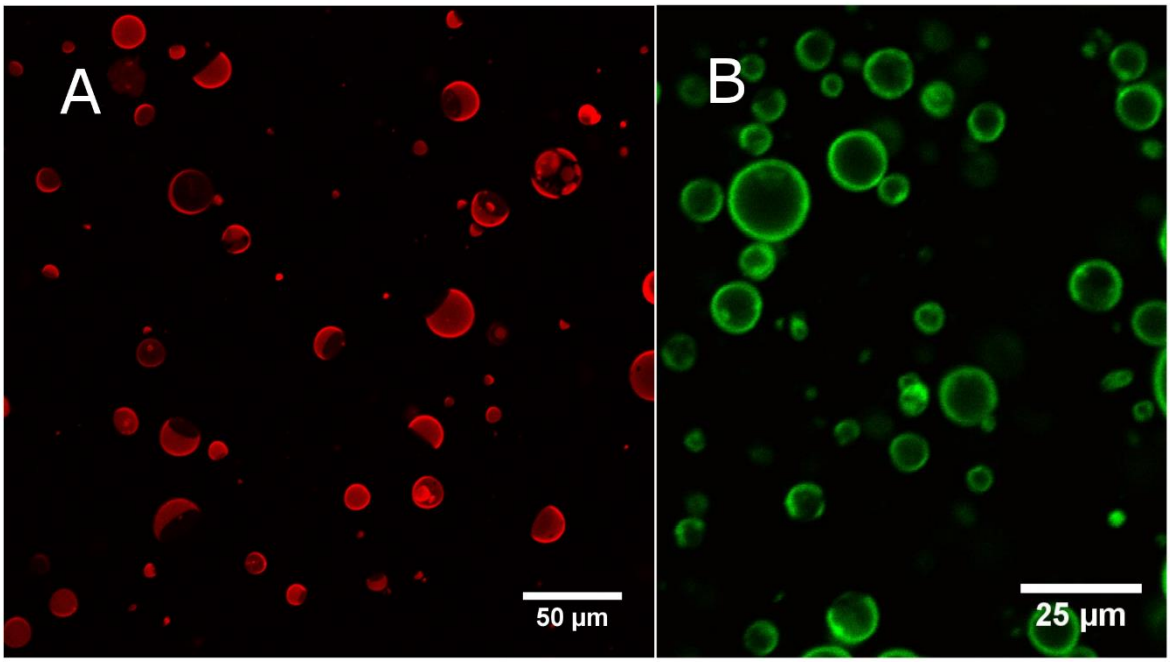

Figure 6.1 Confocal images of (A) Janus anionic giant liposomes and (B) cationic giant liposomes. The anionic giant liposomes labeled with 0.5 mol% Rho-DOPE, are made up of 10 mol% DPPG, 30 mol% DPPC, 40 mol% DOPC and 20 mol% cholesterol. The cationic ones are composed of 10 mol% DPTAP, 30 mol% DOPC, 40 mol% DPPC and 20 mol% cholesterol, and they are doped with 0.5 mol% BODIPY-PC.

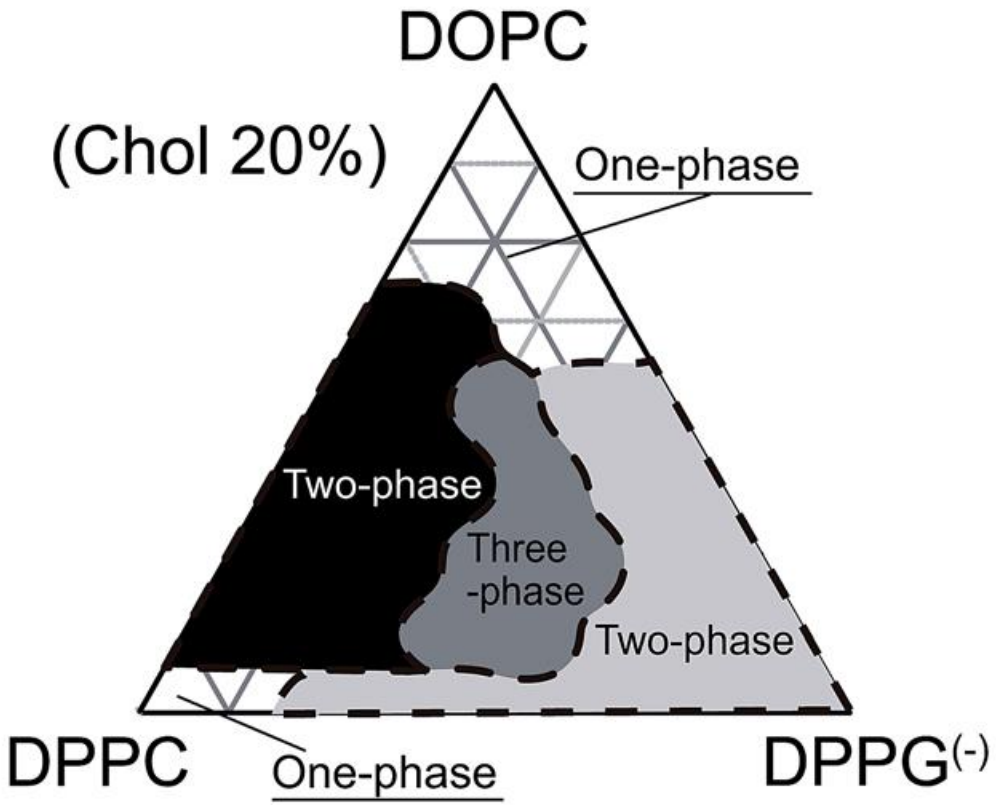

Figure 6.2 Phase diagram of quaternary mixtures of DOPC/DPPC/DPPG/cholesterol (Chol) at a fixed Chol concentration of 20 mol%. Black, grey, and light grey regions represent, l_o/l_d two-phase coexistence, $l_o/l_d/s_o$ three-phase coexistence, and l_d/s_o or l_o/s_o two-phase coexistence, respectively. Reprinted with permission from *Soft Matter*, **2014**, *10*, 7959-7967. Copyright (2014) The Royal Society of Chemistry.

6.3.2 Self-Assembly by Electrostatic Interaction between Cationic Giant Liposomes and Anionic Giant Liposomes

Here, we use electrostatic interaction to drive self-assembly of charged Janus liposomes. Due to variabilities in chemical structure, composition and charge density, interaction between oppositely charged liposomes is rather complex. For example, MacDonald and coworkers spent considerable research effort on studying the interaction between oppositely charged giant

vesicles.[11-13] They directly observed membrane fusion and hemifusion depending on membrane composition by fluorescence microscopy, and fluorescent dye transfer between two vesicles, implying lipid transfer upon membrane adhesion. On the other hand, Lehn and coworkers[9] believe that interaction between two oppositely charged vesicles results in lipid transfer and subsequent de-adhesion. Similarly, Saeki et al.[14] found oppositely charged liposomes first aggregated together, then lipid mixing took place, and ultimately disaggregated.

In this work, we take advantage of cholesterol-induced phase separation, and hence regioselectively locate charged lipids. We mix cationic and anionic giant liposomes together in DI water. In water, the electrostatic interaction is long-range and strong, on the order of k_BT, between oppositely charged lipid headgroups.[23] Confocal images show that dimers, trimers, and tetramers are formed (Fig. 6.4). Note that the binding takes place unambiguously in l_o phase on anionic giant liposomes, confirming the l_o domain is negatively charged, while unfortunately for cationic ones, it is unclear. We can no longer discern l_o phase on cationic giant liposomes after binding, possibly due to domain reorganization. Besides, we found lipid transfer from cationic giant liposomes to anionic ones, indicated by that initially non-fluorescent hemisphere turns into green (Fig. 4A). Taking a careful inspection of Fig. 4, we observed partial membrane fusion. Interestingly, anionic liposomes remain intact and not at all deformed after fusion, while cationic ones are misshapen to some extent. MacDonald and coworkers proposed that cholesterol can stabilize the hemifused structures and inhibit full fusion on the basis of reduced tension of bilayers when oppositely charged liposomes interact.[24] This somehow explains why anionic liposomes are not deformed because the binding region on anionic liposomes is in l_o phase that is enriched in cholesterol. On the other hand, we argue that l_o domain is stiffer than l_d phase, which may be responsible for intact anionic liposomes in the resulting aggregates. For self-assembled trimers, one cationic giant

liposome is sandwiched between two anionic ones. Depending on the relative size of oppositely charged liposomes, linear or bent chain-like structures can be formed. Liposomes with uniform size tend to self-assemble into linear aggregates (Fig. 6.3, Fig. 4B top and middle panel). On the other hand, two smaller anionic giant liposomes can dock on a larger cationic one, forming a "Mickey Mouse" shaped structure (Fig. 6.3, Fig. 6.4B bottom panel). From time to time, we synthesized Janus anionic giant liposomes whose l_d domain is inlaid with a few small circular l_o domain (Fig. 6.2A). These l_o domains are negatively charged and thus can further attach cationic liposomes to extend the chains (Fig. 6.3, Fig. 6.4C).

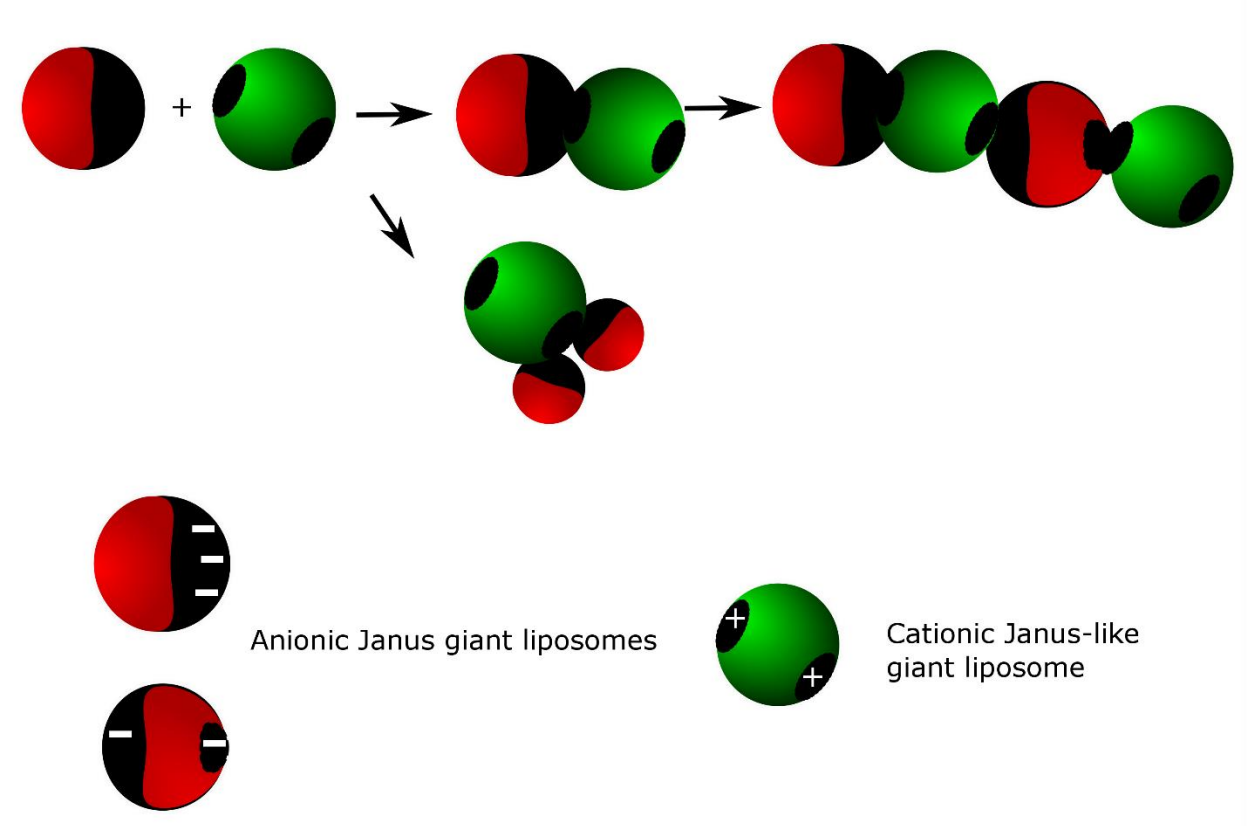

Figure 6.3 Schematic of self-assembly of oppositely charged Janus-like giant lipsomes. In both cationic and anionic lipsomes, non-fluorescent domains are charged (see discussion in main text).

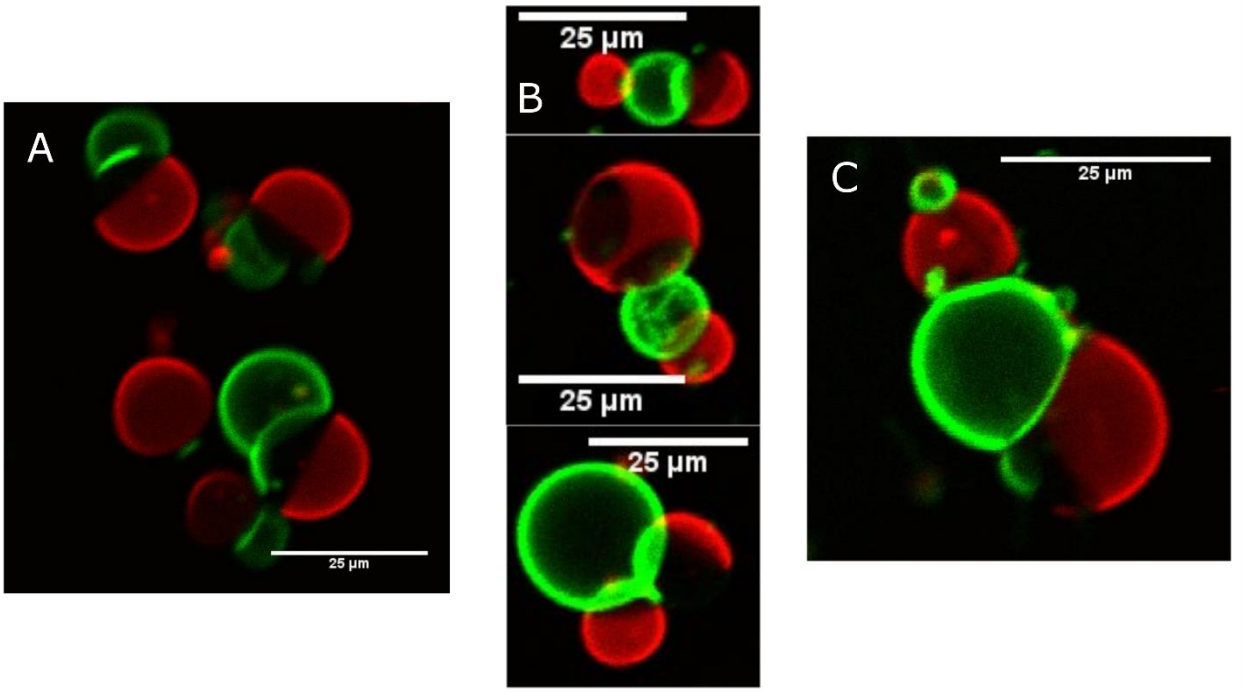

Figure 6.4 Confocal images of self-assemblies of oppositely charged Janus-like giant liposomes. (A) Dimers, (B) trimers, (C) multimer.

6.3.3 Self-Assembly by Electrostatic Interaction between Cationic SUVs and Anionic Giant Liposomes

By bringing SUVs and giant liposomes together through electrostatic attraction, a well-defined lipid interface may be prepared to mimic the intermembrane junctions in the living cells. Such intermembrane junctions are responsible for intercellular communication.[5] Hence, it is of great significance to study interaction between giant liposomes and SUVs. Previously, electrostatic interaction between oppositely charged giant liposomes and SUVs has been investigated. Tabaei et al.,[15] for instance, tethered a population of negatively charged SUVs to a positively charged giant liposome, and found SUVs docked on the giant vesicle executing 2-dimensional Brownian motion by confocal microscopy. Surprisingly, these SUVs did not fuse with GUVs, possibly due

to low charge density in this system. In contrast, Franzin et al. [10] using NMR to investigate the fusion between anionic giant liposomes and cationic SUVs, found that there is a spontaneous fusion of SUVs with the giant liposomes, leading to a complete mixing of the lipids.

In the present work, we employ cationic SUVs to tether adjacent anionic Janus giant liposomes to form aggregates. Again, through cholesterol-triggered phase separation, only one hemisphere (l_o domain) of each giant vesicle carries negative charge. As shown in Fig. 6.5, a population of SUVs with size of 100 nm is mixed with oppositely charged giant vesicles. We envision that spontaneous binding between SUV and l_o domain of giant vesicle (in black) takes place after mixing. Due to the excess of SUVs, the SUV-decorated giant liposomes further bind to another giant vesicle, forming dimers. Indeed, we observed such aggregates by using confocal microscopy (Fig. 6.6A). In order to minimize the liposome fusion, we used SUVs composed of all saturated lipids. From confocal images, however, we found that the two fluorescent probes are intermixing in giant vesicles (Giant vesicles are no longer in red), suggestive of full fusion of SUVs with giant vesicles. This is in line with the finding from Franzin et al.[10] In addition, linear or bent chain-like trimers are observed with the dipole of the middle giant vesicle nearly perpendicular to that of giant vesicles at two ends, as depicted in Fig. 6.5. In similar fashion, a tetramer forms in a pyramidal shape (Fig. 6.5, Fig. 6.6C top panel). At times, as mentioned earlier, we synthesized Janus giant vesicles in which the l_d hemisphere is inlaid with l_o domains, further interacting with positively charged SUVs. In this way, they can bind to another giant liposome, and extend the self-assembled chains (Fig. 6.6C bottom panel, Fig. 6.6D). Often times, introducing oppositely charged SUVs severely disrupts the phase separation of giant liposomes in the resulting aggregates.

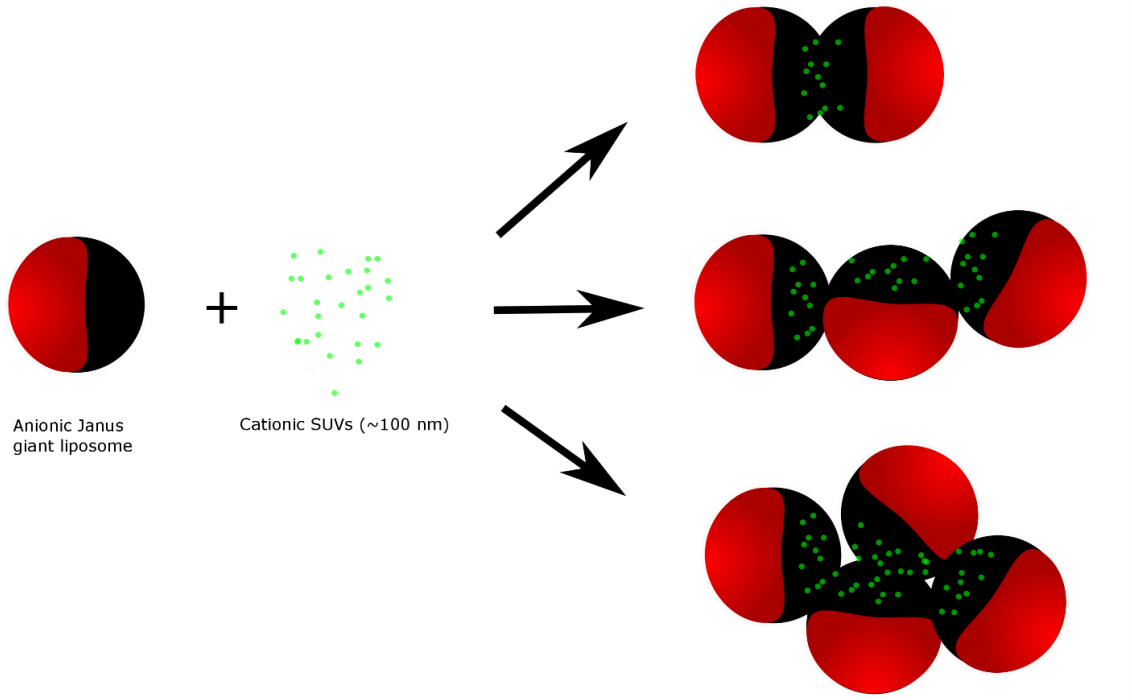

Figure 6.5 Schematic of self-assembly of oppositely charged Janus-like giant liposomes and SUVs.

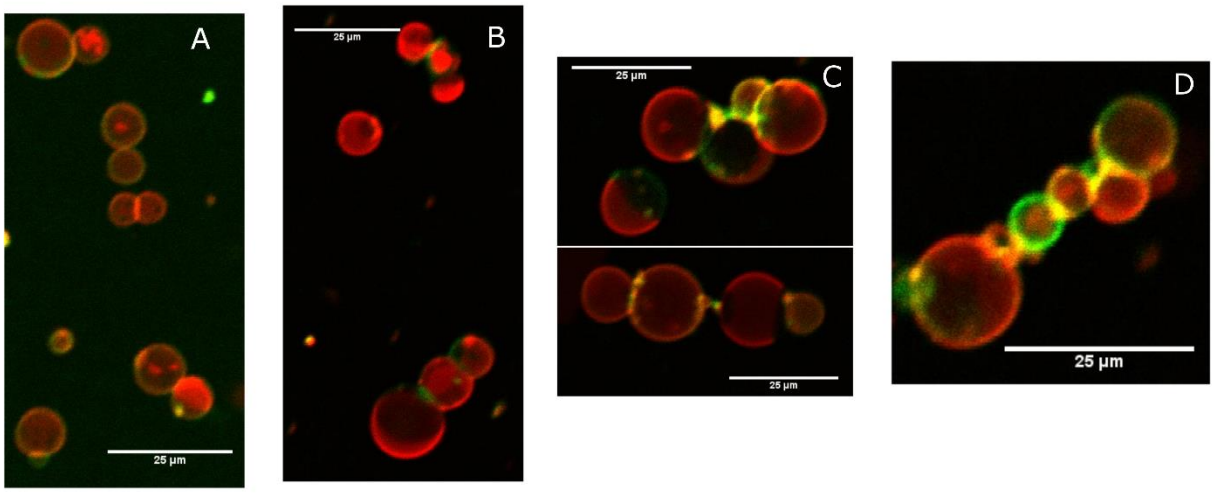

Figure 6.6 Confocal images of self-assemblies of oppositely charged Janus giant liposomes and SUVs. (A) Dimers, (B) trimers, (C) tetramers, (D) chain-like aggregate.

6.4 Conclusions

In this work, we studied the self-assembly of charged Janus liposomes driven by electrostatic interaction. Importantly, in DPPC/DOPC/cholesterol tertiary system, the cholesterol induced phase separation is exploited to create surface asymmetry on individual liposomes, which allows for regio-selectively locating charged lipids. From there, we use two mechanisms to achieve self-assembly. One is by interaction between oppositely charged Janus-like giant liposomes, the other is through electrostatic interaction between oppositely charged giant liposomes and SUVs. Aggregates with interesting structures are formed. One of the future work is to exploit these aggregates to mimic intermembrane junctions in the living cells. To this end, we wish to investigate the self-assembly under physiological conditions. Another research direction is to use computational chemistry to understand how such aggregates are formed, so that we can set out to seek a better controlled way to accomplish the self-assembly.

References

1. Langner, M.; Kubica, K. The Electrostatics of Lipid Surfaces. *Chem. Phys. Lipids* **1999**, *101*, 3-35.
2. Contreras, F.-X.; Ernst, A.M., Wieland, F.; Brügger, B. Specificity of Intramembrane Protein-Lipid Interactions. *Cold Spring Harb. Perspect. Biol.* **2011**, *3*, a004705.
3. Pöyry, S.; Vattulainen, I. Role of Charged Lipids in Membrane Structures-Insight Given by Simulations. *Biochim. Biophys. Acta* **2016**, *1858*, 2322-2333.
4. Czech, M. P. PIP2 and PIP3: Complex Roles at the Cell Surface. *Cell* **2000**, *100*, 603-606.
5. Martin, S.; Reutelingsperger, C.; McGahon, A. J.; Rader, J. A.; Van Schie, R.; LaFace, D. M.; Green, D. R. Early Redistribution of Plasma Membrane Phosphatidylserine is a General

Feature of Apoptosis Regardless of the Initiating Stimulus: Inhibition by Overexpression of Bcl-2 and Abl, *J. Exp. Med.* **1995**, 182, 1545-1556.

6. Boudière, L.; Michaud, M.; Petroutsos, D.; Rébeillé, F.; Falconet, D.; Bastien, O.; Roy, S.; Finazzi, G.; Rolland, N.; Jouhet, J.; Block, M. A.; Maréchal, E. Glycerolipids in Photosynthesis: Composition, Synthesis and Trafficking. *Biochim Biophys Acta* **2014**, *1837*, 470-480.
7. Stamatatos, L.; Leventis, R.; Zuckermann, M. J.; Silvius, J. R. Interactions of Cationic Lipid Vesicles with Negatively Charged Phospholipid Vesicles and Biological Membranes. *Biochemistry* **1988**, *27*, 3917-3925.
8. Duzgunes, N.; Goldstein, J. A.; Friend, D. S.; Felgner, P. L. Fusion of Liposomes Containing a Novel Cationic Lipid, N-[2,3-(Dioleyloxy)Propyl]-N,N,N-Trimethylammonium: Induction by Multivalent Anions and Asymmetric Fusion with Acidic Phospholipid Vesicles. *Biochemistry* **1989**, *28*, 9179-9184.
9. Marchi-Artzner, V.; Jullien, L.; Belloni, L.; Raison, D.; Lacombe, L.; Lehn, J.-M. Interaction, Lipid Exchange, and Effect of Vesicle Size in Systems of Oppositely Charged Vesicles. *J. Phys. Chem*. **1996**, *100*, 13844-13856.
10. Franzin C. M.; Macdonald P. M. Detection and Quantification of Asymmetric Lipid Vesicle Fusion Using Deuterium NMR. *Biochemistry* **1997**, *36*, 2360-2370.
11. Pantazatos, D. P.; MacDonald, R. C. Directly Observed Membrane Fusion Between Oppositely Charged Phospholipid Bilayers. *J. Membr. Biol*. **1999**, 170, 27-38.
12. Pantazatos, D. P.; Pantazatos, S. P.; McDonald, R. C. Bilayer Mixing, Fusion, and Lysis Following the Interaction of Populations of Cationic and Anionic Phospholipid Bilayer Vesicles. *J. Membr. Biol*. **2003**, *194*, 129-139.

13. Lei, G.; MacDonald, R. C. Lipid Bilayer Vesicle Fusion: Intermediates Captured by High-Speed Microfluorescence Spectroscopy. *Biophys. J.* **2003**, *85*, 1585-1599.
14. Saeki, D.; Sugiura, S.; Baba, T.; Kanamori, T.; Satob, S.; Mukataka, S.; Ichikawa, S. Dynamic Interaction Between Oppositely Charged Vesicles: Aggregation, Lipid Mixing, and Disaggregation. *J. Colloid Interface Sci*. **2008**, *320*, 611-614
15. Tabaei, S. R.; Gillissen, J. J. J.; Kim, M. C.; Ho, J. C. S.; Liedberg, B.; Parikh, A. N.; Cho, N.-J. Brownian Dynamics of Electrostatically Adhering Small Vesicles to a Membrane Surface Induces Domains and Probes Viscosity. *Langmuir* **2016**, 32, 5445-5450.
16. Dalu Xu, Jesse C. Hay. Intracellular Membrane Fusion, in: Trafficking Inside Cells Pathways, Mechanisms and Regulation, pp. 282-325(Segev, N. ed), Springer-Verlag, New York, **2009**.
17. Green, C. R. Intercellular Junctions, in: Biology of the Integument, Vol, I, Invertebrates, pp. 5-16 (Bereiter-Hahn, J.; Matoltsy, A. G.; Richards, K. S. eds.), Springer-Verlag, Berlin, Heidelberg, **1984**.
18. Manz, B. N.; Groves, J. T. Spatial Organization and Signal Transduction at Intercellular Junctions. *Nat. Rev. Mol. Cell Biol*. **2010**, *11*, 342-352.
19. Parthasarathy, R.; Groves, J. T. Protein Patterns at Lipid Bilayer Junctions. *Proc. Natl. Acad. Sci. U. S. A.* **2004**, *101*, 12798-12803.
20. Koltover, I.; Salditt, T.; Rädler, J. O.; Safinya, C. R. An Inverted Hexagonal Phase of Cationic Liposome-DNA Complexes Related to DNA Release and Delivery. *Science* **1998**, *281*, 78-81.
21. Himeno, H.; Shimokawa, N.; Komura, S.; Andelman, D.; Hamada, T.; Takagi, M. Charge-Induced Phase Separation in Lipid Membranes. *Soft Matter* **2014**, *10*, 7959-7967.
22. Mukai, M.; Regen, S. L. Exchangeable Mimics of DPPC and DPPG Exhibiting Similar Nearest-Neighbor Interactions in Fluid Bilayers. *Langmuir* **2015**, *31*, 12674-12678.

23. Blosser, M. C.; Starr, J. B.; Turtle, C. W.; Ashcraft, J.; Keller, S. L. Minimal Effect of Lipid Charge on Membrane Miscibility Phase Behavior in Three Ternary Systems. *Biophys. J.* **2013**, *104*, 2629-2638.

24. García, R. A.; Pantazatos, S. P.; Pantazatos, D. P.; MacDonald, R. C. Cholesterol Stabilizes Hemifused Phospholipid Bilayer Vesicles. *Biochim. Biophys. Acta* **2001**, *1511*, 264-270.